

UCSF

UC San Francisco Electronic Theses and Dissertations

Title

Triple-negative breast cancers remodel lipid metabolism in both tumors and surrounding tissue

Permalink

<https://escholarship.org/uc/item/2kp679m1>

Author

Williams, Jeremy LeBoff

Publication Date

2024

Supplemental Material

<https://escholarship.org/uc/item/2kp679m1#supplemental>

Peer reviewed|Thesis/dissertation

Triple-negative breast cancers remodel lipid metabolism in both tumors and surrounding tissue

by
Jeremy LeBoff Williams

DISSERTATION
Submitted in partial satisfaction of the requirements for degree of
DOCTOR OF PHILOSOPHY

in
Biomedical Sciences

in the
GRADUATE DIVISION
of the
UNIVERSITY OF CALIFORNIA, SAN FRANCISCO

Approved:

DocuSigned by:
Isha Jain Isha Jain
DA7944A12D53439... Chair

DocuSigned by:
Andrei Goga Andrei Goga

DocuSigned by:
Suneil Koliwad Suneil Koliwad
94FA558BE5684D9...

Committee Members

Copyright 2024

by

Jeremy LeBoff Williams

To my grandfather, Dr. Gerald LeBoff, PhD. Thank you for kindling my curiosity,
and for teaching through example that education is a lifelong pursuit
worthy of patience and time.

To my mother, Dr. Meryl LeBoff, MD, whose shoulders I stand on.
Thank you for bringing the world within reach.

To my partner Alan Lam, who found me at a difficult time and helped me climb back out.
Thank you for warming me with your light.

And, to my dog Luigi, for joining me on this long journey. Home is wherever you are.

Acknowledgements

I first received keys to a laboratory around the same time that I got my driver's license. Before and throughout my doctoral research, many have extended trust and chances, seen a scientist in me when my I saw other things, and pushed me to focus and grow, sometimes despite my best efforts. In graduate school I learned that I am only as strong as the net beneath me. Failures of varying scope mark the path of most any PhD student, and any of my success at UCSF is owed to those below, and to many more. Thank you all for your kindness, patience and support.

My first mentor in science, Mara Prentiss, PhD, opened her lab to me and my dear friend Julea Vlassakis, when we were in high school. Over many summers to follow, Mara patiently taught the fundamentals of scientific interrogation, and also let me tinker, imagine and build. Working in Mara's lab engaged a desire to contribute to science, and I felt a great sense of place. It was formative being confronted with technical questions and having access to the tools of a lab at that young age, and Mara was supremely charitable to show faith in me. Thank you, Mara, for inspiring an interest in experimental design, and for being the queer role model in science I didn't yet know I would need.

Before reaching the Biomedical Sciences program at UCSF, I took advantage of a liberal arts college curriculum by pivoting from pipettes to study music composition, in healthy counterpoint to ongoing science coursework and projects in Mara's lab. I owe great thanks to my undergraduate advisor Su Tan, for seeing and nurturing both my musical and scientific creativity. Just after college, serendipity brought me the great chance to work for William G. Kaelin Jr., MD, an unforgettable experience that surely carried graduate school at UCSF into orbit. To Dr. Kaelin, thank you for taking the time to mentor me, for affording me an incomparably

challenging and rewarding postbaccalaureate in your lab, and for inspiring with a glimpse into your rigorous experimental world. Thanks to Javid Moslehi, MD, now at UCSF, for seeing the scientist in me and for the opportunities you extended; To Ben Olenchock, MD, PhD for demanding persistence and summoning good work. Thank you to all of Kaelin Lab for taking in this liberal arts generalist and showing me a path towards UCSF.

When I first flew out, full of nerves and visited the Biomedical Sciences program in San Francisco, my eventual mentor Andrei Goga, MD, PhD and his group gave the warmest welcome. I clearly recall first sitting down in Andrei's office — sweaty with imposter syndrome during a full day of interviews — and being grounded by his sincerity. His lab's engaging work identifying therapeutic targets in cancer metabolism was great motivation for me to leap from the Northeast to Northern California. Andrei's deep clinical expertise, knowledge of the literature, skilled grantsmanship and drive to collaborate are all led by kindness, a quality I've not seen falter over these eventful years. Thank you, Andrei, for encouraging perseverance, for giving me rope to explore and experience life during these years, and for your consistent support.

I am only able to pass this milestone with the help of my fellow Goga Lab members. To my former labmate Roman Camarda, who inspired the direction of much of this research, thank you for taking me under your wing, for setting such a positive tone, and for sharing your creative work and letting me shepherd it forward. Thank you to Joyce Lee for always making space to help me out in times of need. Thank you to Dan Van de Mark for your contributions to the lipolysis project, and for calmly fielding my many questions. Thanks to you both for all your great advice. To Joy Gittins, thank you for bringing me so much cheer in lab, and for always taking time to talk and connect. To my dear friend and longtime labmate Rachel Nakagawa, I am keenly aware I would not have been able to complete this degree without your consistent help,

honesty, and camaraderie. Amidst a sort of reset to my scientific confidence upon transplanting to San Francisco, you have been a great friend to me in lab, and grounded me through countless spirals. To my BMS classmates and program-mates, and to other UCSF friends made along the way, thank you for all the support and shared experiences.

I wouldn't have moved so far from home without the encouragement from my Northeast transplant friends, who brought me comfort in once-unfamiliar San Francisco: Thank you to Sara Dinkin, for all the walk-and-talk's through the city, for showing me the way to a good NorCal winter, and for helping me hold on to myself along this road. To Anna Broido, a great friend since childhood, it feels deeply fulfilling to have reconnected with you here. Thank you to Julea Vlassakis, my first labmate, who made bench science fun in high school and showed me how to have fun as a grad student in the Bay Area. And to Aaron Berard back home in New England, thank you for staying so connected from afar, and for sharing the joys of your growing family. I so appreciate these and all the other friends who have stayed in touch.

It's a great fortune to have nuclear family who have championed my interest in academic research, and who've held me close even through great physical distance. I want to thank my grandparents Phyllis and Gerald LeBoff, the gravitational center of my family and an extraordinary example of partnership, who taught patience, compassion and generosity, and embraced me since my birth. My grandpa Jerry pursued his own PhD in Cultural Studies from NYU at around 83 years old, and graduated just shy of his 91st birthday, all with the help (and patience) of his lifelong love, my grandma Phyllis. Both were intently engaged in my ongoing education. My grandpa would often turn his inquisitive mind towards my eventual research with sage questions on logic and intent, and though not a scientist by trade he insisted on reaching understanding. My grandparents' enduring bond was matched only by a love for their family,

and it's hard to grasp the gift of time we've shared on my journey here. Grandma and grandpa, every moment spent with you during these years was an inconceivable blessing, and I carry them forward.

To my mother, Meryl LeBoff, wearer of so many hats — Mom, nana, daughter, immensely talented clinician scientist, friend, and lifelong learner, to name only a few... Mom who is both smart and wise beyond her years, who always picks up the phone and jumps on a plane, and joins me on real and figurative double black diamonds wherever they might approach. Thank you for teaching me the importance of family, the value of education, and what it means to love your work. To my older sister Avery Vafai, the best example of success a sibling could ask for, thank you for your love and support, and for bringing unthinkable joy into our lives during graduate school — The beauty of your family is astonishing. To Madelyn and Benjamin, my niece and nephew, thank you for always inspiring a smile, a priceless resource for any doctoral student. To my brother-in-law Scott Vafai: The cadence of my progress in science is owed in such large part to your thoughtfulness. To my aunt Gail LeBoff, who has helped me know and nurture my creative self since before I can remember — you have fostered so many pieces that lay beyond the bounds of school and science. Thank you for sharing your Vermont, past and future.

And, to my partner Alan, whose bright smile has lit the way through this foggy San Francisco adventure: our connection is the part I treasure most from this experience. Thank you for your unwavering love and support, for bringing me the strength to follow through, for walking this journey by my side, for welcoming me into your family and embracing my family as your own, and for exploring and making a home with me in Northern California. I can't wait to make the leap back East with you to experience it all again.

Contributions

Research detailed in this dissertation was conducted under the supervision of Andrei Goga, MD, PhD. My committee members Isha Jain, PhD and Suneil Koliwad, MD, PhD also provided valuable guidance and support.

Chapter 2 is adopted from a review article previously published as:

Camarda, R., Williams, J., and Goga, A. (2017). In vivo Reprogramming of Cancer Metabolism by MYC. Frontiers in Cell and Developmental Biology. **5**: 1-13.

All authors listed, have made substantial, direct and intellectual contribution to the work, and approved it for publication. This material is based upon work supported by NIH R01- CA170447 and NIH U19 CA179512, UCSF Liver Center grant P30DK026743, a Lymphoma Scholar Award, CDMRP Breast Cancer Research Program (W81XWH-12-1-0272 and W81XWH-16-1-0603) (to AG) and the NIH F99CA212488 (to RC). The authors would also like to thank Dror Assa for providing the drawing in **Fig. 1.1**.

Chapter 3 follows prior work from Mahieu C., Camarda R., Horiuchi D., and Goga A., and was performed with assistance from Nakagawa R., and Durney, S.; Mahieu, C. performed assays shown in **Figs. 3.3A-B** and **3.4E-F**.

Chapter 4 is adopted from a manuscript accepted in principle to *Nature Communications* at the time of this publication. This article was previously published as a preprint:

Williams, J.L. †, Camarda, R. †, Malkov, S., Zimmerman, L., Manning, S., Aran, D., Beardsley, A., Van de Mark, D., Nakagawa, R., Chen, Y., Berdan, C., Louie, S., Mahieu,

C., Superville, D., Winkler, J., Willey, E., Gagnon, J., Avsaroglu, K.S., Kosaku, S., Gruner, M., Nishida, H., Ansel, K.M., Werb, Z., Nomura, D.K., Kajimura, S., Butte, A., Sanders, M., Liebler, D., Rugo, H., Krings, G., Shepherd, J.A., and Goga, A. (2024). "Tumor cell-adipocyte gap junctions activate lipolysis and contribute to breast tumorigenesis."

[bioRxiv: 277939](https://doi.org/10.1101/277939).

† These authors contributed equally to this work

This work was supported, in part, by the US Department of Defense–Congressional Directed Medical Research Programs’ Era of Hope Scholar award W81XWH-12-1-0272 (A.G.), the US National Institutes of Health (NIH) grants R01 CA 0447 (A.G.) and R01 CA056721 (Z.W.), the Atwater Foundation (A.G.), the Breast Cancer Research Fund (H.R.), the EMBO postdoctoral fellowship ALTF 159-2017 (Ju.W.), the US K99/R00 NIH Pathway to Independence Award DK110426 (K.S.), and the US NIH F99/K00 Predoctoral to Postdoctoral Transition Award F99CA212488 (R.C.) and the US NIH F31 Predoctoral Individual National Research Service Award F31CA243468 (J.W.). The authors thank A. Welm for guidance in the use of patient-derived xenografts, A. Tward for technical guidance and helpful discussions, K.A. Fontaine for helpful discussions and comments on the manuscript, and S. Samson for a helpful consumer advocate perspective and guidance on our work. R.C. and A.G. conceived of research. J.W. and R.C. designed and contributed to all *in vitro* and *ex vivo* studies, and to the *in vivo* mouse studies, contributed to all data analysis, and wrote the manuscript. S.M. analyzed 3CB data. L.J.Z. designed LCM and conducted proteomic analyses. S.M. conducted the LCM. D.A. conducted lipolysis signature enrichment and scRNA-seq analyses. A.B. contributed to immunofluorescent staining and microscopy, and generation of Cx31 partial knockout lines. D.V. characterized Cx31 partial depletion lines, generated Cx31 inducible short hairpin lines, contributed to Cx31

knockdown and CL316243 mouse studies and provided helpful discussions. S.K.A. contributed to generation of Cx31 inducible short hairpin lines. R.N. contributed to co-culture studies, immunofluorescent staining, tissue clearing and microscopy, and provided valuable discussions. Y.C. conducted preadipocyte differentiation. C.B. and S.L. conducted mass spectrometry for cAMP. C.M. generated Cas9-expressing cancer cell lines. Ju.W. and E.W. isolated primary mammary adipose tissue. J.D.G. and D.S. conducted FACS analysis. K.S. provided cAMP-dependent lipolysis signature. K.M.A. supervised FACS analysis. Z.W. supervised primary mammary adipose tissue isolation and provided valuable discussion. D.K.N. supervised mass spectrometry for cAMP and provided valuable discussion. S.K. supervised preadipocyte and cAMP-dependent lipolysis studies and provided valuable discussion. A.J.B supervised enrichment analysis. M.E.S. and D.C.L. designed and supervised LCM and proteomics. M.G. contributed to RNA-seq analysis. H.N. contributed to co-culture studies. H.R. provided valuable discussion. G.K. designed and conducted histological analyses and provided valuable discussion. J.A.S. supervised the 3CB study and data analysis, and provided valuable discussion. A.G. supervised the study, and provided valuable discussion and intellectual input. All authors edited the manuscript.

**Triple-negative breast cancers remodel lipid metabolism
in both tumors and surrounding tissue**

Jeremy LeBoff Williams

Abstract

Tumors display altered metabolism, often reflective of their microenvironment. In many cases including breast cancer, the invasive tumor front borders adipocytes. Reliance on mitochondrial fatty acid oxidation (FAO) has been observed in aggressive receptor ‘triple-negative’ breast cancers (TNBC), but the adaptations that permit elevated FAO, and the molecular mechanisms by which tumors coopt adjacent adipocytes for growth, remain elusive. The oncogene MYC dysregulates a range of cellular programs, including metabolism; MYC expression is elevated in most TNBC, and linked to increased FAO. To delineate alterations facilitating FAO in TNBC, I examined fatty acid binding proteins (FABP) thought to traffic FA to the mitochondria. Prior work identified FABP5 elevation in patient TNBC and a model of MYC-driven breast cancer. I observed increased FABP5 transcription in TN compared to ‘receptor-positive’ patient-derived cell lines, yet elevation across MYC-low and -high TNBC suggested levels are not solely MYC-regulated. Treating MYC-driven breast cancer cells with an FABP5/7 inhibitor caused lipid accumulation and impaired proliferation, but I found no growth defect after FABP5 knockout. While compensation by other FABPs may complicate knockout studies, specific inhibitors for FABP5 and other FAM targets are in clinical development. Despite evidence indicating reliance on FAO in TNBC, the source of FA fueling aggressive tumor growth is unclear. I next described a direct interaction linking cancer cell-adipocyte contact to tumor progression. Examining breast tumors and normal adjacent tissue from patient cohorts, patient-derived xenografts and mouse models, we observed activation of lipolysis and lipolytic signaling in neighboring adipose tissue. Using cancer cell adipocyte co-cultures, I found that functional gap junctions (GJ), small

intercellular channels, form and permit cAMP transfer from breast cancer cells to adipocytes, activating lipolysis in a GJ-dependent manner. We identified connexin 31 (GJB3) as a promoter of in vivo TNBC growth and activation of adjacent lipolysis, or FA release. Our findings indicate a pro-tumorigenic role for direct tumor cell-adipocyte interactions. These studies reveal that TNBC dysregulate tumoral lipid metabolism and stimulate altered FAM in surrounding tissue.

Table of Contents

Chapter 1: Introduction	1
Graphical Abstract.....	2
Clinical Impact.....	4
Introduction	6
References	11
Chapter 2: Multiple roles for Myc in altering cancer metabolism.....	21
Abstract	22
Introduction	22
Main Text	26
Conclusion	44
Figures	46
References	49
Chapter 3: Alterations to fatty acid trafficking in triple-negative breast cancer	62
Abstract	63
Introduction	63
Results.....	66
Discussion	67
Figures	71
References	78
Chapter 4: Defining a new role for surrounding adipocytes in TNBC tumor growth.....	83
Abstract	84
Main Text	84
Materials and Methods	98
Figures	113
References	129

Chapter 5: Additional publications from thesis work.....	136
In Vivo Optical Metabolic Imaging of Long-Chain Fatty Acid Uptake in Orthotopic Models of Triple-Negative Breast Cancer.....	137
MYC Dysregulates Mitosis, Revealing Cancer Vulnerabilities	140
Chapter 6: Concluding remarks.....	142
Summary	143
Future Directions.....	146

List of Figures

Figure 1.1. Graphical Abstract: Alterations to lipid metabolism in breast cancers and surrounding adipocytes.....	2
Figure 2.1. A summary of the metabolic alterations found in each MYC-driven cancer type by tissue of origin.....	46
Figure 2.2. MYC-dependent miRNA regulation of glutamine metabolism.....	48
Figure 3.1. Schematic of fatty acid trafficking by fatty acid binding proteins (FABPs) in a breast cancer cell.....	71
Figure 3.2. Schematic of fatty acid trafficking and mitochondrial fatty acid oxidation in a breast cancer cell.	72
Figure 3.3. FABP5 expression is elevated in a MYC-dependent manner in TNBC.	73
Figure 3.4. FABP5 inhibition and silencing selectively impair proliferation and lipid homeostasis in TNBC models.....	74
Figure 3.5. Prolonged FABP5 loss does not impair proliferation, or sensitize to FA trafficking or FA inhibition, in MTB-TOM.	76
Figure 4.1. Lipolysis and lipolytic signaling are activated in breast tumor-adjacent adipocytes from breast cancer patients and mouse models of breast cancer.....	113
Figure 4.2. Breast cancer cells form functional gap junctions and express Cx31.....	115
Figure 4.3. Breast cancer cell-adipocyte gap junctions form, transfer cAMP, and activate lipolytic signaling in a Cx31-dependent manner.	117
Figure 4.4. Cx31 loss impairs breast cancer cell growth in vitro, tumorigenesis, and activation of lipolysis in adjacent adipocytes in vivo.	119

List of Tables

Table 2.1. In vivo transgenic models of MYC-driven cancer (excluding hydrodynamic models).	47
Table S4.2. Sample specifications and study sources for applied clinical samples and datasets.....	127

List of Supplemental Figures

Figure S4.1. NAT lipid content by receptor status and tumor grade, and adipocyte area quantification.....	121
Figure S4.2. Fraction of cells expressing gap junction family by tumor compartment cell type.	122
Figure S4.3. Quantification of lipolysis signaling in primary mammary adipose tissue from indicated cancer cell co-cultures and controls.....	124
Figure S4.4. Flow cytometry gating strategy to identify mCherry-positive, Calcein AM-positive cells.	126

Chapter 1: Introduction

Graphical Abstract

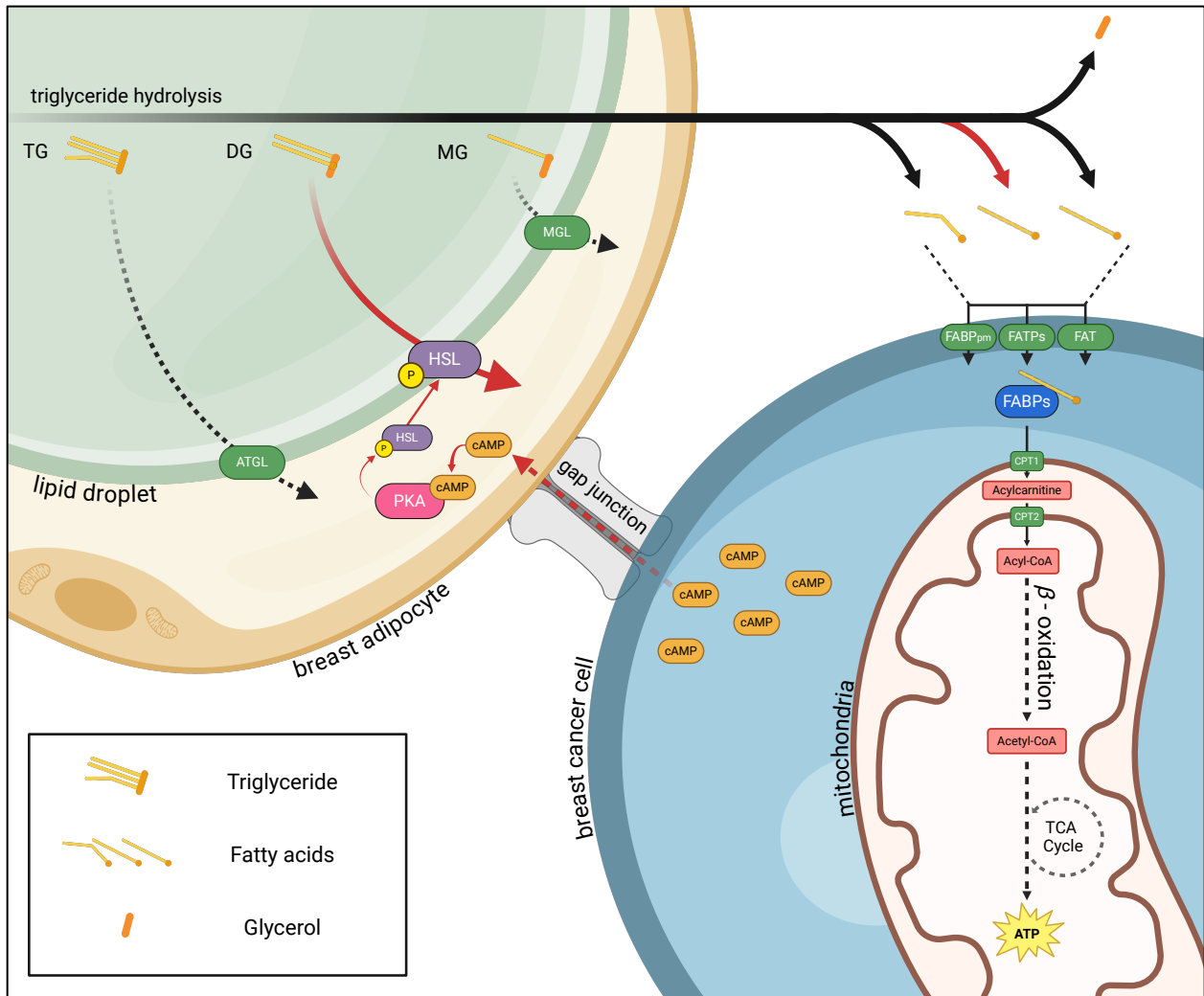


Figure 1.1. Graphical Abstract: Alterations to lipid metabolism in breast cancers and surrounding adipocytes. Figure caption continued on the next page.

Figure caption continued from the previous page. (A) Adipocyte-breast cancer cell gap junctions transduce lipolytic signaling. Gap junction (gray) passively transporting cyclic AMP (cAMP, orange) from breast cancer cell (right) to adjacent adipocyte (left). cAMP, a critical pro-lipolytic signaling molecule, activates key enzyme phospho-kinase A (PKA, pink) to phosphorylate hormone sensitive lipase (HSL, purple). Phospho-HSL translocates to the lipid droplet surface, where it activates the rate-limiting step in triglyceride hydrolysis. An adipocyte undergoes lipolysis, or release of fat: triglyceride hydrolysis in the lipid droplet liberates three fatty acids (FA) and glycerol from stored triglyceride. (B) Altered fatty acid trafficking drives fatty acid oxidation in TNBC. FA are imported into breast cancer cell via transport proteins including specialized plasma membrane fatty acid binding proteins (FABPpm), fatty acid transport proteins (FATPs) and fatty acid translocase (FAT, or CD36). Fatty acid binding proteins (FABPs), some of which are specifically elevated in TNBC, traffic FA to cellular compartments including the mitochondrial membrane. FA are processed by carnitine palmitoyltransferase I (CPT1) to enter the intermembrane space as acylcarnitines, before CPT2 converts them to acyl-CoA for deposit into the mitochondrial matrix. In mitochondrial fatty acid oxidation, acyl-CoAs undergo beta-oxidation and are broken down into acetyl-CoA, which feeds the citric acid cycle (TCA Cycle), producing ATP [1].

Clinical Impact

To grasp the clinical need for targeted therapies in TNBC, it is essential to address breast cancer's prevalence, the historical development of targeted therapies, and the current clinical standard of care. Prognosis for breast cancer patients has improved steadily over the last 50 years, yet as groundbreaking advancements in decoding hereditary risk factors [2] have bolstered conventional screening methodologies [3], the rate of new breast cancer diagnoses has increased over the same period [4]. The majority (80-85%) of new breast cancer patients report no family history of breast cancer or known genetic predictor [5]. Current standard of care for primary breast cancer treatment emphasizes a multidisciplinary approach, typically with some combination of surgery (mastectomy or lumpectomy), radiation therapy, chemotherapy (most commonly anthracyclines, cyclophosphamide, taxanes), and hormone therapy (see below), tailored to specific subtype, cancer stage and other patient characteristics [3]. But despite this raft of therapeutic tools, breast cancer is still the second leading cause of cancer-related death for women worldwide, with an estimated 2.3 million new cases and 670,000 deaths in 2022 alone [6,7].

Breast cancers can be classified into many subtypes, some based on expression of three surface receptors that both drive cell growth and facilitate targeted therapies: hormone receptor-positive cancers express estrogen (ER) and/or progesterone receptors (PR), allowing treatments that target these receptors (tamoxifen); HER2-positive cancers overexpress the human epidermal growth factor receptor 2 (HER2) protein, and are candidates for HER2-targeted therapies (commonly trastuzumab). These hormonal and HER2-targeted therapies are seminal developments in targeted therapeutics and in breast cancer treatment. As described above,

TNBC, which comprise 10-20% of all breast cancers [8], lack expression of ER, PR, and HER2 surface receptors, resulting in limited treatment options and a more aggressive clinical course.

Current standard of care for TNBC primarily involves systemic chemotherapies, including agents like doxorubicin, cyclophosphamide, paclitaxel, and approved immunotherapies. Doxorubicin, first found to be an effective chemotherapy in metastatic breast cancer in 1974 [9], is an anthracycline which intercalates DNA and generates free radicals that damage cellular components. Cyclophosphamide, an alkylating agent which crosslinks DNA to inhibit replication and transcription, would become part of the ‘gold standard’ two decades later in combination with doxorubicin [10]. Paclitaxel, a taxane which stabilizes microtubules preventing cell division, was approved by the FDA as a metastatic breast cancer therapy in 1994 and is often combined with these other agents [11,12]. Recent advances include the development of several PARP inhibitors [13-17] targeting TNBC with BRCA mutations (a majority) by disrupting dysregulated DNA repair to inhibit cell replication [3].

Immunotherapy has also emerged as a promising approach in TNBC treatment [3,18]. Antibodies that target tumor immune evasion by inhibiting the PD-1/PD-L1 immune checkpoint response have undergone extensive clinical trials. There is FDA approval of anti-PD-1 antibody pembrolizumab for treatment of high-risk early-stage TNBC [19,20], and clinical trials have shown mixed success targeting PD-L1 with atezolizumab for metastatic TNBC [21-23]. Recent work from our laboratory shows promise in preventing TNBC recurrence by using combinatorial immunotherapies to target immune evasion driven by overexpression of MYC [24]. These developments have significantly improved TNBC prognosis, but a greater understanding of the molecular and metabolic features that support its aggressive growth phenotype can address a lingering clinical need for targeted therapies.

Introduction

Altered metabolism is a hallmark of cancer, and is observed in all cancers compared to their tissue of origin [25]. Since alterations to cancer metabolism were first noted by Otto Warburg in 1956 [26], therapies targeting metabolic dependencies such as glycolysis in tumors have been of interest [27], however challenges remain in delineating pathways that selectively control cancer cell growth without impacting healthy tissues [28,29]. To characterize the molecular features that enable altered metabolism in cancer, we must understand the oncogenic drivers that regulate metabolic adaptation during cellular transformation [30]. In the Goga laboratory, most studies focus on c-MYC (MYC), a potent proto-oncogene and transcription factor that is aberrantly expressed in a majority (70%) of human cancers [31]. MYC is pleiotropic and constitutively expressed in tumor cells, and dynamically regulates a breadth of cellular functions during transformation, including metabolism. In many tissues MYC upregulation alone is sufficient to drive tumorigenesis [32], but unfortunately no direct inhibitor of MYC is available for clinical use. MYC has been demonstrated to influence multiple metabolic pathways [33-35], as discussed in *Chapter 2*, and regulation of programs including glycolysis [36,37] and glutaminolysis [38] has been studied, but less well understood is its role in fatty acid metabolism (FAM), a central focus of this dissertation.

Changes to FAM have been observed across cancers, including in the breast [39]. The breast tumor microenvironment provides a unique setting in which to study altered FAM in carcinogenesis and tumor progression, as it is predominately adipose in composition. Breast and other cancers have previously been shown to support production of cell membranes and lipid signaling precursors for tumor growth by upregulating fatty acid synthesis (FAS) [40-42]. However, in one particularly aggressive subtype of breast cancer, termed receptor ‘triple-

negative' (TNBC), recent evidence suggests that both primary [43] and metastatic [44] tumors rely on an alternative pathway, mitochondrial fatty acid oxidation (FAO). TN breast cancers (TNBC) are termed for distinct lack of surface receptor expression targeted in other, 'receptor-positive' (RP) breast tumors (see *Clinical Impact*, above). Unlike most RP tumor cells, the majority of TNBC feature elevated MYC [45], and *in vivo* studies indicate that FAO is elevated in and essential for progression of MYC-driven TNBC [43]. This is perhaps an unexpected feature, as upregulation of FAS to support cell proliferation is observed across many cancers [40-42]. It has not been well-addressed in the literature what special features of TNBC permit increased FAO.

During FAO, long chain fatty acids (LCFAs) such as C16 palmitate are catabolically processed to form acetyl-CoA, a major source of fuel for bioenergetic and biosynthetic metabolism [46] (**Fig. 1.1**). In normal cells, FAO can serve as a primary source of energy particularly during nutrient deprivation, and provides an important mechanism for metabolic adaptation to available fuel. In most tumors, FAS supports functions critical to cell proliferation, and although certain cancers can utilize FA from FAS to fuel mitochondrial FAO in an energetically inefficient 'futile cycle,' [47] most cells require uptake of extracellular FA to fuel FAO [46]. Extracellular FA are imported into the cell by membrane-bound active transporters including fatty acid transport proteins (FATPs) and CD36 (FAT) [48], and bind to fatty acid binding proteins (FABPs) for trafficking to various intracellular compartments, including to the mitochondrial membrane for FAO (**Fig. 1.1**). Given evidence that elevated FAO supports rapid tumor progression in MYC-driven TNBC, this dissertation research aims to describe the distinct intracellular adaptations to FA trafficking, and intercellular interactions with the breast tumor niche, that facilitate this metabolic shift.

To address the molecular features of TNBC that permit elevated mitochondrial FAO, we first probed how TNBC cells maintain flux of FA to the mitochondria. Prior studies in our laboratory [49] examined TN and RP patient tumors and a mouse allograft model for inducible MYC-driven breast cancer [50] for changes to FA trafficking machinery. Elevated expression of fatty acid binding protein 5 (FABP5) was identified in patient TN tumors, and *in vivo* data indicated a link between MYC and higher FABP5 levels. Further studies describing contributions of FABP5 to TNBC growth and lipid homeostasis are described in *Chapter 3*. Questions remain as to how TNBC derive FA to support elevated FAO, and one possibility is that the adipose-rich tumor microenvironment in the breast plays a role in cellular shift towards FAO, rather than *de novo* FA synthesis. A mechanistic link between MYC-driven TNBC and surrounding breast adipocytes is explored in *Chapter 4*.

While these studies center on TNBC, identifying pro-tumorigenic cancer-fat interactions in the breast, a major adipose depot in the female body, may bear broader significance in elucidating links between obesity and cancer, and in revealing how cancer cell metabolism adapts not only through primary tumorigenesis but also in metastasis. Prior studies have explored the connection between adipocytes and cancer cell growth to understand mechanisms behind obesity-induced cancer development[51] in breast [52,53], ovarian [54], endometrial, prostate [55], and pancreas [56]. Many focus on altered inflammatory state in adipose tissue as a potential connection between obesity and cancer [57], but precise pathways linking obesity to cancer risk are not yet well-defined.

In multiple cancers including ovarian [58,59], gastric [19-20], roles for adipose tissue have been identified in supporting tumor metastasis to the omentum, the body's primary adipose tissue depot. Vicinity to the body's fat depots is a notably common shared feature of numerous

cancers with obesity-linked risk factors and omental tropism — primary gastric, pancreatic, endometrial, prostate, renal, and ovarian cancers, for example, are proximate to the omentum; the primary breast tumor microenvironment is predominately adipose in composition. Numerous studies have also interrogated metabolic reprogramming of adipocytes on the invasive tumor front, often termed ‘Cancer Associated Adipocytes’ (CAAs) [60]. CAAs have been found to secrete pro-tumorigenic signals such as adipokines, chemokines, cytokines and growth factors [61] in breast [62], renal, and ovarian [63,64] and other cancers, and are thought to indirectly signal tumor and microenvironment cells through mechanisms broadly described as paracrine and endocrine.

Adipocytes store excess energy in the form of triglycerides, and a fundamental cellular function that contributes to metabolic tumor reprogramming and tumor progression is lipolysis, or the liberation of free FA and glycerol from triglyceride stores (**Fig. 1.1**). Roles for adipocyte lipolysis in cancer progression have been described in various cancers such as breast [65], gastric [66]. Endocrine, paracrine and neural signals have been identified as regulators of lipolytic signaling in adipocytes [67]. Lipolytic signaling and lipolysis are relevant in linking obesity to cancer [65], and a feature of obesity is raised levels of circulatory FA. Indirect lipolytic signaling is also of interest in cancer cachexia [68-70]. Contributions of tumor cell contact to adipocyte lipolysis have not been well-defined.

Work in *Chapter 4* describes a previously unestablished mechanism by which *direct* cancer cell-adipocyte contact stimulates release of FA in the breast tumor microenvironment, and promotes breast tumorigenesis. Many prior studies elucidating the role of adjacent adipocytes in cancer progression, in contrast, have examined autocrine, paracrine and endocrine pro-tumorigenic signals, *indirect* mechanisms that are not contact-dependent. Notably, cancer cell-

adipocyte interactions have often been modeled using transwell assays where tumor cells and adipocytes are separated by a semipermeable membrane, thus excluding contributions of direct cell-cell signaling [48,58,71-75]. A major focus of this doctoral research is to delineate contributions of cancer cell-adipocyte contact to tumorigenesis, using primary patient data and tissue samples, direct *in vitro* and *ex vivo* co-cultures, and *in vivo* models of tumor progression. While this work addresses broader questions about the role of adipocyte contact in tumor progression, a clear aim is to identify metabolic vulnerabilities in TNBC.

A limitation in our ability to identify targetable metabolic dependencies in MYC-driven TNBC is an incomplete understanding of the intracellular and tumor microenvironment features that support their distinct FAM. In this dissertation work, I therefore aim to address A) the influence of MYC on cancer cell metabolism (*Chapter 2*), B) the intracellular features of TNBC that permit elevated FAO (*Chapter 3*), and C) contributions of the adipose breast tumor microenvironment to tumorigenesis in aggressive MYC-driven TNBC (*Chapter 4*). These interrelated studies tell a story of altered FAM both in and near tumor cells: changes to intracellular FA trafficking machinery, and pro-tumorigenic cancer cell signaling that alters FAM in the tumor microenvironment.

References

- 1 Created in BioRender. Williams, J.L. (2024). <https://BioRender.com/z87r007>
- 2 Hall, J. M. *et al.* Linkage of Early-Onset Familial Breast Cancer to Chromosome 17q21. *Science* **250**, 1684-1689 (1990). <https://doi.org/doi:10.1126/science.2270482>
- 3 UpToDate. *ER/PR negative, HER2-negative (triple-negative) breast cancer*, <https://www.uptodate.com/contents/er-pr-negative-her2-negative-triple-negative-breast-cancer>.
- 4 NCI Surveillance, Epidemiology, and End Results (SEER) Program. *Cancer Stat Facts: Female Breast Cancer*, <https://seer.cancer.gov/statfacts/html/breast.html> (2024).
- 5 Haber, G., Ahmed, N. U. & Pekovic, V. Family history of cancer and its association with breast cancer risk perception and repeat mammography. *Am J Public Health* **102**, 2322-2329 (2012). <https://doi.org/10.2105/ajph.2012.300786>
- 6 World Health Organization. *Fact Sheets: Breast Cancer*, <https://www.who.int/news-room/fact-sheets/detail/breast-cancer> (2022).
- 7 The American Cancer Society. *Key Statistics for Breast Cancer*, <https://www.cancer.org/cancer/types/breast-cancer/about/how-common-is-breast-cancer.html> (2024).
- 8 Perou, C. M. *et al.* Molecular portraits of human breast tumours. *Nature* **406**, 747-752 (2000). <https://doi.org/10.1038/35021093>
- 9 Cole, M. P., Todd, I. D. & Wilkinson, P. M. A preliminary trial of doxorubicin in advanced breast cancer and other malignant disease. *Br J Cancer* **29**, 114-116 (1974). <https://doi.org/10.1038/bjc.1974.47>

- 10 Fisher, B. *et al.* Two months of doxorubicin-cyclophosphamide with and without interval reinduction therapy compared with 6 months of cyclophosphamide, methotrexate, and fluorouracil in positive-node breast cancer patients with tamoxifen-nonresponsive tumors: results from the National Surgical Adjuvant Breast and Bowel Project B-15. *Journal of Clinical Oncology* **8**, 1483-1496 <https://doi.org/10.1200/JCO.1990.8.9.1483>
- 11 Nabholz, J. M. *et al.* Multicenter, randomized comparative study of two doses of paclitaxel in patients with metastatic breast cancer. *Journal of Clinical Oncology* **14**, 1858-1867 <https://doi.org/10.1200/JCO.1996.14.6.1858>
- 12 Sledge, G. W. *et al.* Past, present, and future challenges in breast cancer treatment. *J Clin Oncol* **32**, 1979-1986 (2014). <https://doi.org/10.1200/jco.2014.55.4139>
- 13 Tutt, A. *et al.* Phase II trial of the oral PARP inhibitor olaparib in BRCA-deficient advanced breast cancer. *Journal of Clinical Oncology* **27**, CRA501-CRA501 https://doi.org/10.1200/jco.2009.27.18_suppl.cra501
- 14 Fong, P. C. *et al.* Inhibition of poly(ADP-ribose) polymerase in tumors from BRCA mutation carriers. *N Engl J Med* **361**, 123-134 (2009). <https://doi.org/10.1056/NEJMoa0900212>
- 15 Tutt, A. *et al.* Oral poly(ADP-ribose) polymerase inhibitor olaparib in patients with BRCA1 or BRCA2 mutations and advanced breast cancer: a proof-of-concept trial. *Lancet* **376**, 235-244 (2010). [https://doi.org/10.1016/s0140-6736\(10\)60892-6](https://doi.org/10.1016/s0140-6736(10)60892-6)
- 16 Gelmon, K. A. *et al.* Can we define tumors that will respond to PARP inhibitors? A phase II correlative study of olaparib in advanced serous ovarian cancer and triple-negative breast cancer. *Journal of Clinical Oncology* **28**, 3002-3002 https://doi.org/10.1200/jco.2010.28.15_suppl.3002

- 17 Dent, R. A. *et al.* Safety and efficacy of the oral PARP inhibitor olaparib (AZD2281) in combination with paclitaxel for the first- or second-line treatment of patients with metastatic triple-negative breast cancer: Results from the safety cohort of a phase I/II multicenter trial. *Journal of Clinical Oncology* **28**, 1018-1018
https://doi.org/10.1200/jco.2010.28.15_suppl.1018
- 18 Li, Y. *et al.* Recent advances in therapeutic strategies for triple-negative breast cancer. *Journal of Hematology & Oncology* **15**, 121 (2022). <https://doi.org/10.1186/s13045-022-01341-0>
- 19 Schmid, P. *et al.* Pembrolizumab for Early Triple-Negative Breast Cancer. *New England Journal of Medicine* **382**, 810-821 (2020). <https://doi.org/10.1056/NEJMoa1910549>
- 20 U.S. Food and Drug Administration. *Pembrolizumab injection. United States Prescribing Information*,
https://www.accessdata.fda.gov/drugsatfda_docs/label/2020/125514s088lbl.pdf.
- 21 Schmid, P. *et al.* Atezolizumab and Nab-Paclitaxel in Advanced Triple-Negative Breast Cancer. *New England Journal of Medicine* **379**, 2108-2121 (2018).
<https://doi.org/10.1056/NEJMoa1809615>
- 22 Miles, D. *et al.* Primary results from IMpassion131, a double-blind, placebo-controlled, randomised phase III trial of first-line paclitaxel with or without atezolizumab for unresectable locally advanced/metastatic triple-negative breast cancer. *Ann Oncol* **32**, 994-1004 (2021). <https://doi.org/10.1016/j.annonc.2021.05.801>
- 23 Emens, L. A. *et al.* First-line atezolizumab plus nab-paclitaxel for unresectable, locally advanced, or metastatic triple-negative breast cancer: IMpassion130 final overall survival analysis. *Ann Oncol* **32**, 983-993 (2021). <https://doi.org/10.1016/j.annonc.2021.05.355>

- 24 Lee, J. V. *et al.* Combinatorial immunotherapies overcome MYC-driven immune evasion in triple negative breast cancer. *Nature Communications* **13**, 3671 (2022).
<https://doi.org/10.1038/s41467-022-31238-y>
- 25 Hanahan, D. The cancer wars 2 Rethinking the war on cancer. *The Lancet* **383**, 558-563 (2014). [https://doi.org/10.1016/S0140-6736\(13\)62226-6](https://doi.org/10.1016/S0140-6736(13)62226-6)
- 26 Warburg, O. On respiratory impairment in cancer cells. *Science* **124**, 269-270 (1956).
- 27 Vander Heiden, M. G. Targeting cancer metabolism: a therapeutic window opens. *Nature Reviews Drug Discovery* **10**, 671-684 (2011). <https://doi.org/10.1038/nrd3504>
- 28 Stine, Z. E., Schug, Z. T., Salvino, J. M. & Dang, C. V. Targeting cancer metabolism in the era of precision oncology. *Nature Reviews Drug Discovery* **21**, 141-162 (2022).
<https://doi.org/10.1038/s41573-021-00339-6>
- 29 Martinez-Outschoorn, U. E., Peiris-Pagés, M., Pestell, R. G., Sotgia, F. & Lisanti, M. P. Cancer metabolism: a therapeutic perspective. *Nature Reviews Clinical Oncology* **14**, 11-31 (2017). <https://doi.org/10.1038/nrclinonc.2016.60>
- 30 Levine, A. J. & Puzio-Kuter, A. M. The Control of the Metabolic Switch in Cancers by Oncogenes and Tumor Suppressor Genes. *Science* **330**, 1340-1344 (2010).
<https://doi.org/doi:10.1126/science.1193494>
- 31 Madden, S. K., de Araujo, A. D., Gerhardt, M., Fairlie, D. P. & Mason, J. M. Taking the Myc out of cancer: toward therapeutic strategies to directly inhibit c-Myc. *Molecular Cancer* **20**, 3 (2021). <https://doi.org/10.1186/s12943-020-01291-6>
- 32 Meyer, N. & Penn, L. Z. Reflecting on 25 years with MYC. *Nature Reviews Cancer* **8**, 976-990 (2008). <https://doi.org/10.1038/nrc2231>

- 33 Hu, S. *et al.* 13C-pyruvate imaging reveals alterations in glycolysis that precede c-Myc-induced tumor formation and regression. *Cell Metabolism* **14**, 131-142 (2011).
<https://doi.org/10.1016/j.cmet.2011.04.012>
- 34 Cunningham, J. T., Moreno, M. V., Lodi, A., Ronen, S. M. & Ruggero, D. Protein and nucleotide biosynthesis are coupled by a single rate-limiting enzyme, PRPS2, to drive cancer. *Cell* **157**, 1088-1103 (2014). <https://doi.org/10.1016/j.cell.2014.03.052>
- 35 Wahlström, T. & Arsenian Henriksson, M. Impact of MYC in regulation of tumor cell metabolism. *Biochimica et Biophysica Acta - Gene Regulatory Mechanisms* **1849**, 563-569 (2015). <https://doi.org/10.1016/j.bbagrm.2014.07.004>
- 36 Tateishi, K. *et al.* Myc-Driven Glycolysis Is a Therapeutic Target in Glioblastoma. *Clin Cancer Res* **22**, 4452-4465 (2016). <https://doi.org/10.1158/1078-0432.Ccr-15-2274>
- 37 Dong, Y., Tu, R., Liu, H. & Qing, G. Regulation of cancer cell metabolism: oncogenic MYC in the driver's seat. *Signal Transduction and Targeted Therapy* **5**, 124 (2020).
<https://doi.org/10.1038/s41392-020-00235-2>
- 38 Gao, P. *et al.* c-Myc suppression of miR-23a/b enhances mitochondrial glutaminase expression and glutamine metabolism. *Nature* **458**, 762-765 (2009).
<https://doi.org/10.1038/nature07823>
- 39 Koundouros, N. & Poulogiannis, G. Reprogramming of fatty acid metabolism in cancer. *British Journal of Cancer* **122**, 4-22 (2020). <https://doi.org/10.1038/s41416-019-0650-z>
- 40 Mashima, T., Seimiya, H. & Tsuruo, T. De novo fatty-acid synthesis and related pathways as molecular targets for cancer therapy. *British Journal of Cancer* **100**, 1369-1372 (2009). <https://doi.org/10.1038/sj.bjc.6605007>

- 41 Röhrig, F. & Schulze, A. The multifaceted roles of fatty acid synthesis in cancer. *Nature Reviews Cancer* **16**, 732-749 (2016). <https://doi.org/10.1038/nrc.2016.89>
- 42 Yoshii, Y., Furukawa, T., Saga, T. & Fujibayashi, Y. Acetate/acetyl-CoA metabolism associated with cancer fatty acid synthesis: Overview and application. *Cancer Letters* **356**, 211-216 (2015). <https://doi.org/10.1016/j.canlet.2014.02.019>
- 43 Camarda, R. *et al.* Inhibition of fatty acid oxidation as a therapy for MYC-overexpressing triple-negative breast cancer. *Nat Med* **22**, 427-432 (2016).
<https://doi.org/https://10.1038/nm.4055>
- 44 Park, J. H. *et al.* Fatty Acid Oxidation-Driven Src Links Mitochondrial Energy Reprogramming and Oncogenic Properties in Triple-Negative Breast Cancer. *Cell Reports* **14**, 2154-2165 (2016). <https://doi.org/10.1016/j.celrep.2016.02.004>
- 45 Horiuchi, D. *et al.* MYC pathway activation in triple-negative breast cancer is synthetic lethal with CDK inhibition. *The Journal of Experimental Medicine* **209**, 679-696 (2012).
<https://doi.org/10.1084/jem.20111512>
- 46 Bonnefont, J. P. *et al.* Carnitine palmitoyltransferases 1 and 2: Biochemical, molecular and medical aspects. *Molecular Aspects of Medicine* **25**, 495-520 (2004).
<https://doi.org/10.1016/j.mam.2004.06.004>
- 47 Melone, M. A. B. *et al.* The carnitine system and cancer metabolic plasticity. *Cell Death Dis* **9**, 228 (2018). <https://doi.org/10.1038/s41419-018-0313-7>
- 48 Balaban, S., Lee, L. S., Schreuder, M. & Hoy, A. J. Obesity and cancer progression: Is there a role of fatty acid metabolism? *BioMed Research International* **2015** (2015).
<https://doi.org/10.1155/2015/274585>

- 49 Mahieu, C. *The story of a power couple: importance of FABP5 and MYC for fatty acid oxidation in triple negative breast cancer*, University of California, San Francisco, (2015).
- 50 D'Cruz, C. M. *et al.* c-MYC induces mammary tumorigenesis by means of a preferred pathway involving spontaneous Kras2 mutations. *Nature medicine* **7**, 235-239 (2001). <https://doi.org/10.1038/84691>
- 51 Zhang, Y. *et al.* White Adipose Tissue Cells Are Recruited by Experimental Tumors and Promote Cancer Progression in Mouse Models. *Cancer Research* **69**, 5259-5266 (2009). <https://doi.org/10.1158/0008-5472.Can-08-3444>
- 52 Bray, F. *et al.* Global cancer statistics 2018: GLOBOCAN estimates of incidence and mortality worldwide for 36 cancers in 185 countries. *CA: A Cancer Journal for Clinicians* **68**, 394-424 (2018). <https://doi.org/https://doi.org/10.3322/caac.21492>
- 53 Kolb, R. *et al.* Obesity-associated NLRC4 inflammasome activation drives breast cancer progression. *Nature Communications* **7**, 13007 (2016). <https://doi.org/10.1038/ncomms13007>
- 54 Liu, Y. *et al.* Obesity Contributes to Ovarian Cancer Metastatic Success through Increased Lipogenesis, Enhanced Vascularity, and Decreased Infiltration of M1 Macrophages. *Cancer Research* **75**, 5046-5057 (2015). <https://doi.org/10.1158/0008-5472.Can-15-0706>
- 55 Laurent, V. *et al.* Periprostatic adipocytes act as a driving force for prostate cancer progression in obesity. *Nature Communications* **7**, 10230 (2016). <https://doi.org/10.1038/ncomms10230>

- 56 Incio, J. *et al.* Obesity-Induced Inflammation and Desmoplasia Promote Pancreatic Cancer Progression and Resistance to Chemotherapy. *Cancer Discovery* **6**, 852-869 (2016). <https://doi.org/10.1158/2159-8290.Cd-15-1177>
- 57 Deng, T., Lyon, C. J., Bergin, S., Caligiuri, M. A. & Hsueh, W. A. Obesity, Inflammation, and Cancer. *Annu Rev Pathol* **11**, 421-449 (2016). <https://doi.org/10.1146/annurev-pathol-012615-044359>
- 58 Nieman, K. M. *et al.* Adipocytes promote ovarian cancer metastasis and provide energy for rapid tumor growth. *Nat Med* **17**, 1498-1503 (2011).
- 59 Ladanyi, A. *et al.* Adipocyte-induced CD36 expression drives ovarian cancer progression and metastasis. *Oncogene* **37**, 2285-2301 (2018). <https://doi.org/10.1038/s41388-017-0093-z>
- 60 Dirat, B. *et al.* in *Adipose Tissue Development: From Animal Models to Clinical Conditions* 3rd ESPE Advanced Seminar in Developmental Endocrinology, Paris, March 2009 Vol. 19 (eds C. Levy-Marchal & L. Pénicaud) 0 (S.Karger AG, 2010).
- 61 Wu, Q. *et al.* Cancer-associated adipocytes: key players in breast cancer progression. *Journal of Hematology & Oncology* **12**, 95 (2019). <https://doi.org/10.1186/s13045-019-0778-6>
- 62 He, J.-Y. *et al.* Adipocyte-derived IL-6 and leptin promote breast Cancer metastasis via upregulation of Lysyl Hydroxylase-2 expression. *Cell Communication and Signaling* **16**, 100 (2018). <https://doi.org/10.1186/s12964-018-0309-z>
- 63 John, B. *et al.* Regulation of the bi-directional cross-talk between ovarian cancer cells and adipocytes by SPARC. *Oncogene* **38**, 4366-4383 (2019). <https://doi.org/10.1038/s41388-019-0728-3>

- 64 Iyoshi, S. *et al.* Pro-tumoral behavior of omental adipocyte-derived fibroblasts in tumor microenvironment at the metastatic site of ovarian cancer. *Int J Cancer* **149**, 1961-1972 (2021). <https://doi.org/10.1002/ijc.33770>
- 65 Balaban, S. *et al.* Adipocyte lipolysis links obesity to breast cancer growth: adipocyte-derived fatty acids drive breast cancer cell proliferation and migration. *Cancer & Metabolism* **5**, 1 (2017). <https://doi.org/10.1186/s40170-016-0163-7>
- 66 Kawabata, K. *et al.* Lipolysis-stimulated lipoprotein receptor promote lipid uptake and fatty acid oxidation in gastric cancer. *Gastric Cancer* **27**, 1258-1272 (2024). <https://doi.org/10.1007/s10120-024-01552-z>
- 67 Arner, P. & Langin, D. Lipolysis in lipid turnover, cancer cachexia, and obesity-induced insulin resistance. *Trends in Endocrinology & Metabolism* **25**, 255-262 (2014). <https://doi.org/https://doi.org/10.1016/j.tem.2014.03.002>
- 68 Agustsson, T. *et al.* Mechanism of Increased Lipolysis in Cancer Cachexia. *Cancer Research* **67**, 5531-5537 (2007). <https://doi.org/10.1158/0008-5472.Can-06-4585>
- 69 Cao, D.-x. *et al.* Role of β 1-adrenoceptor in increased lipolysis in cancer cachexia. *Cancer Science* **101**, 1639-1645 (2010). <https://doi.org/https://doi.org/10.1111/j.1349-7006.2010.01582.x>
- 70 Rydén, M. *et al.* Lipolysis—Not inflammation, cell death, or lipogenesis—Is involved in adipose tissue loss in cancer cachexia. *Cancer* **113**, 1695-1704 (2008). <https://doi.org/https://doi.org/10.1002/cncr.23802>
- 71 Wang, Y. Y. *et al.* Mammary adipocytes stimulate breast cancer invasion through metabolic remodeling of tumor cells Mammary adipocytes stimulate breast cancer

- invasion through metabolic remodeling of tumor cells. **2** (2017).
<https://doi.org/10.1172/jci.insight.87489>
- 72 Wen, Y. A. *et al.* Adipocytes activate mitochondrial fatty acid oxidation and autophagy to promote tumor growth in colon cancer. *Cell Death Dis* **8**, e2593 (2017).
<https://doi.org/10.1038/cddis.2017.21>
- 73 Muller, C. Tumour-surrounding adipocytes are active players in breast cancer progression. *Annales d'Endocrinologie* **74**, 108-110 (2013).
<https://doi.org/10.1016/j.ando.2013.02.007>
- 74 Dirat, B. *et al.* Cancer-associated adipocytes exhibit an activated phenotype and contribute to breast cancer invasion. *Cancer Research* **71**, 2455-2465 (2011).
<https://doi.org/10.1158/0008-5472.CAN-10-3323>
- 75 Dirat, B. A., Bochet, L., Escourrou, G., Valet, P. & Muller, C. Unraveling the obesity and breast cancer links: a role for cancer-associated adipocytes? *Endocr Dev* **19**, 45-52 (2010). <https://doi.org/10.1159/000316896>

Chapter 2: Multiple roles for Myc in altering cancer metabolism

A version of this chapter was previously published as:

Camarda, R., Williams, J., and Goga, A. (2017). In vivo Reprogramming of Cancer Metabolism by MYC. Frontiers in Cell and Developmental Biology. **5**: 1-13.

Abstract

The past few decades have welcomed tremendous advancements toward understanding the functional significance of altered metabolism during tumorigenesis. However, many conclusions drawn from studies of cancer cells in a dish (i.e., in vitro) have been put into question as multiple lines of evidence have demonstrated that the metabolism of cells can differ significantly from that of primary tumors (in vivo). This realization, along with the need to identify tissue-specific vulnerabilities of driver oncogenes, has led to an increased focus on oncogene-dependent metabolic programming in vivo. The oncogene c-MYC (MYC) is overexpressed in a wide variety of human cancers, and while its ability to alter cellular metabolism is well-established, translating the metabolic requirements, and vulnerabilities of MYC-driven cancers to the clinic has been hindered by disparate findings from in vitro and in vivo models. This review will provide an overview of the in vivo strategies, mechanisms, and conclusions generated thus far by studying MYC's regulation of metabolism in various cancer models.

Introduction

Cancer is a disease of uncontrolled growth, and proliferating cells change their metabolic demands compared to quiescent cells [1,2]. Tumor cells can outcompete normal cells, regardless of the proliferative capacity of the tissue of origin. Dysregulated metabolism is a hallmark of tumorigenesis [3], and such altered metabolism permits tumor cells to survive and proliferate despite adverse conditions.

Historical studies of altered metabolism in cancer pointed to increased glycolysis, and later glutaminolysis, as defining characteristic of tumor cells. Significant progress has been made studying glycolysis and glutaminolysis, and therapeutic targeting of these pathways is actively being pursued in the clinic [4,5]. However, it has become increasingly apparent that while glycolysis and glutaminolysis certainly play major roles in some tumors [4,5], alternative sources of “fuel” can be just as, if not more, important[6]. Notably, targeting of alternative metabolic pathways, for example lipid biosynthesis, is currently in clinical trials against a variety of tumor types, and cannot be undervalued [7].

A critical link between understanding cancer metabolism and targeting it therapeutically is identifying the upstream effectors that reshape tumor metabolism. The proto-oncogene MYC is a pleiotropic transcription factor and is one of the most commonly amplified or overexpressed genes in human cancers [8]. While MYC expression is dysregulated in a wide variety of cancers, its oncogenic role has most thoroughly been studied *in vivo* in the context of transgenic models of aggressive breast, liver, lung, prostate, and kidney cancers, as well as neuroblastoma and lymphoma (see references below; **Fig. 1.1** and **Table 1.1**). For example, we and others have demonstrated that MYC expression is elevated in the estrogen, progesterone and human epidermal growth factor receptor- 2 (HER2), receptor triple-negative subtype of breast cancer (TNBC) [9,10]. Additionally, MYC translocation to the IgG locus plays a causal role in Burkitt’s Lymphoma [8,11]. As a transcription factor, MYC’s primary mode of transformation is through the pro-tumorigenic transcriptional dysregulation of a wide variety of processes including proliferation, cell size, apoptosis, and metabolism [8]. Regulation of MYC’s transcriptional activity [12], and the role of MYC’s transcriptional binding partners in the regulation of metabolism [13] have been studied and reviewed, and will not be discussed here. It is also

important to note that given the broadly important role of MYC in cancer, a direct MYC inhibitor could be of great clinical utility. However, such an inhibitor has yet to be created, and the strategy of targeting MYC directly remains challenging [14,15]. Thus, alternative strategies of targeting MYC-driven cancers via selective inhibition of cellular pathways, like metabolism, that may selectively kill MYC-overexpressing cells have attractive therapeutic potential. Indeed, the concept of specifically targeting metabolism to induce synthetic lethality in a MYC-dependent manner was pioneered by Shim et al. (1997) [16], and expanded upon by many others [17,18].

The ability of MYC to dynamically regulate cellular metabolism in cancer is well-established [19,20]. However, it is important to note that many studies describing MYC's ability to reprogram tumor cell metabolism have been conducted *in vitro*, primarily using inducible/repressible transgenic and human cancer cell line models [19,20]. While the importance and utility of *in vitro* cell culture models is undeniable, results from these models must be considered with caution when studying a process such as metabolism that is dependent on tumor cell environment [21]. Further, the dynamic nature of metabolic stressors and plasticity *in vivo* is difficult to model *in vitro*, particularly en masse. Primary tumors develop to form a complex tissue that is exposed to varying levels of oxygenation, and fluctuating concentrations of glucose, glutamine, amino acids and countless other metabolites that cannot be readily modeled in tissue culture [21]. Recent studies have also revealed an intimate connection between circadian rhythms and tissue-specific metabolism that has yet to be fully considered in the context of cancer metabolism [22]. This last point is particularly prescient given the recent demonstration by Altman et al. that MYC itself can dysregulate circadian gene expression and metabolism [23], however, these findings have yet to be validated *in vivo*.

The disparate nature of *in vitro* and *in vivo* metabolism is exemplified by a recent study that took advantage of two transgenic mouse models of KRAS-driven non-small cell lung cancer (NSCLC) [24]. Davidson et al. [24] found that both models displayed increased utilization of glucose-derived carbon to fuel the tricarboxylic acid (TCA) cycle compared to normal lung *in vivo*, while neither tumor nor non-tumor utilized glutamine-derived carbon for the TCA cycle to a large extent. This is in stark contrast to a cell line derived from one of the transgenic models, which *in vitro* decreases its utilization of glucose for the TCA cycle and increases its utilization of glutamine to that end [24]. Thus, glutamine oxidation in this model system appears to be an artifact of the *in vitro* culture methods and is not observed *in vivo*. Such results thus raise doubt about the utility of targeting the glutamine pathway as a therapeutic target for primary KRAS-driven lung tumors.

Given the dynamic nature of MYC's function in diverse cellular contexts, and the potential for cell culture to confound our understanding of tumor metabolism, the goal of this review is to focus on the regulation of cancer metabolism by MYC *in vivo*. To clarify, our definition of *in vivo* refers to studies of metabolism with findings based on *de novo* MYC-driven tumorigenesis, usually in the form of transgenic mouse models. While we acknowledge that many findings from *in vitro* studies of MYC-driven cancer metabolism hold true *in vivo* [19,20], we will discuss here the various models used to study the regulation of cancer metabolism by MYC *in vivo* (summarized in **Table 2.1**), and provide broader context on some of the questions that remain to be answered.

Main Text

Use of Transgenic Mouse Models and Consideration of Tissue-Specific Effects

The study of cancer metabolism *in vivo* is of course limited by the methods and unique challenges and considerations that the metabolism of complex tissues warrants[21]. One particularly important consideration is the difference between “snap-shot” strategies of studying metabolism vs. kinetic flux analyses, and how the use of chemically labeled metabolites factors into both approaches. The most common snap-shot method for studying metabolism is mass spectrometry-based metabolomics, which can be “targeted” for known metabolites or “untargeted” for unbiased detection of all metabolites present within a particular sample, and does not require any labeled metabolite [25]. A second snap-shot strategy is ¹³C tracer analysis, in which a ¹³C-labeled metabolite is infused or fed to the subject, and mass spectrometry is used to identify downstream metabolite labeling patterns [26]. The use of ¹³C-labeled metabolites shifts from a snap-shot tracing study to a formal kinetic flux analysis when a much more complex series of considerations (metabolite uptake and secretion, as well as the kinetics of the biochemical reaction network to be probed) are taken into account [26]. A common approach to achieve flux analysis is with constant infusion of an isotopically labeled tracer, ¹³C-glucose for example, that will achieve isotopic steady state as ¹³C enrichment becomes stable over time [26]. Understanding the differences between these methods, and the conclusions that can be drawn from them, is vital. In particular, snap-shot metabolomics is often used to prematurely draw conclusions about the activity of a metabolic pathway, when the elevation or decrease of a particular metabolite does not necessarily reflect activation or inhibition of an entire pathway [25,26]. Moreover, interpretation and validation of metabolic data is critical, as for example, accumulation of a particular metabolite could have multiple potential interpretations (i.e., increased activity of an upstream anabolic pathway or decreased activity of a downstream

catabolic pathway). An important caveat to the study of *in vivo* metabolism is that tumor tissue is often analyzed at a bulk level, and as the work of Aran et al. [27] and many others has demonstrated, the composition of solid tumors includes a number of different cell types [27] whose metabolism is rarely accounted for in such bulk analyses.

With a cadre of strategies in hand, the study of cancer metabolism *in vivo* then becomes a function of the models or the clinical samples available for analysis. In this section, we will address some of the most thoroughly used models to study the metabolism of MYC-driven cancer (**Table 2.1**). The overall message is that while MYC-driven metabolism during tumorigenesis is quite tissue-specific, some shared pathways also emerge (**Fig. 2.1**).

MYC Dysregulates Glucose and Glutamine Metabolism

In hepatocellular carcinoma (HCC), MYC is found to be frequently amplified and/or overexpressed, and is associated with poorly differentiated tumors and poor prognosis [28-31]. In addition, MYC expression is commonly found to be upregulated in hepatoblastoma (HB), a liver tumor type that predominates in pediatric patients [32].

To study MYC-dependent metabolism in HCC, we and others have utilized the MYC-driven LAP-tTA/TRE-MYC (LT2-MYC) transgenic mouse model of liver cancer initially developed in the lab of J.M. Bishop, which allows for MYC overexpression specifically in hepatocytes in the absence of doxycycline [30]. Importantly, mRNA expression analysis reveals that LT2-MYC tumors effectively model poorly differentiated, aggressive liver cancer [33]. Using this model, we probed for changes in glycolytic metabolism using hyperpolarized ¹³C-pyruvate magnetic resonance spectroscopic imaging (MRSI) during *de novo* tumorigenesis and inducible tumor regression. More specifically, hyperpolarized ¹³C-pyruvate MRSI allows for *in*

in vivo flux analysis of pyruvate to lactate and/or alanine conversion. With this modality, we found that MYC induction led to increased pyruvate to alanine conversion in the liver that preceded overt tumor formation, while full-blown tumors displayed increased pyruvate to lactate conversion. Both of these phenotypes were reversed during tumor regression. Mechanistically, mRNA expression analysis revealed coordinate changes in the levels of TCA cycle and glycolytic enzymes that supported the observed metabolic changes. In particular, there was a specific elevation of glutamate pyruvate transaminase 1, which converts pyruvate to alanine, in pre-tumorigenic liver, while lactate dehydrogenase A (LDHA), which converts pyruvate to lactate, was specifically upregulated in tumors [34]. Studies such as this indicate that imaging of downstream glycolysis pathway events can identify the earliest stages of tumor formation and regression and that these metabolic changes are indeed MYC dependent.

The notion that MYC drives increased glycolysis in liver cancer was further bolstered by a parallel study of MYC- driven metabolism using the same LT2-MYC model. Yuneva et al. utilized a combination of steady-state profiling techniques including nuclear magnetic resonance spectroscopy with or without ¹³C-glucose and ¹³C-glutamine labeling, as well as ¹⁸F-fluorodeoxyglucose positron emission tomography and mass spectrometry [35]. The authors found that MYC-driven liver tumors displayed increased glucose uptake and catabolism to lactate and TCA cycle intermediates, as well as increased glutamine catabolism to support the TCA cycle. These findings were supported by increased expression of LDHA, hexokinase 2 (Hk2), and glutaminase 1 (Gls1), and decreased expression of glutamine synthetase (Glul). The importance of glutamine catabolism in MYC-driven HCC was further demonstrated by Xiang et al. who demonstrated that genetic ablation of one copy of Gls1 or treatment with two different inhibitors of Gls1 could significantly prolong survival in this same model [36]. This was in direct

contrast to glucose and glutamine utilization in transgenic MYC-driven lung tumors [37,38]. Unlike MYC-driven liver tumors, MYC-driven lung tumors displayed elevated lactate and glutamine levels, which was suggestive of increased glucose catabolism, but not glutamine catabolism. MYC-driven lung tumors displayed increased LDHA, Hk2, Gls1 as well as Glul. Likewise, a similar model of transgenic MYC-driven lung cancer displayed increased LDHA and Hk2, as well as enzymes from several other metabolic pathways, at the mRNA level [39].

Although MYC pathway activation is elevated in the majority of renal cell carcinoma (RCC) cases, a formal study of MYC's role in the pathogenesis and the metabolism of RCC had been lacking. To study MYC in RCC, Shroff et al. created an inducible transgenic model of renal cell carcinoma (GGT-tTA/TRE-MYC) in which MYC is specifically overexpressed in the kidney in the absence of doxycycline [40]. Using desorption electrospray ionization mass spectrometry imaging (DESI-MSI), the authors studied the metabolic profiles of non-tumor kidney, MYC-driven kidney tumors at 2 and 4 weeks post-MYC induction, and regressed tumors after 4 weeks of switching MYC off. The authors noted multiple metabolic changes, including in the relative abundance of a variety of long-chain fatty acids in tumors compared to non-tumor kidneys and regressed tumors. Shroff and colleagues focused on glutamine metabolism after mRNA expression analysis revealed a downregulation in many glycolytic genes, but an upregulation in genes associated with glutaminolysis. The authors confirmed that glutamate and TCA cycle intermediates were elevated in tumors using DESI-MSI, and found that their transgenic tumors, as well as MYC^{high} human RCC, stained positively for Gls1 and Gls2, suggesting an elevation in glutaminolysis. Decreased staining of the transgenic tumors for Hk1 and LDHA further supported diminished glycolysis. Finally, the authors found that pharmacological inhibition of Gls1 with bis-2-(5-phenylacetamido-1,2,4-thiadiazol-2-yl) ethyl

sulfide (BPTES) abrogated the growth of MYC-driven kidney tumors [40], implicating glutamine utilization as critical for MYC-driven RCCs, similar to what was found in MYC-driven HCC [36].

Additional evidence that MYC dysregulates glutamine metabolism was provided by a recent study that found elevation of the glutamine synthetase (Glu) enzyme and glutamine abundance in a transgenic mouse model of dual MYC and KRAS-driven pancreatic cancer, compared to tumors driven by KRAS alone [41]. These studies suggested Glu is induced by MYC. Further support that MYC dysregulates glucose metabolism was provided when mass spectrometry- based metabolomic analysis was used to compare the metabolic profiles of established transgenic mouse models of MYC- or AKT-driven prostate cancer [42,43], as well as human prostate cancer samples that had been profiled for activated phospho-AKT and MYC levels. The authors found coordinately decreases in glucose- related metabolites and downregulation of HK2 and the glucose transporter GLUT-1 in mouse and human prostate tumors that were MYC^{high}, compared to control tissue and AKT^{high} tumors. In addition, the authors found specific dysregulation of several long-chain fatty acids in MYC^{high} tumors, but the functional significance of these changes was not addressed[44].

In summary, the ability of MYC to alter glucose and glutamine metabolism in cancer is clear. However, the studies of MYC- driven liver, lung, kidney, pancreatic, and prostate cancers studied above highlight the fact that MYC can up- or down- regulate either or both of these pathways depending on tissue context. Furthermore, Shroff et al. were the only group to formally demonstrate that dysregulation of one of these pathways leads to a reliance upon it that may have therapeutic potential [40]. Further, studies in the remaining cancer types discussed above will be necessary to determine if targeting glucose or glutamine metabolism will have therapeutic utility.

Myc Regulates Downstream Glutamine Utilization

Although the LT2-MYC model had multiple changes in glucose and glutamine metabolism [18,34], other metabolic pathways had not been fully explored. Using the conditional MYC-driven liver cancer model we conducted global mRNA expression and mass spectrometry-based metabolomic analyses on LT2-MYC tumors vs. control uninduced transgenic livers [28]. Using an integrated bioinformatics approach, we probed for metabolic pathways coordinately dysregulated in both transcript and metabolite levels. Of the six pathways identified: glutathione metabolism; glycine, serine, and threonine metabolism; aminoacyl-tRNA biosynthesis; cysteine and methionine metabolism; ABC transporters; and mineral absorption, we focused on glutathione metabolism [28]. We found a marked decrease in the reduced and oxidized form of glutathione, as well as the enzyme responsible for *de novo* glutathione biosynthesis, glutamate-cysteine ligase, catalytic subunit (GCLC). Because glutathione is synthesized downstream of glutamine conversion to glutamate, we performed mass spectrometry-based tracing analysis with ¹³C-glutamine in a somatic transgenic model of MYC-driven liver cancer [45]. We found that glutamine-derived carbons preferentially fueled the TCA cycle vs. glutathione production in MYC-driven liver tumors compared to control liver tissue. Mechanistically, we found that GCLC expression was downregulated by miR-18a in a MYC-dependent manner. Treatment of LT2-MYC tumor-bearing mice with a locked-nucleic acid antagonist of miR-18a significantly rescued GCLC expression and glutathione levels *in vivo*. In addition, miR-18a was significantly elevated in human HCC compared to non-tumor liver, was negatively correlated with GCLC expression in human HCC, and was positively correlated with alpha-fetoprotein (AFP) expression, which is associated with aggressive liver cancer. Finally, we found that LT2-MYC tumors displayed increased sensitivity to an oxidative stress inducer, diquat, compared to non-tumor liver. In particular, diquat-treated tumors displayed a specific and significant increase in

cell loss, TUNEL staining as a marker of apoptosis, and decreased MYC expression [28]. Notably, it had been previously demonstrated *in vitro* that MYC-dependent suppression of miR-23a/b results in increased Gls1 and glutaminolysis activity[46,47]. Thus, MYC can alter the expression of specific miRNAs (i.e., miR18a and miR23a) which in turn regulate glutamine metabolism. MYC-dependent regulation of miRNAs may be a common mechanism through which MYC reprograms tumor metabolism (**Fig. 2.1**) and deserves broader consideration beyond HCC.

In neuroblastoma, the MYC-related transcription factor MYCN is found to be amplified in ~20% of neuroblastomas, and its amplification is associated with poor prognosis [48]. To study the role of MYCN in neuroblastoma metabolism, Carter et al. [48] utilized the TH-MYCN transgenic model of MYCN- driven neuroblastoma in which MYCN is overexpressed in cells of the neural crest [49]. Using mass spectrometry-based metabolomics, the authors performed global metabolic profiling of MYCN-driven neuroblastoma at multiple time-points representing hyperplastic ganglia, early tumors, and advanced tumors. Grouping the metabolomic data into pathway analysis, it was found that glutathione metabolism was the most significantly dysregulated pathway, with all metabolites associated with glutathione biosynthesis elevated in MYCN- driven tumors compared to control ganglia. Interestingly, the majority of enzymes associated with glutathione biosynthesis, including GCLC, were found to be downregulated at the mRNA level. Therefore, the authors speculated that increased protein biosynthesis, which was evidenced by a significant increase in the expression of ribosome biogenesis genes, was responsible for the observed increase in glutathione, although this contention was not formally tested. Regardless, the increase in glutathione led the authors to hypothesize that MYCN-driven neuroblastoma could have an increased dependence upon glutathione metabolism. Indeed, the

authors found that BSO, an inhibitor of GCLC, could reduce sympathetic ganglia hyperplasia and delay tumor onset when given prophylactically. In addition, GCLC inhibitors did not have an effect on the growth of established tumors when given alone, but did have a significant benefit when given with the clinically relevant chemotherapeutic agent vincristine, compared to BSO alone or vincristine alone [48]. Thus, in both MYC driven liver and neuroblastoma models GCLC expression is suppressed, though the effects on glutathione production appear to be contextually dependent. We postulate that in the setting of low GCLC expression, and consequently low GSH production that some MYC-driven tumors, such as liver cancers, may be especially sensitive to exogenous oxidative stress [28].

Terunuma et al. conducted mass spectrometry-based metabolomics on primary breast cancer samples and adjacent non-tumor tissue [50]. The authors found a number of differences in metabolite abundance between tumor and non-tumor samples, and probed further into the differences between ER-positive and ER-negative tumors as well as tumors from individuals with African ancestry vs. European ancestry. The authors chose to focus on 2-hydroxyglutarate (2-HG), a known “oncometabolite,” which was found to be preferentially elevated in ER-negative tumors. Interestingly, 2-HG accumulation normally occurs in the context of isocitrate dehydrogenase (IDH) 1 or 2 mutation, but the authors did not find evidence of IDH mutation in breast cancer. It was recently demonstrated that 2-HG can be produced via LDHA in the context of hypoxia [51,52], but Terunuma et al. did not address whether hypoxia could explain 2-HG production in the breast tumors analyzed [50]. However, they did find a strong correlation between 2-HG levels, MYC pathway activity, glutaminolysis-associated metabolites, and Gls1 expression. Further, the authors provided *in vitro* evidence that 2-HG production occurs during glutamine catabolism, and that MYC is both necessary and sufficient for elevated 2-HG levels

[50] in breast cell lines. These data suggest that MYC, albeit via a yet unclear mechanism, is able to promote glutamine utilization for 2-HG production in cancer. It is of course tempting to speculate that MYC-dependent regulation of LDHA, as discussed above, may contribute to the 2-HG production observed, but this remains to be determined.

In summary, MYC's regulation of glutamine metabolism is extensive. In the case of glutathione, relative decreases [28] and increases [48] were observed depending on the cancer type. With a decrease, tumors were found to be sensitive to an inducer of oxidative stress [28], while an increase led the tumors to be sensitive to GCLC inhibition during the early phase of tumor formation [48]. Interestingly, in neuroblastoma the elevation of glutathione occurred despite a downregulation in GCLC mRNA levels. It would be interesting to determine if the decrease in GCLC observed in neuroblastoma is miR-18a-dependent. An alternative downstream use of glutamine to generate 2-HG has also been postulated in primary breast cancers. It remains unclear how MYC activity could induce 2-HG production, thus the therapeutic utility and potential to target this pathway have not been explored [50].

Myc Dysregulates Lipid Metabolism

The role of MYC in HB metabolism has not been studied as extensively as HCC [53], but it is worth noting that a recent study performed global mRNA expression analysis in a somatic transgenic model of β -catenin/YAP-driven HB performed in mice with either MYC-wildtype (WT) or MYC-knockout (KO) hepatocytes. The authors found that MYC promoted tumor progression, but not initiation, and were able to identify several metabolic pathways with differential enzyme expression and pathway activity in MYC-WT vs. MYC-KO tumors [32]. For example, MYC-KO tumors displayed reduced expression of the fatty acid transporter CD36,

with a concomitant decrease in lipid droplet levels and fatty acid oxidation (FAO) [32]. Given these results in HB, it would be interesting to determine if MYC also dysregulated lipid metabolism in HCC. To that end, Perry et al. [54] utilized DESI- MSI to not only detect differential abundance of lipid species in non-tumor liver, early LT2-MYC tumors, late tumors, and regressed tumors, but also generate a spatial localization of the detected lipids with $\sim 200 \mu\text{m}$ resolution [54]. The authors found that a number of lipid species displayed differential abundance in tumor vs. non-tumor tissue, but did not pursue the functional significance of these changes.

The work of Perry et al. in MYC-driven liver cancer [54] later led the same lab to use DESI-MSI to study MYC-driven lymphoma. MYC is known to be broadly dysregulated in aggressive lymphomas, and in Burkitt's lymphoma the MYC gene is translocated next to the immunoglobulin heavy chain enhancer in virtually all cases [8,11]. To study MYC-driven lymphoma Eberlin et al. [11] utilized the conditional E μ -tTA/TRE-MYC transgenic mouse model in which MYC is specifically expressed in lymphocytes only in the absence of doxycycline [55]. The authors reported a number of lipids that displayed differential abundance in MYC-driven lymphoma compared to control non- tumor thymus. In addition, the authors performed DESI-MSI on 15 human lymphoma samples, including five cases of Burkitt's lymphoma, that were profiled for MYC expression such that they were classified as MYC^{high} or MYC^{low}. Interestingly, there were many similarities between the lipid profiles of the mouse MYC-driven lymphomas and the human MYC^{high} lymphomas, and both were distinct from the human MYC^{low} lymphomas [11]. In addition, some of the most differentially increased lipids in MYC-driven lymphomas were multiple cardiolipin species, which are known to play critical roles in mitochondrial membrane integrity. Thus, although Eberlin et al. [11] did not pursue the

functional significance of dysregulated lipid metabolism, these changes could support alternative aspects of MYC-driven metabolism in lymphoma. Additionally, it is interesting that Eberlin et al. acknowledge in their discussion a potential relationship between altered lipid abundance and FAO, and a separate study indeed found that inhibition of FAO was able to significantly delay tumorigenesis in a constitutive model of transgenic MYC-driven lymphoma (E μ -MYC) [56,57].

As mentioned above, we and others have demonstrated that MYC expression is disproportionately elevated in TNBC compared to receptor-positive (RP) tumors [9,10]. Thus, we were particularly interested in the use of the MYC-driven MMTV-rtTA/TRE-MYC (MTB-TOM) transgenic mouse model of breast cancer, in which MYC is overexpressed specifically in mammary epithelial cells in a doxycycline-inducible manner [58]. It is important to note that while MYC is certainly overexpressed in this model, which mimics the clinically observed increase in MYC expression in TNBC, it was also confirmed by unbiased clustering of mRNA expression analysis that the MTB-TOM model does resemble the Basal/TN subtype of breast cancer [59]. Using this model, we performed steady-state metabolomics and ¹³C-tracing analysis and found that FAO was dysregulated. We then used a ¹⁴C-oleic acid oxidation assay to confirm that FAO was elevated specifically in MYC-overexpressing TNBC. Given the elevation in FAO, a pathway known to fuel the TCA cycle and ATP production, we hypothesized this pathway could be required to fuel bioenergetic metabolism in MYC-overexpressing TNBC, and could have therapeutic potential. To address this hypothesis in a more clinically relevant model, we utilized a recently described panel of breast cancer patient-derived xenografts (PDX)[60]. Using a specific inhibitor of the FAO pathway, etomoxir, we found that inhibition of FAO decreased bioenergetic metabolism and inhibited tumorigenesis in a MYC^{high} TN PDX, but did not inhibit tumorigenesis in a MYC^{low} TN PDX model [61]. Notably, a separate study found elevated FAO

in TNBC, and described an additional downstream role for FAO in promoting autophosphorylation and activation of the oncogenic Src kinase [62]. It remains to be seen whether or not there is a functional interaction between MYC and Src in TNBC, and whether Src could be a mechanism of FAO upregulation in MYC-driven TNBC, or vice versa. In addition, as mentioned above, Terunuma et al. found elevation of acyl- carnitines, the bottleneck intermediate of FAO, in ER-negative human tumors compared to ER-positive or non-tumor tissue [50], supporting our findings of dysregulated FAO in TNBC [61].

Although several studies have now indicated that MYC is capable of dysregulating lipid metabolism, and in particular FAO, no study has yet to validate a downstream mechanism by which MYC activation dysregulates lipid metabolism and/or FAO *in vivo*. It is worth noting that several potential mechanisms have been described *in vitro*, including MYC-dependent induction of mitochondrial biogenesis [63], which has been functionally linked to FAO in the context of MYC inhibition [64]. In addition, there are several other hypotheses supported by the literature that are worth noting. First, we found a marked downregulation in acetyl- CoA carboxylase 2 (ACC2) protein expression in MYC^{high}, but not MYC^{low} PDXs, and it has been demonstrated that downregulation of ACC2 in transgenic mice is sufficient to upregulate FAO *in vivo* [65]. Second, fatty acid binding proteins (FABPs) are known to play a supporting role in fatty acid oxidation as they are responsible for trafficking fatty acids throughout the cell[66]. In ovarian cancer that metastasizes to the omentum it was demonstrated that FABP4 is upregulated in tumor cells and expressed in omental adipocytes, and is necessary in both cell types to support metastatic tumorigenesis [66]. Furthermore, FABP5 has been found to be upregulated in TNBC, and is associated with poor prognosis and recurrence-free survival in TNBC [67]. Thus, we postulate

that MYC reprograms lipid metabolism in TNBCs via coordinated suppression of fatty acid synthesis and upregulation of oxidation to support tumor metabolic demands.

Finally, we and others recently described the necessity for PIM kinase activity in MYC-overexpressing TNBC [68,69]. PIM expression can promote PGC1 α expression, a master regulator of FAO [70]. In addition, a recent study suggests that there may be functional redundancy between PIM and PI3K in breast cancer, and because PI3K is a known regulator of glycolysis, PIM may then play a role in regulation of glycolysis in MYC-overexpressing TNBC [71,72]. Further studies are necessary to determine which, if any, of these potential mechanisms are indeed at play in the regulation of FAO in MYC-overexpressing TNBC.

In summary, MYC is capable of dysregulating lipid metabolism in multiple cancer types, but a mechanism has yet to be described. Given that our work found that inhibition of FAO is a therapeutic strategy against MYC-overexpressing TNBC [61], and a separate study found similar results in a model of MYC-driven lymphoma [57], it will be interesting to determine if this strategy could be expanded to MYC-driven HB and/or HCC.

Studies Of Protein and Nucleotide Metabolism in Myc-Driven Lymphoma

In addition to studies of lipid metabolism, the E μ -MYC model has also been used for studies of protein and nucleotide metabolism. E μ -MYC lymphomas display elevated protein translation, a common feature of many cancer types [73]. Barna et al. created a bi-allelic model in which haploinsufficiency of the ribosomal protein RPL24 results in reduced protein translation back to non-tumor levels. When this model was bred to the E μ -MYC model it resulted in decreased tumorigenesis [73]. With this model, the same lab recently utilized NMR-based

metabolomic analysis to profile changes in a number of metabolic pathways in non-tumor lymphocytes, pre-tumor MYC- driven lymphocytes, lymphocytes with reduced translation, MYC-driven lymphocytes with normalized translation, and tumorigenic MYC-driven lymphocytes. Cunningham et al. [74] found that the most notable translation-dependent difference detected was a reduction in nucleotide-related metabolites, specifically inosine monophosphate and adenosine mono-, di-, and triphosphate. The authors then demonstrated that a single enzyme, phosphoribosyl-pyrophosphate synthetase 2 (PRPS2), is responsible for increased nucleotide metabolism in MYC-driven lymphoma via a cis-regulatory element in its 5' UTR that is activated by translation initiation factor eIF4E, which is itself hyperactivated in tumors. Additionally, MYC-driven lymphomagenesis is at least in part dependent upon PRPS2 as E μ -MYC crossed with PRPS2-null mice have a significant delay in tumor initiation as well as a significant increase in survival[74]. Interestingly, elevated protein synthesis in this model has also been linked to increased activation of the unfolded protein response, which ultimately promotes tumor cell survival via autophagy[75]. Thus, a combined increase in translation and autophagy may contribute to MYC-driven metabolic adaptation in lymphomas.

Regulation of Myc by Metabolism

While MYC reprograms metabolism, there is also mounting evidence of metabolic regulation of MYC in cancer and tissue homeostasis. One notable example is the regulation of MYC protein levels by HMG-CoA reductase, which has been demonstrated in the E μ -tTA/TRE-MYC model of lymphoma, as well as the LT2-MYC model of liver cancer[76,77]. Mechanistically, HMG-CoA reductase inhibition via atorvastatin reduced RAS and ERK1/2 signaling in lymphoma, resulting in decreased ERK-dependent MYC phosphorylation, and

reduced MYC levels[77]. In liver cancer, however, atorvastatin was found to decrease MYC phosphorylation and protein levels downstream of Rac GTPase activity[76]. The broader implication of this finding is that a HMG-CoA reductase inhibitor such as atorvastatin deserves further consideration in MYC-overexpressing tumor types, and indeed atorvastatin did have anti-tumorigenic activity in the aforementioned models of MYC-driven liver cancer and lymphoma[76,77]. A second example is the regulation of MYC protein levels by the enzyme O-linked N-acetylglucosamine transferase (OGT), which catalyzes post-translational O-GlcNAcylation of proteins. This phenomenon was demonstrated in a transgenic mouse model of liver cancer with elevated OGT activity[78]. Interestingly, it has been previously demonstrated that MYC can be glycosylated on threonine 58, a key regulatory residue that is also phosphorylated, but the functional significance of this modification remains to be elucidated[79].

Studying Myc and Metabolism in Human Patients

While transgenic and PDX mouse models are invaluable in studying the role of MYC in cancer metabolism, the ultimate goal of these studies is to translate the findings from mouse models to the clinic. The study of cancer metabolism in the clinic has actually been a common practice for more than two decades via the use of the glucose analog 18F-fluorodeoxyglucose (FDG)[80]. Specifically, intravenous injection of 18F- FDG coupled with positron emission tomography (PET) allows for the imaging of a variety of tumor types, which preferentially take up glucose to a higher degree than most non-tumor tissues[80]. Upregulation of hexokinase, which is very likely a MYC transcriptional target in at least some tumor tissues given its strong MYC-dependent regulation as discussed above and elsewhere[81], results in phosphorylation and trapping of the FDG probe in cancers[80]. Although 18F-FDG-PET imaging has generally

been used to detect tumors, recent advancements in our understanding of the biology of tumorigenesis have led to much more specific uses for 18F-FDG-PET. For example, Palaskas et al. [82] reasoned that a correlation between the expression of some mRNAs and 18 F-FDG uptake may allow 18 F-FDG-PET to identify the driver oncogene(s) or oncogenic pathway(s) active in a patient's tumor. The authors integrated mRNA expression analysis and 18F- FDG uptake from a panel of cancer cell lines and 18 patients with breast cancer. Gene set enrichment analysis revealed a number of upregulated molecular pathways in the cell lines and patients with higher 18F-FDG uptake including, not surprisingly, glycolysis. The authors then probed further for associations between the 18F-FDG signature and breast cancer subtypes and molecular drivers, and found that the 18F-FDG signature correlated best with the TN/basal subtype and MYC-dependent transcriptional activity. In addition, the authors retrospectively stained biopsies from the 18 breast cancer patients, and found a significant increase in MYC protein staining of the tumors with high 18F-FDG uptake[82]. To our knowledge, further studies correlating MYC expression with 18F-FDG uptake in human tumors have not been conducted, but should be of further consideration.

Although glucose uptake measurement via 18F-FDG-PET is an invaluable clinical tool, some tumors are inherently 18F-FDG- negative[80]. Likewise, some non-tumor tissues demonstrate high glucose utilization (i.e., brain and liver), making discernment of tumors via 18F-FDG-PET challenging. Thus, alternative metabolites with high avidity for certain tumor types are needed. To that end, preclinical studies have been performed in the MTB-TOM MYC-driven breast cancer model with 18 F-(2S,4R)4-fluoroglutamine[83], which could be useful in a number of MYC-driven tumors that upregulate glutaminolysis as discussed above. In addition, acetate was recently described by two studies as a critical carbon fuel for a variety of primary

tumors and tumors that have metastasized to the brain[84,85]. The critical acetate oxidation enzyme in cancer appears to be the acetyl-CoA synthetase enzyme ACSS2, which was found to be essential for tumorigenesis in a MYC-driven model of liver cancer, and increased expression of ACSS2 was associated with poor prognosis in TNBC[84]. Notably, this study that focused on both primary brain tumors and tumors that metastasized to the brain. Four patients were infused with [1,2-¹³C]acetate during surgical resection of their tumors. Post-operative NMR revealed *de novo* oxidation of acetate to fuel the TCA cycle[85]. Thus, acetate deserves broader consideration as a bioenergetics substrate in MYC-overexpressing tumors, both in terms of therapeutic targeting and for imaging purposes. Finally, hyperpolarized 1-¹³C-pyruvate MRSI has been used pre-clinically[34], but has also been adopted for imaging of patient tumors as part of a first-in-man clinical trial[86]. Indeed, there is clear interest and opportunity for this modality to enter the clinic, especially with expanded probes beyond 1-¹³C-pyruvate, which so far has been the most well-studied[87].

Finally, it is worth taking note of several studies that focused almost entirely on the analysis of clinical samples. Importantly, these studies did not make a functional connection between the metabolic phenotypes observed and MYC activity, even though MYC has established functional roles in the cancer types studied. For those interested, we refer to metabolic profiling performed on primary tumors and serum samples from patients with HCC[88,89], as well as breast cancer[90-92]. In addition, integrated metabolomic and proteomic analysis has been performed on primary RCC tumors[93].

Broader Implications

In this review, we have focused on the role of MYC in regulating cancer metabolism *in vivo*. The majority of studies to date have used transgenic mouse models or primary tumors. Thus, there remains a tremendous amount of work to be done looking outside the confines of the primary tumor to the role of MYC in metastatic tumors, as well as cells within the microenvironment and non-adjacent normal tissue, both of which will ultimately have tremendous influence on which therapeutic strategies can be translated to the clinic. With respect to metastasis, we recently performed single-cell mRNA expression analysis on *de novo* low- and high-burden metastases from orthotopic TNBC PDXs and found that MYC expression was significantly elevated in high-burden metastases[94]. Given that cancer cell metabolism has been shown to change in metastasis initiating cells[95], when the metastatic cells are in circulation[96], and depending on which organ the metastatic tumor colonizes[97], further studies will need to determine whether the reliance on FAO, glucose, glutamine or other metabolites present in primary MYC-overexpressing TNBC is maintained in high- burden metastases.

Another aspect of the microenvironment that deserves significant consideration is the immune cell component. A recent study demonstrated that tumors with elevated glucose consumption effectively drain glucose from the microenvironment, resulting in decreased T-effector cell function, which also relies upon glucose oxidation[98]. Notably, one of the effectors used in this study to promote glycolysis in a tumor line that would otherwise succumb to T-effector surveillance was MYC[98]. Of course, T-effector cells are just one of a large number of immune cell types present in the tumor microenvironment, and the metabolic reliance of each of them could be effected by either the tumor itself or therapies that specifically target metabolism. The metabolism of other non-tumor cell types beyond the immune compartment are also

important to consider with respect to MYC. Indeed, a recent study demonstrated that mice heterozygous for MYC throughout their entire body are smaller, live longer, and are more metabolically active[99]. Thus, targeting MYC-dependent metabolism in cancer could likely impact MYC-dependent metabolism in non-tumor cell types.

Conclusion

In summary, the role of MYC in the regulation of cancer metabolism is as complex as the diverse functions of MYC itself. What becomes clear after considering the multitude of studies conducted is that the function of MYC, like other oncogenes such as KRAS, is incredibly tissue-specific. However, while the overall metabolic phenotype is usually tissue-specific, dysregulations of individual metabolic pathways are often conserved across tissues, and the combination of these considerations should inform treatment decisions. Cancer research seeks to develop better and potentially curative treatments for MYC driven tumors. Studies of specific oncogene-driven transgenic cancer models allow for discoveries of new metabolic pathways that are deregulated in primary tumors, which could not be otherwise identified in cultured cells. We anticipated that effectively translating findings from studying cancer metabolism and its regulation by oncogenes like MYC or KRAS to the clinic will be accelerated through our understanding of how these oncogenes affect tissue specific metabolism *in vivo*.

Conflict of Interest Statement: The authors declare that the research was conducted in the absence of any commercial or financial relationships that could be construed as a potential conflict of interest.

Copyright © 2017 Camarda, Williams and Goga. This is an open-access article distributed under the terms of the Creative Commons Attribution License (CC BY). The use, distribution or reproduction in other forums is permitted, provided the original author(s) or licensor are credited and that the original publication in this journal is cited, in accordance with accepted academic practice. No use, distribution or reproduction is permitted which does not comply with these terms.

Figures

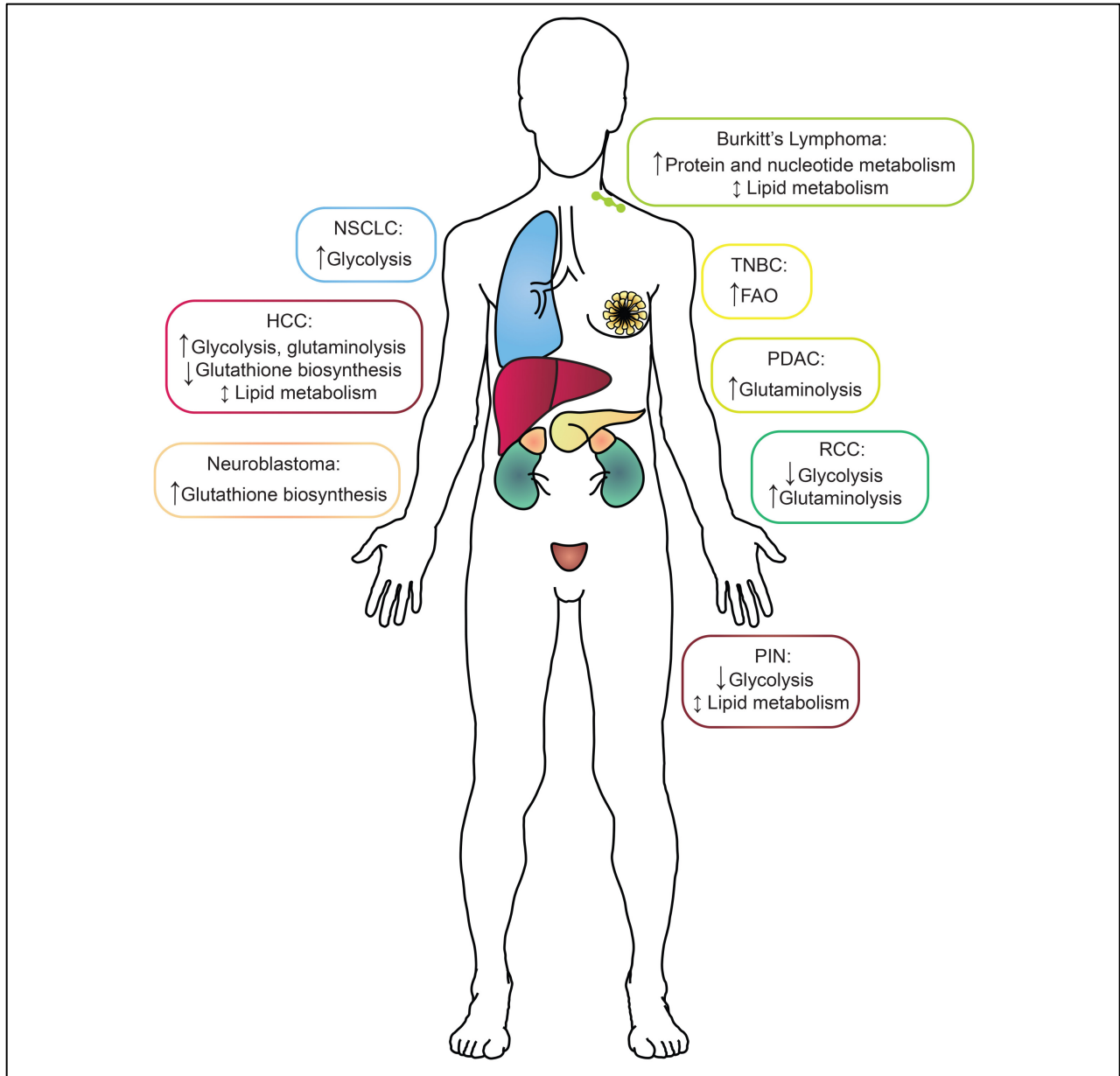


Figure 2.1. A summary of the metabolic alterations found in each MYC-driven cancer type by tissue of origin.

Boxes surrounding each cancer indication are color-coded to match the tissue of origin. HCC, hepatocellular carcinoma; NSCLC, non-small-cell lung cancer; RCC, renal cell carcinoma; PDAC, pancreatic ductal adenocarcinoma; PIN, prostatic intraepithelial neoplasia; TNBC, triple-negative breast cancer.

Table 2.1. In vivo transgenic models of MYC-driven cancer (excluding hydrodynamic models).

A summary of the transgenic mouse models used thus far to study MYC-driven cancer metabolism in vivo. The tissue of origin, specific transgenes and primary altered metabolic pathway(s) studied in each model are noted. References for the models can be found in the main text. HCC, hepatocellular carcinoma; NSCLC, non-small-cell lung cancer; RCC, renal cell carcinoma; PDAC, pancreatic ductal adenocarcinoma; PIN, prostatic intraepithelial neoplasia; NB, neuroblastoma; BL, Burkitt's lymphoma; TNBC, triple-negative breast cancer.

Tissue/cancer specificity	Model	MYC-dependent metabolic pathways altered
Liver—HCC	LAP-tTA/TRE-MYC	Glycolysis (Medina-Cleghorn and Nomura, 2014; Buescher et al., 2015), glutaminolysis (Buescher et al., 2015), glutathione biosynthesis (Altman et al., 2015), lipid metabolism (Bott et al., 2015)
Lung—NSCLC	SPC-rtTA/TRE-MYC	Glycolysis (Buescher et al., 2015)
Kidney—RCC	GGT-tTA/TRE-MYC	Glycolysis (Anderton et al., 2017), glutaminolysis (Anderton et al., 2017)
Pancreatic—PDAC	Pdx1-Cre/LSL-KRASG12D/R26-LSL-MYC	Glutaminolysis (Calvisi and Thorgeirsson, 2005)
Prostate—PIN	Pbsn-MYC	Glycolysis (Hu et al., 2011), lipid metabolism (Hu et al., 2011)
Neural crest—NB	TH-MYCN	Glutathione biosynthesis (Allen et al., 2011)
Lymphocytes—BL	E μ -tTA/TRE-MYC E μ -MYC/RPL24 ^{+/-}	Lipid metabolism (Eberlin et al., 2014) Protein metabolism (D'Cruz et al., 2001), nucleotide metabolism (Pfefferle et al., 2013)
Breast—TNBC	MMTV-rtTA/TRE-MYC	Fatty acid oxidation (Carter et al., 2016)

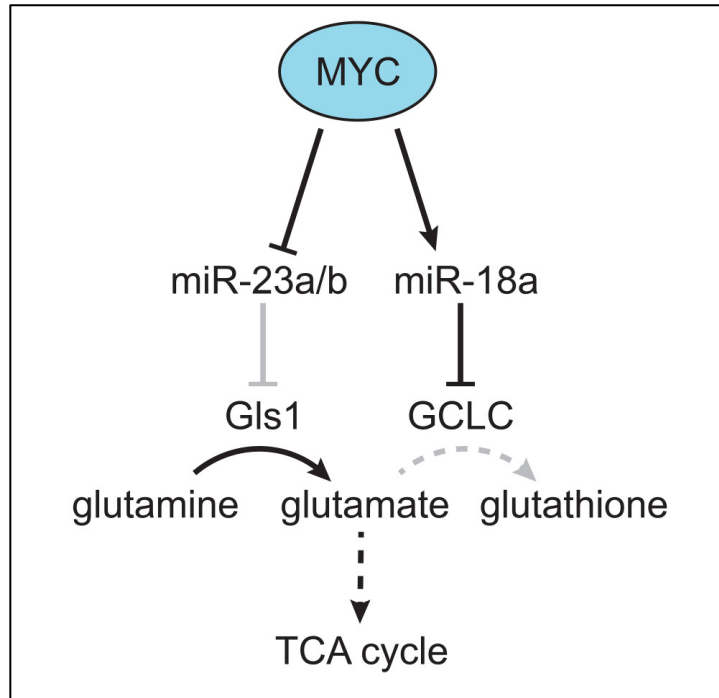


Figure 2.2. MYC-dependent miRNA regulation of glutamine metabolism.

MYC-dependent miRNA regulation of glutamine metabolism. MYC was found to downregulate miR-23a/b, which targets GlS, resulting in increased production of glutamate from glutamine [46]. In addition, MYC was found to upregulate miR-18a, which targets GCLC, resulting in decreased production of glutathione from glutamate, and increased flow of glutamine-derived carbon into the TCA cycle[28]. Gray lines indicate a decreased effect, and dotted lines indicate a multi-step metabolic pathway.

References

- 1 DeBerardinis, R. J., Lum, J. J., Hatzivassiliou, G. & Thompson, C. B. The Biology of Cancer: Metabolic Reprogramming Fuels Cell Growth and Proliferation. *Cell Metabolism* **7**, 11-20 (2008). <https://doi.org/10.1016/j.cmet.2007.10.002>
- 2 Vander Heiden, M. G., Cantley, L. C. & Thompson, C. B. Understanding the Warburg effect: the metabolic requirements of cell proliferation. *Science* **324**, 1029-1033 (2009). <https://doi.org/10.1126/science.1160809>
- 3 Hanahan, D. & Weinberg, R. A. Hallmarks of cancer: the next generation. *Cell* **144**, 646-674 (2011). <https://doi.org/10.1016/j.cell.2011.02.013>
- 4 Altman, B. J., Stine, Z. E. & Dang, C. V. From Krebs to clinic: glutamine metabolism to cancer therapy. *Nature Reviews Cancer* **16**, 619-634 (2016). <https://doi.org/10.1038/nrc.2016.71>
- 5 Hay, N. Reprogramming glucose metabolism in cancer: can it be exploited for cancer therapy? *Nat Rev Cancer* **16**, 635-649 (2016). <https://doi.org/10.1038/nrc.2016.77>
- 6 Cairns, R. A. & Mak, T. W. The current state of cancer metabolism. *Nature Reviews Cancer* **16**, 613-614 (2016). <https://doi.org/10.1038/nrc.2016.100>
- 7 Galluzzi, L., Kepp, O., Vander Heiden, M. G. & Kroemer, G. Metabolic targets for cancer therapy. *Nat Rev Drug Discov* **12**, 829-846 (2013). <https://doi.org/10.1038/nrd4145>
- 8 Meyer, N. & Penn, L. Z. Reflecting on 25 years with MYC. *Nat Rev Cancer* **8**, 976-990 (2008). <https://doi.org/10.1038/nrc2231>

- 9 Horiuchi, D. *et al.* MYC pathway activation in triple-negative breast cancer is synthetic lethal with CDK inhibition. *The Journal of Experimental Medicine* **209**, 679-696 (2012). <https://doi.org/10.1084/jem.20111512>
- 10 Comprehensive molecular portraits of human breast tumours. *Nature* **490**, 61-70 (2012). <https://doi.org/10.1038/nature11412>
- 11 Eberlin, L. S. *et al.* Alteration of the lipid profile in lymphomas induced by MYC overexpression. *Proc Natl Acad Sci U S A* **111**, 10450-10455 (2014). <https://doi.org/10.1073/pnas.1409778111>
- 12 Kress, T. R., Sabò, A. & Amati, B. MYC: connecting selective transcriptional control to global RNA production. *Nat Rev Cancer* **15**, 593-607 (2015). <https://doi.org/10.1038/nrc3984>
- 13 Sloan, E. J. & Ayer, D. E. Myc, mondo, and metabolism. *Genes Cancer* **1**, 587-596 (2010). <https://doi.org/10.1177/1947601910377489>
- 14 Lockwood, W. W., Zejnullahu, K., Bradner, J. E. & Varmus, H. Sensitivity of human lung adenocarcinoma cell lines to targeted inhibition of BET epigenetic signaling proteins. *Proc Natl Acad Sci U S A* **109**, 19408-19413 (2012). <https://doi.org/10.1073/pnas.1216363109>
- 15 McKeown, M. R. & Bradner, J. E. Therapeutic strategies to inhibit MYC. *Cold Spring Harb Perspect Med* **4** (2014). <https://doi.org/10.1101/cshperspect.a014266>
- 16 Shim, H. *et al.* c-Myc transactivation of LDH-A: implications for tumor metabolism and growth. *Proc Natl Acad Sci U S A* **94**, 6658-6663 (1997). <https://doi.org/10.1073/pnas.94.13.6658>

- 17 Dang, C. V. Therapeutic targeting of Myc-reprogrammed cancer cell metabolism. *Cold Spring Harb Symp Quant Biol* **76**, 369-374 (2011).
<https://doi.org/10.1101/sqb.2011.76.011296>
- 18 Yuneva, M., Zamboni, N., Oefner, P., Sachidanandam, R. & Lazebnik, Y. Deficiency in glutamine but not glucose induces MYC-dependent apoptosis in human cells. *J Cell Biol* **178**, 93-105 (2007). <https://doi.org/10.1083/jcb.200703099>
- 19 Stine, Z. E., Walton, Z. E., Altman, B. J., Hsieh, A. L. & Dang, C. V. MYC, Metabolism, and Cancer. *Cancer Discov* **5**, 1024-1039 (2015). <https://doi.org/10.1158/2159-8290.Cd-15-0507>
- 20 Wahlström, T. & Henriksson, M. A. Impact of MYC in regulation of tumor cell metabolism. *Biochim Biophys Acta* **1849**, 563-569 (2015).
<https://doi.org/10.1016/j.bbagr.2014.07.004>
- 21 Mayers, J. R. & Vander Heiden, M. G. Famine versus feast: understanding the metabolism of tumors in vivo. *Trends Biochem Sci* **40**, 130-140 (2015).
<https://doi.org/10.1016/j.tibs.2015.01.004>
- 22 Abbondante, S., Eckel-Mahan, K. L., Ceglia, N. J., Baldi, P. & Sassone-Corsi, P. Comparative Circadian Metabolomics Reveal Differential Effects of Nutritional Challenge in the Serum and Liver. *J Biol Chem* **291**, 2812-2828 (2016).
<https://doi.org/10.1074/jbc.M115.681130>
- 23 Altman, B. J. *et al.* MYC Disrupts the Circadian Clock and Metabolism in Cancer Cells. *Cell Metab* **22**, 1009-1019 (2015). <https://doi.org/10.1016/j.cmet.2015.09.003>

- 24 Davidson, S. M. *et al.* Environment Impacts the Metabolic Dependencies of Ras-Driven Non-Small Cell Lung Cancer. *Cell Metab* **23**, 517-528 (2016).
<https://doi.org/10.1016/j.cmet.2016.01.007>
- 25 Medina-Cleghorn, D. & Nomura, D. K. Exploring metabolic pathways and regulation through functional chemoproteomic and metabolomic platforms. *Chem Biol* **21**, 1171-1184 (2014). <https://doi.org/10.1016/j.chembiol.2014.07.007>
- 26 Buescher, J. M. *et al.* A roadmap for interpreting (13)C metabolite labeling patterns from cells. *Curr Opin Biotechnol* **34**, 189-201 (2015).
<https://doi.org/10.1016/j.copbio.2015.02.003>
- 27 Aran, D., Sirota, M. & Butte, A. J. Systematic pan-cancer analysis of tumour purity. *Nature Communications* **6**, 8971 (2015). <https://doi.org/10.1038/ncomms9971>
- 28 Anderton, B. *et al.* MYC-driven inhibition of the glutamate-cysteine ligase promotes glutathione depletion in liver cancer. *EMBO reports* **18**, 569-585-585 (2017). <https://doi.org/https://doi.org/10.15252/embr.201643068>
- 29 Calvisi, D. F. & Thorgeirsson, S. S. Molecular mechanisms of hepatocarcinogenesis in transgenic mouse models of liver cancer. *Toxicol Pathol* **33**, 181-184 (2005).
<https://doi.org/10.1080/01926230590522095>
- 30 Shachaf, C. M. *et al.* MYC inactivation uncovers pluripotent differentiation and tumour dormancy in hepatocellular cancer. *Nature* **431**, 1112-1117 (2004).
<https://doi.org/10.1038/nature03043>
- 31 Kaposi-Novak, P. *et al.* Central role of c-Myc during malignant conversion in human hepatocarcinogenesis. *Cancer Res* **69**, 2775-2782 (2009). <https://doi.org/10.1158/0008-5472.Can-08-3357>

- 32 Wang, H. *et al.* Coordinated Activities of Multiple Myc-dependent and Myc-independent Biosynthetic Pathways in Hepatoblastoma. *J Biol Chem* **291**, 26241-26251 (2016).
<https://doi.org/10.1074/jbc.M116.754218>
- 33 Lim, L. *et al.* MicroRNA-494 within an oncogenic microRNA megacluster regulates G1/S transition in liver tumorigenesis through suppression of mutated in colorectal cancer. *Hepatology* **59**, 202-215 (2014). <https://doi.org/10.1002/hep.26662>
- 34 Hu, S. *et al.* ¹³C-pyruvate imaging reveals alterations in glycolysis that precede c-Myc-induced tumor formation and regression. *Cell Metab* **14**, 131-142 (2011).
<https://doi.org/10.1016/j.cmet.2011.04.012>
- 35 Yuneva, M. O. *et al.* The metabolic profile of tumors depends on both the responsible genetic lesion and tissue type. *Cell Metab* **15**, 157-170 (2012).
<https://doi.org/10.1016/j.cmet.2011.12.015>
- 36 Xiang, Y. *et al.* Targeted inhibition of tumor-specific glutaminase diminishes cell-autonomous tumorigenesis. *J Clin Invest* **125**, 2293-2306 (2015).
<https://doi.org/10.1172/jci75836>
- 37 Allen, T. D. *et al.* Interaction between MYC and MCL1 in the genesis and outcome of non-small-cell lung cancer. *Cancer Res* **71**, 2212-2221 (2011).
<https://doi.org/10.1158/0008-5472.Can-10-3590>
- 38 Wang, R., Ferrell, L. D., Faouzi, S., Maher, J. J. & Bishop, J. M. Activation of the Met receptor by cell attachment induces and sustains hepatocellular carcinomas in transgenic mice. *J Cell Biol* **153**, 1023-1034 (2001). <https://doi.org/10.1083/jcb.153.5.1023>

- 39 Ciribilli, Y., Singh, P., Inga, A. & Borlak, J. c-Myc targeted regulators of cell metabolism in a transgenic mouse model of papillary lung adenocarcinoma. *Oncotarget* **7**, 65514-65539 (2016). <https://doi.org/10.18632/oncotarget.11804>
- 40 Shroff, E. H. *et al.* MYC oncogene overexpression drives renal cell carcinoma in a mouse model through glutamine metabolism. *Proc Natl Acad Sci U S A* **112**, 6539-6544 (2015). <https://doi.org/10.1073/pnas.1507228112>
- 41 Bott, A. J. *et al.* Oncogenic Myc Induces Expression of Glutamine Synthetase through Promoter Demethylation. *Cell Metab* **22**, 1068-1077 (2015). <https://doi.org/10.1016/j.cmet.2015.09.025>
- 42 Ellwood-Yen, K. *et al.* Myc-driven murine prostate cancer shares molecular features with human prostate tumors. *Cancer Cell* **4**, 223-238 (2003). [https://doi.org/10.1016/s1535-6108\(03\)00197-1](https://doi.org/10.1016/s1535-6108(03)00197-1)
- 43 Majumder, P. K. *et al.* Prostate intraepithelial neoplasia induced by prostate restricted Akt activation: the MPAKT model. *Proc Natl Acad Sci U S A* **100**, 7841-7846 (2003). <https://doi.org/10.1073/pnas.1232229100>
- 44 Priolo, C. *et al.* AKT1 and MYC induce distinctive metabolic fingerprints in human prostate cancer. *Cancer Res* **74**, 7198-7204 (2014). <https://doi.org/10.1158/0008-5472.Can-14-1490>
- 45 Tward, A. D. *et al.* Genomic progression in mouse models for liver tumors. *Cold Spring Harb Symp Quant Biol* **70**, 217-224 (2005). <https://doi.org/10.1101/sqb.2005.70.058>
- 46 Gao, P. *et al.* c-Myc suppression of miR-23a/b enhances mitochondrial glutaminase expression and glutamine metabolism. *Nature* **458**, 762-765 (2009). <https://doi.org/10.1038/nature07823>

- 47 Kota, J. *et al.* Therapeutic microRNA delivery suppresses tumorigenesis in a murine liver cancer model. *Cell* **137**, 1005-1017 (2009). <https://doi.org/10.1016/j.cell.2009.04.021>
- 48 Carter, D. R. *et al.* Glutathione biosynthesis is upregulated at the initiation of MYCN-driven neuroblastoma tumorigenesis. *Mol Oncol* **10**, 866-878 (2016).
<https://doi.org/10.1016/j.molonc.2016.02.004>
- 49 Weiss, W. A., Aldape, K., Mohapatra, G., Feuerstein, B. G. & Bishop, J. M. Targeted expression of MYCN causes neuroblastoma in transgenic mice. *Embo j* **16**, 2985-2995 (1997). <https://doi.org/10.1093/emboj/16.11.2985>
- 50 Terunuma, A. *et al.* MYC-driven accumulation of 2-hydroxyglutarate is associated with breast cancer prognosis. *J Clin Invest* **124**, 398-412 (2014).
<https://doi.org/10.1172/jci71180>
- 51 Intlekofer, A. M. *et al.* Hypoxia Induces Production of L-2-Hydroxyglutarate. *Cell Metab* **22**, 304-311 (2015). <https://doi.org/10.1016/j.cmet.2015.06.023>
- 52 Oldham, W. M., Clish, C. B., Yang, Y. & Loscalzo, J. Hypoxia-Mediated Increases in L-2-hydroxyglutarate Coordinate the Metabolic Response to Reductive Stress. *Cell Metab* **22**, 291-303 (2015). <https://doi.org/10.1016/j.cmet.2015.06.021>
- 53 Cairo, S. *et al.* Hepatic stem-like phenotype and interplay of Wnt/beta-catenin and Myc signaling in aggressive childhood liver cancer. *Cancer Cell* **14**, 471-484 (2008).
<https://doi.org/10.1016/j.ccr.2008.11.002>
- 54 Perry, R. H. *et al.* Characterization of MYC-induced tumorigenesis by in situ lipid profiling. *Anal Chem* **85**, 4259-4262 (2013). <https://doi.org/10.1021/ac400479j>
- 55 Felsher, D. W. & Bishop, J. M. Reversible tumorigenesis by MYC in hematopoietic lineages. *Mol Cell* **4**, 199-207 (1999). [https://doi.org/10.1016/s1097-2765\(00\)80367-6](https://doi.org/10.1016/s1097-2765(00)80367-6)

- 56 Harris, A. W. *et al.* The E mu-myc transgenic mouse. A model for high-incidence spontaneous lymphoma and leukemia of early B cells. *J Exp Med* **167**, 353-371 (1988). <https://doi.org/10.1084/jem.167.2.353>
- 57 Pacilli, A. *et al.* Carnitine-acyltransferase system inhibition, cancer cell death, and prevention of myc-induced lymphomagenesis. *J Natl Cancer Inst* **105**, 489-498 (2013). <https://doi.org/10.1093/jnci/djt030>
- 58 D'Cruz, C. M. *et al.* c-MYC induces mammary tumorigenesis by means of a preferred pathway involving spontaneous Kras2 mutations. *Nat Med* **7**, 235-239 (2001). <https://doi.org/10.1038/84691>
- 59 Pfefferle, A. D. *et al.* Transcriptomic classification of genetically engineered mouse models of breast cancer identifies human subtype counterparts. *Genome Biol* **14**, R125 (2013). <https://doi.org/10.1186/gb-2013-14-11-r125>
- 60 DeRose, Y. S. *et al.* Tumor grafts derived from women with breast cancer authentically reflect tumor pathology, growth, metastasis and disease outcomes. *Nat Med* **17**, 1514-1520 (2011). <https://doi.org/10.1038/nm.2454>
- 61 Camarda, R. *et al.* Inhibition of fatty acid oxidation as a therapy for MYC-overexpressing triple-negative breast cancer. *Nat Med* **22**, 427-432 (2016). <https://doi.org/https://10.1038/nm.4055>
- 62 Park, J. H. *et al.* Fatty Acid Oxidation-Driven Src Links Mitochondrial Energy Reprogramming and Oncogenic Properties in Triple-Negative Breast Cancer. *Cell Reports* **14**, 2154-2165 (2016). <https://doi.org/10.1016/j.celrep.2016.02.004>

- 63 Li, F. *et al.* Myc stimulates nuclearly encoded mitochondrial genes and mitochondrial biogenesis. *Mol Cell Biol* **25**, 6225-6234 (2005). <https://doi.org/10.1128/mcb.25.14.6225-6234.2005>
- 64 Zirath, H. *et al.* MYC inhibition induces metabolic changes leading to accumulation of lipid droplets in tumor cells. *Proc Natl Acad Sci U S A* **110**, 10258-10263 (2013). <https://doi.org/10.1073/pnas.1222404110>
- 65 Abu-Elheiga, L., Matzuk, M. M., Abo-Hashema, K. A. & Wakil, S. J. Continuous fatty acid oxidation and reduced fat storage in mice lacking acetyl-CoA carboxylase 2. *Science* **291**, 2613-2616 (2001). <https://doi.org/10.1126/science.1056843>
- 66 Nieman, K. M. *et al.* Adipocytes promote ovarian cancer metastasis and provide energy for rapid tumor growth. *Nat Med* **17**, 1498-1503 (2011). <https://doi.org/10.1038/nm.2492>
- 67 Liu, R. Z. *et al.* Association of FABP5 expression with poor survival in triple-negative breast cancer: implication for retinoic acid therapy. *Am J Pathol* **178**, 997-1008 (2011). <https://doi.org/10.1016/j.ajpath.2010.11.075>
- 68 Brasó-Maristany, F. *et al.* PIM1 kinase regulates cell death, tumor growth and chemotherapy response in triple-negative breast cancer. *Nature Medicine* **22**, 1303-1313 (2016). <https://doi.org/10.1038/nm.4198>
- 69 Horiuchi, D. *et al.* PIM1 kinase inhibition as a targeted therapy against triple-negative breast tumors with elevated MYC expression. *Nat Med* **22**, 1321-1329 (2016). <https://doi.org/10.1038/nm.4213>
- 70 Beharry, Z. *et al.* The Pim protein kinases regulate energy metabolism and cell growth. *Proceedings of the National Academy of Sciences* **108**, 528-533 (2011). <https://doi.org/10.1073/pnas.1013214108>

- 71 Hu, H. *et al.* Phosphoinositide 3-Kinase Regulates Glycolysis through Mobilization of Aldolase from the Actin Cytoskeleton. *Cell* **164**, 433-446 (2016).
<https://doi.org/10.1016/j.cell.2015.12.042>
- 72 Le, X. *et al.* Systematic Functional Characterization of Resistance to PI3K Inhibition in Breast Cancer. *Cancer Discov* **6**, 1134-1147 (2016). <https://doi.org/10.1158/2159-8290.Cd-16-0305>
- 73 Barna, M. *et al.* Suppression of Myc oncogenic activity by ribosomal protein haploinsufficiency. *Nature* **456**, 971-975 (2008). <https://doi.org/10.1038/nature07449>
- 74 Cunningham, J. T., Moreno, M. V., Lodi, A., Ronen, S. M. & Ruggero, D. Protein and nucleotide biosynthesis are coupled by a single rate-limiting enzyme, PRPS2, to drive cancer. *Cell* **157**, 1088-1103 (2014). <https://doi.org/10.1016/j.cell.2014.03.052>
- 75 Hart, L. S. *et al.* ER stress-mediated autophagy promotes Myc-dependent transformation and tumor growth. *J Clin Invest* **122**, 4621-4634 (2012). <https://doi.org/10.1172/jci62973>
- 76 Cao, Z. *et al.* MYC phosphorylation, activation, and tumorigenic potential in hepatocellular carcinoma are regulated by HMG-CoA reductase. *Cancer Res* **71**, 2286-2297 (2011). <https://doi.org/10.1158/0008-5472.Can-10-3367>
- 77 Shachaf, C. M. *et al.* Inhibition of HMGcoA reductase by atorvastatin prevents and reverses MYC-induced lymphomagenesis. *Blood* **110**, 2674-2684 (2007).
<https://doi.org/10.1182/blood-2006-09-048033>
- 78 Burén, S. *et al.* Regulation of OGT by URI in Response to Glucose Confers c-MYC-Dependent Survival Mechanisms. *Cancer Cell* **30**, 290-307 (2016).
<https://doi.org/10.1016/j.ccell.2016.06.023>

- 79 Chou, T. Y., Hart, G. W. & Dang, C. V. c-Myc is glycosylated at threonine 58, a known phosphorylation site and a mutational hot spot in lymphomas. *J Biol Chem* **270**, 18961-18965 (1995). <https://doi.org/10.1074/jbc.270.32.18961>
- 80 Fletcher, J. W. *et al.* Recommendations on the use of 18F-FDG PET in oncology. *J Nucl Med* **49**, 480-508 (2008). <https://doi.org/10.2967/jnumed.107.047787>
- 81 Kim, J. W., Gao, P., Liu, Y. C., Semenza, G. L. & Dang, C. V. Hypoxia-inducible factor 1 and dysregulated c-Myc cooperatively induce vascular endothelial growth factor and metabolic switches hexokinase 2 and pyruvate dehydrogenase kinase 1. *Mol Cell Biol* **27**, 7381-7393 (2007). <https://doi.org/10.1128/mcb.00440-07>
- 82 Palaskas, N. *et al.* 18F-fluorodeoxy-glucose positron emission tomography marks MYC-overexpressing human basal-like breast cancers. *Cancer Res* **71**, 5164-5174 (2011). <https://doi.org/10.1158/0008-5472.Can-10-4633>
- 83 Lieberman, B. P. *et al.* PET imaging of glutaminolysis in tumors by 18F-(2S,4R)4-fluoroglutamine. *J Nucl Med* **52**, 1947-1955 (2011). <https://doi.org/10.2967/jnumed.111.093815>
- 84 Comerford, S. A. *et al.* Acetate dependence of tumors. *Cell* **159**, 1591-1602 (2014). <https://doi.org/10.1016/j.cell.2014.11.020>
- 85 Mashimo, T. *et al.* Acetate is a bioenergetic substrate for human glioblastoma and brain metastases. *Cell* **159**, 1603-1614 (2014). <https://doi.org/10.1016/j.cell.2014.11.025>
- 86 Nelson, S. J. *et al.* Metabolic imaging of patients with prostate cancer using hyperpolarized [1-¹³C]pyruvate. *Sci Transl Med* **5**, 198ra108 (2013). <https://doi.org/10.1126/scitranslmed.3006070>

- 87 Kurhanewicz, J. *et al.* Analysis of cancer metabolism by imaging hyperpolarized nuclei: prospects for translation to clinical research. *Neoplasia* **13**, 81-97 (2011).
<https://doi.org/10.1593/neo.101102>
- 88 Huang, Q. *et al.* Metabolic characterization of hepatocellular carcinoma using nontargeted tissue metabolomics. *Cancer Res* **73**, 4992-5002 (2013).
<https://doi.org/10.1158/0008-5472.Can-13-0308>
- 89 Liu, Y. *et al.* NMR and LC/MS-based global metabolomics to identify serum biomarkers differentiating hepatocellular carcinoma from liver cirrhosis. *Int J Cancer* **135**, 658-668 (2014). <https://doi.org/10.1002/ijc.28706>
- 90 Cao, M. D. *et al.* Metabolic characterization of triple negative breast cancer. *BMC Cancer* **14**, 941 (2014). <https://doi.org/10.1186/1471-2407-14-941>
- 91 Cui, M., Wang, Q. & Chen, G. Serum metabolomics analysis reveals changes in signaling lipids in breast cancer patients. *Biomed Chromatogr* **30**, 42-47 (2016).
<https://doi.org/10.1002/bmc.3556>
- 92 Kanaan, Y. M. *et al.* Metabolic profile of triple-negative breast cancer in African-American women reveals potential biomarkers of aggressive disease. *Cancer Genomics Proteomics* **11**, 279-294 (2014).
- 93 Wettersten, H. I. *et al.* Grade-Dependent Metabolic Reprogramming in Kidney Cancer Revealed by Combined Proteomics and Metabolomics Analysis. *Cancer Res* **75**, 2541-2552 (2015). <https://doi.org/10.1158/0008-5472.Can-14-1703>
- 94 Lawson, D. A. *et al.* Single-cell analysis reveals a stem-cell program in human metastatic breast cancer cells. *Nature* **526**, 131-135 (2015). <https://doi.org/10.1038/nature15260>

- 95 Pascual, G. *et al.* Targeting metastasis-initiating cells through the fatty acid receptor CD36. *Nature* **541**, 41-45 (2017). <https://doi.org/10.1038/nature20791>
- 96 LeBleu, V. S. *et al.* PGC-1 α mediates mitochondrial biogenesis and oxidative phosphorylation in cancer cells to promote metastasis. *Nat Cell Biol* **16**, 992-1003, 1001-1015 (2014). <https://doi.org/10.1038/ncb3039>
- 97 Dupuy, F. *et al.* PDK1-Dependent Metabolic Reprogramming Dictates Metastatic Potential in Breast Cancer. *Cell Metab* **22**, 577-589 (2015). <https://doi.org/10.1016/j.cmet.2015.08.007>
- 98 Chang, C. H. *et al.* Metabolic Competition in the Tumor Microenvironment Is a Driver of Cancer Progression. *Cell* **162**, 1229-1241 (2015). <https://doi.org/10.1016/j.cell.2015.08.016>
- 99 Hofmann, J. W. *et al.* Reduced expression of MYC increases longevity and enhances healthspan. *Cell* **160**, 477-488 (2015). <https://doi.org/10.1016/j.cell.2014.12.016>

**Chapter 3: Alterations to fatty acid trafficking in triple-negative
breast cancer**

Abstract

A reliance on fatty acid catabolism has been observed in an aggressive class of breast cancer, triple-negative breast cancer (TNBC), the majority of which feature elevated levels of potent oncogene MYC. The intracellular adaptations that facilitate this metabolic shift, however, are not well defined. Elevated levels of mitochondrial fatty acid oxidation (FAO) have been shown to drive rapid tumor growth in MYC^{High} TNBC, but the alterations that enable flux of fatty acids (FA) to the mitochondria to satisfy elevated FAO and their connection to MYC are unclear. This study investigates the role of Fatty Acid Binding Protein 5 (FABP5) in lipid homeostasis and cell growth in MYC^{High} TNBC. I observed that transient inhibition, but not genetic knockout of FABP5 impaired cell proliferation in a mouse model for MYC-driven TNBC. Expression analysis in patient-derived breast cancer cell lines revealed specific elevation of FABP5 in TNBC, but did not confirm an association MYC expression. I found that FABP5 inhibition was sufficient to disrupt lipid homeostasis, congruent with prior studies, suggesting its potential as a therapeutic target in TNBC. These results underscore the importance of defining the intracellular features that facilitate elevated FAO in TNBC.

Introduction

Breast and other cancers have previously been shown to support production of cell membranes and lipid signaling precursors, key processes in proliferation, through fatty acid synthesis (FAS). While c-MYC (MYC) has been established to dysregulate metabolic pathways governing glucose [1,2] and glutamine utilization[3-5] in cancer (see *Chapter 1*), recent work from our laboratory and others indicates that in triple-negative breast cancer (TNBC), the proto-oncogene may also moderate fatty acid oxidation (FAO) [6,7]. In mouse PDX models of MYC-high TNBC, FAO is increased compared to MYC-low TNBC and receptor-positive (RP) cells,

and *in vivo* FAO inhibition with CPT1 inhibitor etomoxir is sufficient to impair tumor growth [6] (**Fig. 1.1**). This FAO dependency falls in contrast to reliance on FAS observed in other cancer context; the specific alterations that permit elevated FAO in *MYC*-driven TNBC are, however, still unclear. To that end, in this study aimed to delineate the intracellular adaptations to FA trafficking that permit increased mitochondrial FAO, in *MYC*-driven TNBC.

Cellular uptake of long-chain fatty acids (LCFA) can occur via passive and active transport mechanisms, but protein-mediated transport is the major model for LCFA uptake and activation to acetyl-CoA. The majority of extracellular, circulatory LCFAs are albumin-bound, but are released from albumin before entering the PM, becoming hydrophobic and requiring active transport. Several known FA transporters reside at the PM, including plasma membrane Fatty Acid Binding Proteins, CD36 (or fatty acid transporter, FAT) and fatty acid transport proteins (FATPs) [8] (**Fig. 1.1**). In the breast, it is possible that the adipose tumor microenvironment release FA for tumor uptake (*Chapter 4*).

Once across the PM, LCFAs are bound by fatty acid binding proteins (FABPs) in the cytoplasm [9]. FABPs are a family of at least 9 small intracellular lipid chaperones expressed across a range of tissues, most abundantly in those involved in active lipid metabolism—the liver, intestine, heart, adipose, epidermal, ileum, brain, myelin and testis FABP (FABP1-9, respectively). Each FABP binds LCFAs, but with variation in binding selectivity, affinity and mechanism [10], possibly reflecting specific LCFA abundance in different tissues. FABPs can also bind a host of other molecules, also potentially reflecting the microenvironment—FABP1 (liver) binds haem, and FABP4 (adipose) binds hormone-sensitive lipase (HSL). Given their apparent promiscuity, it's incompletely understood how these chaperones achieve binding specificity [11,12]. While certain tissues show elevation of a specific FABP, no known FABPs

are exclusive to one tissue or cell type. Increased FA exposure leads to increased FABP expression in most cell types [13], suggesting that some adaptive cellular mechanism regulates FABPs to sustain lipid homeostasis and stoichiometry with available lipid supply. FABP protein content in most cells is also proportional to their rate of FAM [13], further indicating an important role in maintenance of bioenergetic homeostasis [9,14].

LCFA-bound FABPs are thought to chaperone lipids to a host of different intracellular compartments (**Fig. 4.1**). One established function is trafficking to lipid droplets (LD) for storage. Other proposed functions include delivery to the endoplasmic reticulum (ER) for use in signaling, trafficking, or membrane synthesis, to the peroxisome for oxidation, to enzymes that regulate FA homeostasis in the cytosol or elsewhere, to the nucleus for modulation of lipid-responsive transcription factor activity, and possibly to the extracellular compartment for autocrine or paracrine signaling purposes [11]. In this study we focus on the role of FABPs in chaperoning lipids to the mitochondria for FAO.

Because elevated mitochondrial FAO suggests an increased FA pool at the mitochondria available for import across the carnitine shuttle (**Fig. 4.2**), our laboratory probed intracellular alterations to FA trafficking machinery. Indeed, one component of this trafficking machinery, fatty acid binding protein 5 (FABP5), is upregulated in TNBC in a MYC-dependent manner [15]. A strong association between elevated FABP5 and poor survival has previously been identified in TNBC [16]. Intriguingly, preliminary studies indicate that inhibition of FABP5 in a mouse model for MYC-high TNBC is sufficient to cause defects in cellular metabolism and proliferation [15]. One possibility is that FABP5 elevation in TNBC could satisfy the requirement for increased FA at the mitochondria, thus permitting increased FAO observed in

this subtype. I therefore further investigated the role of FABP5 in increased FAO, and its contribution to cell survival and proliferation, in TNBC.

Results

To examine what alterations within TNBC permit increased FAO, we investigated mechanisms of intracellular FA trafficking. FABPs at the mitochondria donate FA to fatty acyl-CoA synthetases (ACSSs) for activation into fatty acyl CoAs, enabling import through the mitochondrial membrane. During FAO, activated FA are then catabolically processed to form acetyl-CoA, a major fuel source for bioenergetic and biosynthetic metabolism. Indeed, prior assessment of available data on patient TN and RP tumors indicated specific elevation of FABP5 in TN tumors (**Fig. 3.3A**) [15]. Former Master's student Céline Mahieu in our laboratory also utilized a genetically engineered mouse model for MYC-driven TNBC (MTB-TOM) [17] wherein breast epithelial MYC expression can be activated with doxycycline expression, and resulting tumors are allografted into the mammary fat pad of wild-type FVBN mice. She assessed FABP5 expression in allografts both from mice receiving doxycycline chow, activating MYC-driven tumor progression, and from mice who were subsequently switched to control chow, for which tumors regressed. Studies in MTB-TOM indicated that FABP5 expression was MYC-dependent (**Fig. 3.3B**) [15]. I first performed validation studies using RNA-seq on an established[18] panel of patient-derived TN and RP PDX cell lines to assess FABP levels, and found that FABP5 was specifically upregulated in TN lines(**Fig. 3.3C**), and was also the most expressed FABP across TN and RP lines. However, expression was significantly elevated in both TN MYC^{Low} and MYC^{High} lines in comparison to RP (data not shown), suggesting that expression may not be MYC-driven as observed in MTB-TOM tumors (**Fig. 3.3B**).

Second, I employed pharmacological inhibition to delineate the contributions of FABP5 to TNBC progression. I used a commercially available FABP5/7 inhibitor (Cayman SBI126) which has been well tolerated in animal studies [19], to assay MTB-TOM cells, and in the MYC-high group we observed significant, marked loss of proliferation with inhibitor treatment compared to vehicle (**Fig. 3.4A-B**). Then, to examine effects of inhibition on lipid homeostasis, I used Nile red staining [20] to assay lipid droplet (LD) formation. I observed increased LD and decreased total ATP in MYC-high MTB-TOM cells, while MYC-low MTB-TOM cells exhibited no significant change with inhibition (**Fig. 3.4C-D**). These data mirror prior siRNA studies in MTB-TOM, in which transient FABP5 silencing decreased cell proliferation and increased lipid accumulation specifically in MYC-high MTB-TOM cells (**Fig. 3.4E-F**) [15], and suggest that transient inhibition may be sufficient to impair proliferation and lipid homeostasis in MYC-driven TNBC.

Finally, using CRISPR-Cas9 engineered FABP5 null MTB-TOM cell lines (**Fig. 3.5A**) we assessed the impact of FABP5 deletion on MYC-driven TNBC proliferation and FA metabolism. Notably, prolonged FABP5 loss did not significantly alter cell proliferation compared to controls in this model (**Fig. 3.5B**). Furthermore, FABP5 deletion did not sensitize cells to inhibition of either FABP5/7 (FA trafficking) or CPT1 (mitochondrial FAO) (**Fig. 3.5C-D**).

Discussion

Dysregulation of FABPs has been observed across many cancer types including breast [21], prostate [22], squamous cell carcinomas [23,24], renal cell carcinoma [25], and melanoma [26], compared with normal tissue. Furthermore, multiple cancer models support that

overexpression or depletion of one FABP species can be sufficient to increase cell growth, and even metastatic potential [27,28]. In a human TNBC study, patients with FABP7- positive tumors had better outcomes than those with FABP7-negative tumors, and elevated nuclear FABP7 was associated with longer disease-free survival [29], indicating a potential role of FABP- or LCFA-transcription factor interactions in regulating cancer growth and survival. In melanoma, metastatic tumors show decreased FABP7 compared with primary tumor, and metastatic FABP7 expression is associated with decreased relapse-free survival and overall survival [30], implying that FABP levels could also play a role in metabolic reprogramming upon metastasis. These prior studies support the importance of delineating FABP function and therapeutic potential in TNBC and beyond breast cancer.

Complicating matters, multiple mouse models have also shown that loss of one FABP can be met with compensatory upregulation of others [31,32]. In MYC-on MTB-TOM we observed a distinct proliferative defect with FABP5 inhibition and silencing (**Fig. 3.4E-F**), while CRISPR-Cas9 deletion in the same model did not impact cell growth (**Fig. 3.5A-B**). It is possible that CRISPR/Cas9 deletion of FABP5 in MTB-TOM dysregulated expression of other FABPs, however assessment of FABP transcriptional levels is required. The lack of proliferative phenotype observed *in vitro* in this engineered model precluded using these cell lines for subsequent *in vivo* experiments.

Despite limited scope, this work lends insight into the functionality of an understudied FA chaperone, and suggests that transient FABP5 inhibition could be sufficient to disrupt TNBC proliferation and lipid homeostasis. There is an established link in TNBC between elevated MYC and increased FAO level [6], and as described in *Chapter 4* there is also specific activation of lipolysis (FA release) in the adipose tumor microenvironment for MYC-high TNBC. FABP5

expression data in patient-derived cell lines, however, contrasts this trend and prior evidence in MTB-TOM tumors that elevated FABP5 is a specific feature of MYC-high TNBCs. Limitations of this FABP5 knockout model in recapitulating parallel siRNA studies may also point to difficulties in isolating FABP5 contributions to FAM using complete genetic knockout. In an interventional setting, FABP5 could prove a challenging target for prolonged inhibition due to the potential for compensation of other FABP family members. Better understanding the binding specificity of each FABP for LCFAs and other ligands would help to delineate their respective roles in supporting FAO and lipid homeostasis.

Development of FABP5-specific drugs (as opposed to the FABP5/7 inhibitor used in these assays) would facilitate more precise pharmacological studies. There is currently a specific FABP5 inhibitor in development for chemotherapy-induced peripheral neuropathy(ART26.12), which is expected to begin clinical trials in 2025. Inhibition of FA import machinery (FATPs, FAT/CD36 and plasma membrane FABPs) could present another avenue for disrupting FA supply to the mitochondria and blocking FAO-fueled growth in TNBC. Multiple preclinical trials have assessed the impact of blocking CD36-mediated FA uptake using anti-CD36 antibodies, in mouse xenograft models of ovarian cancer [33] and of oral squamous cell carcinoma metastasis [34]. A small molecule CD36 inhibitor SMS121 has shown promise in impairing FA uptake and viability in acute myeloid leukemia cells [35]. Furthermore, in breast cancer CD36 and FABP4 have been shown to interact and regulate FA uptake, while also altering adipocyte metabolism in *indirect* co-culture models [36] (using transwell assays where a semipermeable barrier separates adipocytes from cancer cells, see *Chapter 4*). Future studies could evaluate the roles of CD36 and other FA uptake machinery, and of adipocytes in the tumor microenvironment, in supporting TNBC tumorigenesis [6,7]. As outlined in *Chapter 2*, *in vivo* models and approaches that

account for tumor microenvironment are critical for capturing tumor metabolism. A mechanistic role for direct cancer cell-adipocyte contact in TNBC tumorigenesis is described next in

Chapter 4.

Figures

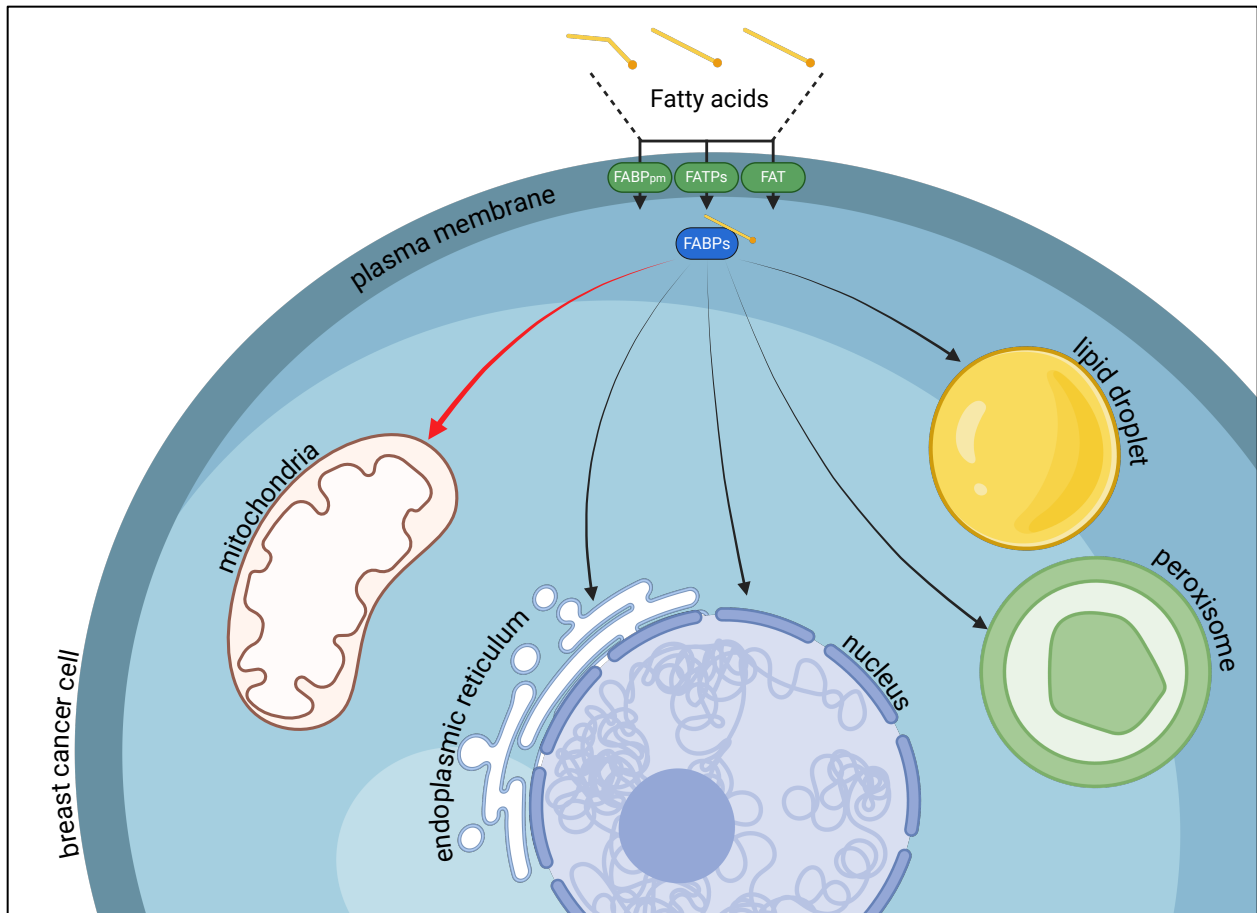


Figure 3.1. Schematic of fatty acid trafficking by fatty acid binding proteins (FABPs) in a breast cancer cell.

FA are imported into breast cancer cell via transport proteins including specialized plasma membrane fatty acid binding proteins (FABP_{pm}), fatty acid transport proteins (FATPs) and fatty acid translocase (FAT, or CD36). Fatty acid binding proteins (FABPs), some of which are specifically elevated in TNBC, traffic FA to cellular compartments including the nucleus, endoplasmic reticulum, peroxisomes, lipid droplets, and mitochondria[37].

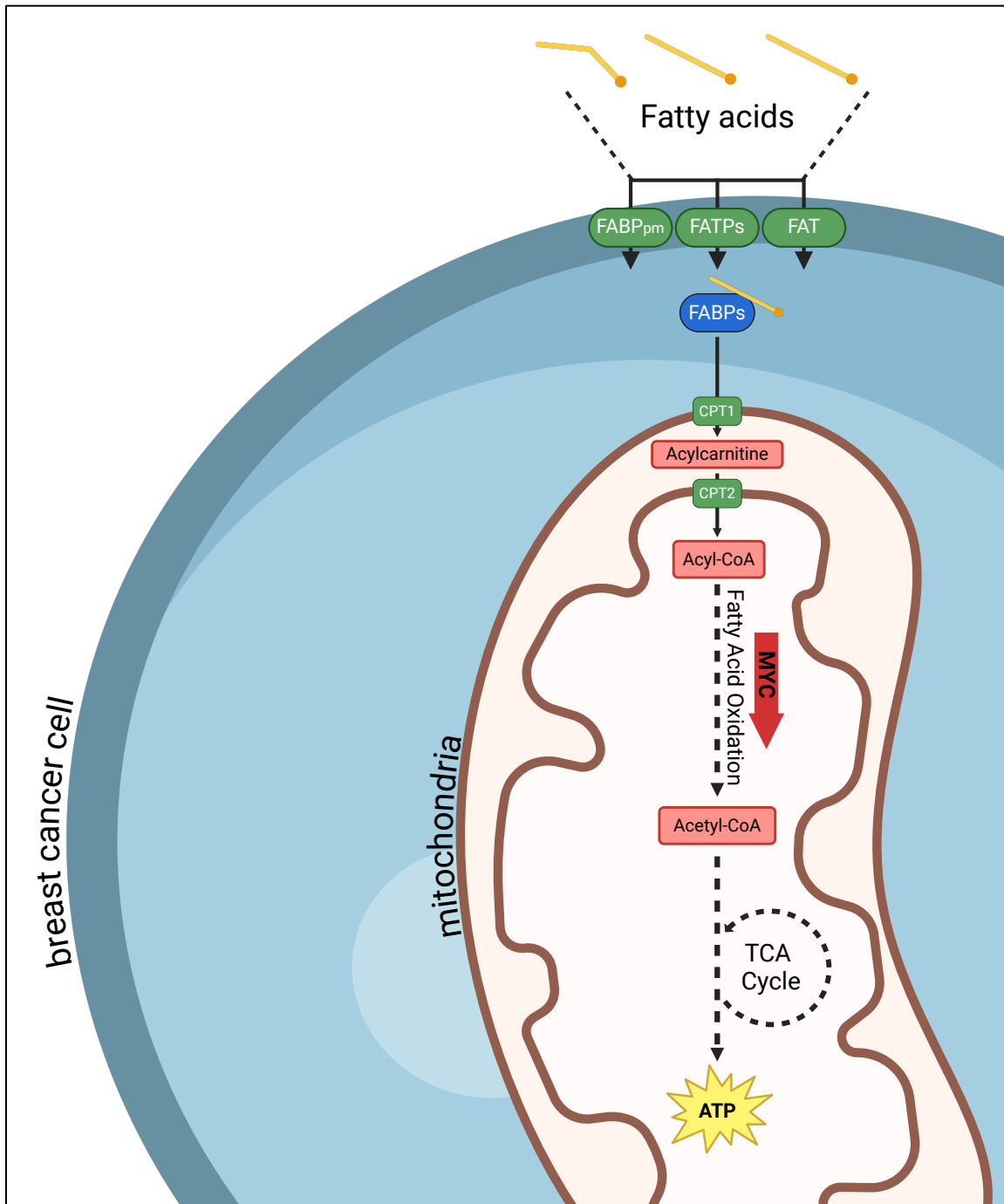


Figure 3.2. Schematic of fatty acid trafficking and mitochondrial fatty acid oxidation in a breast cancer cell.

FABP-bound FA trafficked to the mitochondrial membrane are then processed by carnitine palmitoyltransferase I (CPT1) to enter the intermembrane space as acylcarnitines, before CPT2 converts them to acyl-CoA for deposit into the mitochondrial matrix. In mitochondrial fatty acid oxidation, acyl-CoAs undergo beta-oxidation and are broken down into acetyl-CoA, which feeds the citric acid cycle (TCA Cycle), producing ATP[38].

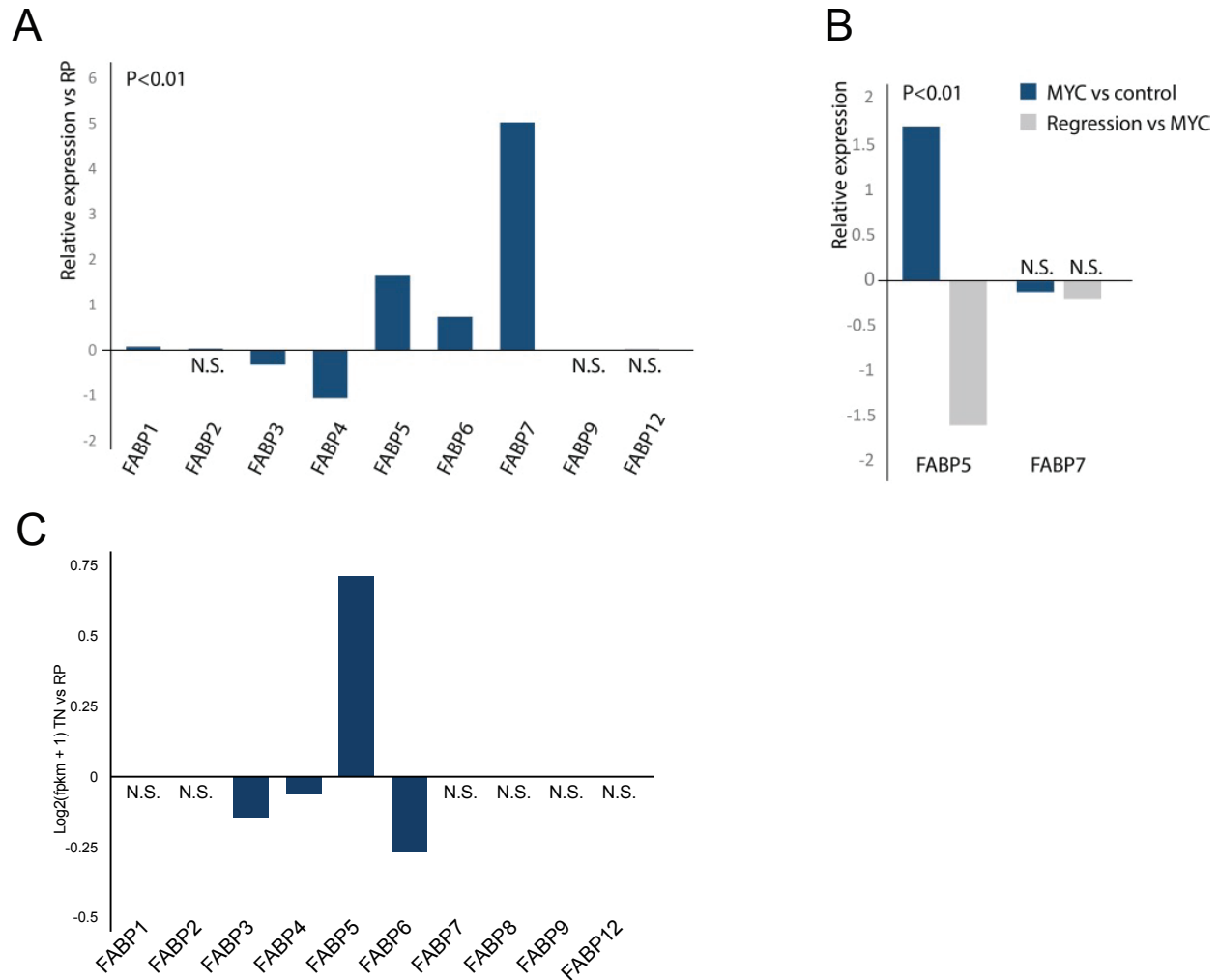


Figure 3.3. FABP5 expression is elevated in a MYC-dependent manner in TNBC.

(A) Fold change (\log_2) expression of indicated FABP genes in TN ($n = 123$) versus RP ($n = 648$) tumors based on RNA-seq data acquired from TCGA of 771 breast cancer patients[15]. (B) Fold change (\log_2) expression of indicated FABP genes in MTB- TOM MYC-high tumor versus control tissue (blue), and during tumor progression (dox administration) versus regression (dox withdrawal) (gray)[15]. (C) Fold change (\log_2) expression of indicated FABP genes from RNA-seq of patient-derived TN ($n = 4$) versus RP ($n = 2$) cell lines.

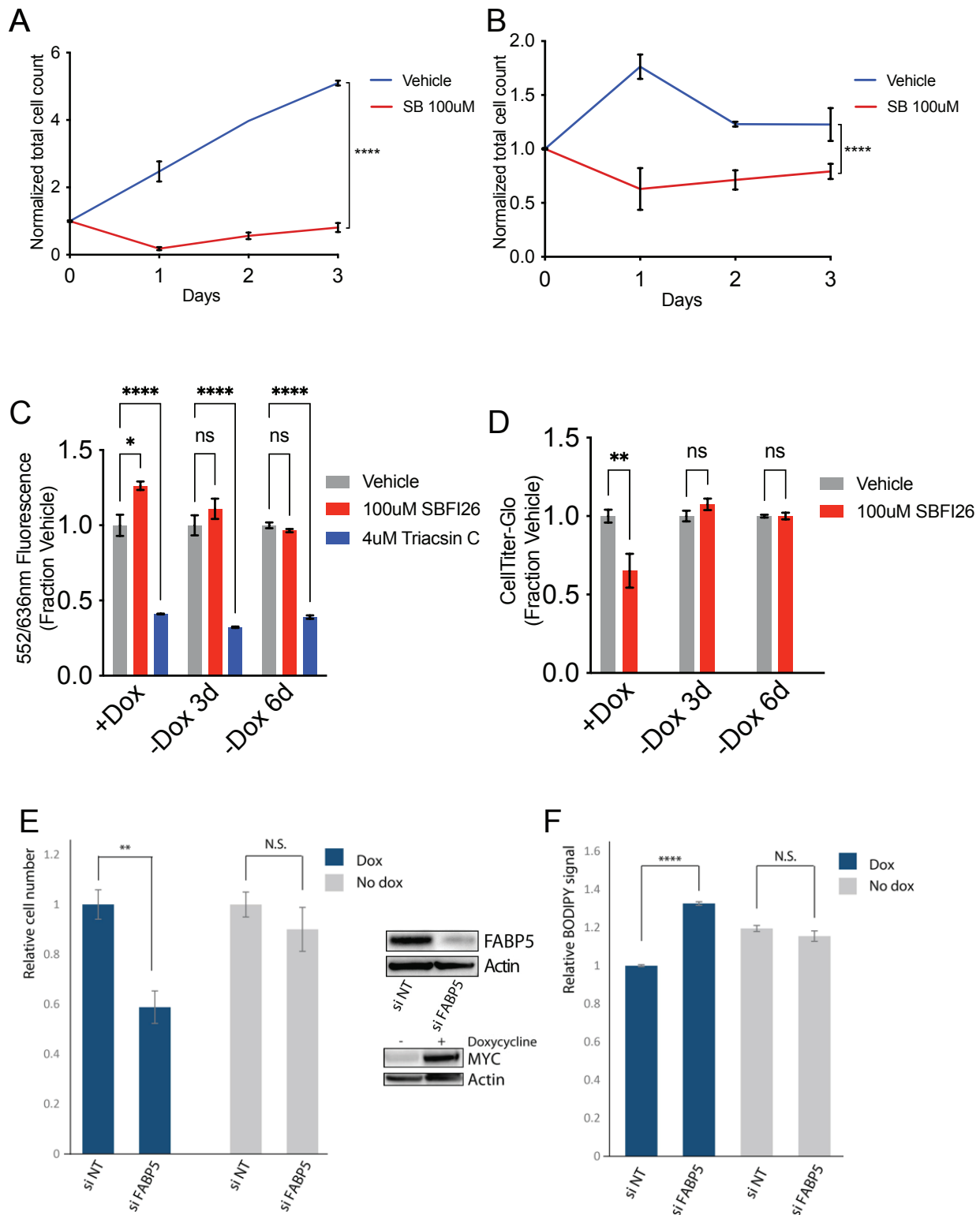


Figure 3.4. FABP5 inhibition and silencing selectively impair proliferation and lipid homeostasis in TNBC models. Figure caption continued on the next page.

Figure caption continued from the previous page. (A) Relative proliferation of MYC-high (+dox) MTB-TOM cells treated with vehicle or 100 μ M FABP5/7 inhibitor (SB); drug and doxycycline changed daily. (B) Relative proliferation of MYC-low (-dox) MTB-TOM cells treated with vehicle or 100 μ M FABP5/7 inhibitor (SB); drug and doxycycline changed daily. (C) Nile red signal in MTB-TOM cells with doxycycline (MYC-high) or after doxycycline removal (MYC withdrawal); cells treated 48H with indicated vehicle or drug; Triacsin C is a negative control for LD formation. (D) Total ATP (CellTiter-GLO) signal in MTB-TOM cells with doxycycline (MYC-high) or after doxycycline removal (MYC withdrawal); cells treated 48H with vehicle or inhibitor. (E) Relative cell counts in MYC-high (with dox) or MYC-low (without dox) MTB-TOM cells with indicated siRNA. Immunoblots (right) indicate protein levels for siRNA targets and for MYC[15]. (F) Relative intracellular lipid levels in MYC-high (with dox) or MYC-low (without dox) MTB-TOM cells with indicated siRNA[15].

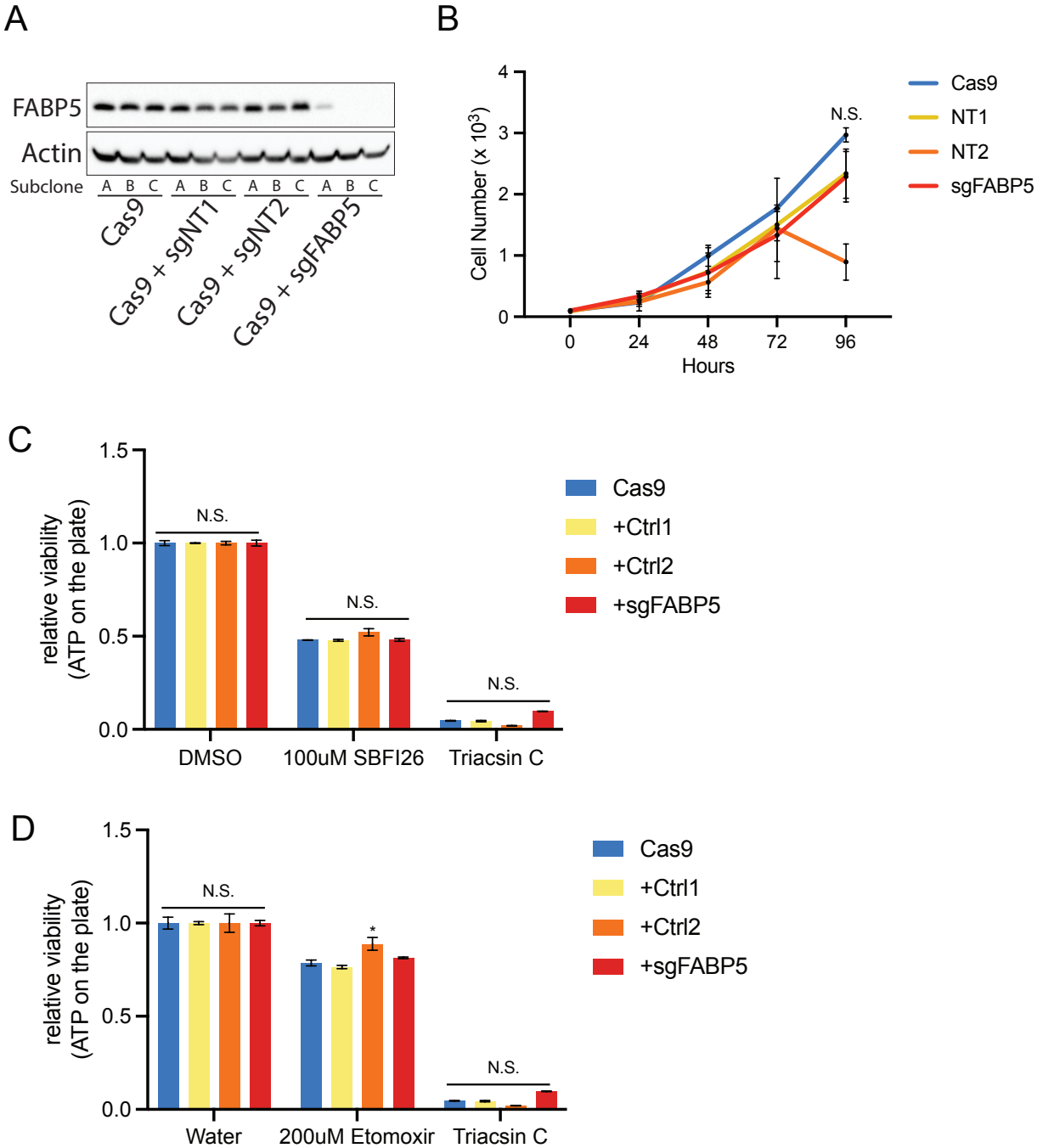


Figure 3.5. Prolonged FABP5 loss does not impair proliferation, or sensitize to FA trafficking or FA inhibition, in MTB-TOM.

(A) Immunoblot showing FABP5 expression in clonal MTB-TOM cell lines with CRISPR-Cas9 and indicated non-targeting or FABP5-targeting sgRNA. Respective subclones ‘B’ are used in subsequent panels. (B) Cell proliferation for indicated MTB-TOM cell lines; doxycycline changed daily. (C) Relative viability of indicated MTB-TOM cell lines (MYC-high; with dox) following 48H treatment with indicated vehicle or drug. Figure caption continued on the next page.

Figure caption continued from the previous page. (D) Relative viability of indicated MTB-TOM cell lines (MYC-high; with dox) following 48H treatment with indicated vehicle or drug. Etomoxir inhibits the comital step in fatty acid oxidation.

References

- 1 Yuneva, Mariia O. *et al.* The Metabolic Profile of Tumors Depends on Both the Responsible Genetic Lesion and Tissue Type. *Cell Metabolism* **15**, 157-170 (2012). <https://doi.org/10.1016/j.cmet.2011.12.015>
- 2 Ellwood-Yen, K. *et al.* Myc-driven murine prostate cancer shares molecular features with human prostate tumors. *Cancer Cell* **4**, 223-238 (2003). [https://doi.org/10.1016/s1535-6108\(03\)00197-1](https://doi.org/10.1016/s1535-6108(03)00197-1)
- 3 Stine, Z. E., Walton, Z. E., Altman, B. J., Hsieh, A. L. & Dang, C. V. MYC, Metabolism, and Cancer. *Cancer Discov* **5**, 1024-1039 (2015). <https://doi.org/10.1158/2159-8290.Cd-15-0507>
- 4 Xiang, Y. *et al.* Targeted inhibition of tumor-specific glutaminase diminishes cell-autonomous tumorigenesis. *The Journal of Clinical Investigation* **125**, 2293-2306 (2015). <https://doi.org/10.1172/JCI75836>
- 5 Camarda, R., Williams, J. & Goga, A. In vivo Reprogramming of Cancer Metabolism by MYC. *Frontiers in Cell and Developmental Biology* **5**, 1-13 (2017). <https://doi.org/10.3389/fcell.2017.00035>
- 6 Camarda, R. *et al.* Inhibition of fatty acid oxidation as a therapy for MYC-overexpressing triple-negative breast cancer. *Nat Med* **22**, 427-432 (2016). <https://doi.org/https://10.1038/nm.4055>
- 7 Park, J. H. *et al.* Fatty Acid Oxidation-Driven Src Links Mitochondrial Energy Reprogramming and Oncogenic Properties in Triple-Negative Breast Cancer. *Cell Reports* **14**, 2154-2165 (2016). <https://doi.org/10.1016/j.celrep.2016.02.004>

- 8 Balaban, S., Lee, L. S., Schreuder, M. & Hoy, A. J. Obesity and cancer progression: Is there a role of fatty acid metabolism? *BioMed Research International* **2015** (2015).
<https://doi.org/10.1155/2015/274585>
- 9 Furuhashi, M. & Hotamisligil, G. S. Fatty acid-binding proteins: Role in metabolic diseases and potential as drug targets. *Nature Reviews Drug Discovery* **7**, 489-503 (2008). <https://doi.org/10.1038/nrd2589>
- 10 Chmurzyńska, A. The multigene family of fatty acid-binding proteins (FABPs): Function, structure and polymorphism. *Journal of Applied Genetics* **47**, 39-48 (2006).
<https://doi.org/10.1007/BF03194597>
- 11 Anderson, C. & Stahl, A. SLC27 fatty acid transport proteins. *Molecular aspects of medicine* **34**, 516-528 (2013). <https://doi.org/10.1016/j.mam.2012.07.010.SLC27>
- 12 Smathers, R. & DR, P. The human fatty acid-binding protein family: Evolutionary divergences and functions. *Human genomics* **5**, 485-496 (2011).
<https://doi.org/10.1186/1479-7364-5-3-170>
- 13 Veerkamp, J. H., van Moerkerk, H. T. Molecular and cellular biochemistry. *Molecular and Cellular Biochemistry* **123**, 101-106 (1993).
- 14 Amiri, M. *et al.* Diverse roles of fatty acid binding proteins (FABPs) in development and pathogenesis of cancers. *Gene* **676**, 171-183 (2018).
<https://doi.org/https://doi.org/10.1016/j.gene.2018.07.035>
- 15 Mahieu, C. *The story of a power couple: importance of FABP5 and MYC for fatty acid oxidation in triple negative breast cancer*, University of California, San Francisco, (2015).

- 16 Liu, R. Z. *et al.* Association of FABP5 expression with poor survival in triple-negative breast cancer: Implication for retinoic acid therapy. *American Journal of Pathology* **178**, 997-1008 (2011). <https://doi.org/10.1016/j.ajpath.2010.11.075>
- 17 D'Cruz, C. M. *et al.* c-MYC induces mammary tumorigenesis by means of a preferred pathway involving spontaneous Kras2 mutations. *Nature medicine* **7**, 235-239 (2001). <https://doi.org/10.1038/84691>
- 18 Neve, R. M. *et al.* A collection of breast cancer cell lines for the study of functionally distinct cancer subtypes. *Cancer Cell* **10**, 515-527 (2006). <https://doi.org/10.1016/j.ccr.2006.10.008>
- 19 Al-Jameel, W. *et al.* Inhibitor SBFI26 suppresses the malignant progression of castration-resistant PC3-M cells by competitively binding to oncogenic FABP5. *Oncotarget* **8**, 31041-31056 (2017). <https://doi.org/10.18632/oncotarget.16055>
- 20 Greenspan, P., Mayer, E. P. & Fowler, S. D. Nile red: a selective fluorescent stain for intracellular lipid droplets. *J Cell Biol* **100**, 965-973 (1985). <https://doi.org/10.1083/jcb.100.3.965>
- 21 Adamson, J. *et al.* High-level expression of cutaneous fatty acid-binding protein in prostatic carcinomas and its effect on tumorigenicity. *Oncogene* **22**, 2739-2749 (2003). <https://doi.org/10.1038/sj.onc.1206341>
- 22 Fujii, K. *et al.* Proteomic study of human hepatocellular carcinoma using two-dimensional difference gel electrophoresis with saturation cysteine dye. *Proteomics* **5**, 1411-1422 (2005). <https://doi.org/10.1002/pmic.200401004>

- 23 Han, J. *et al.* Identification of potential therapeutic targets in human head & neck squamous cell carcinoma. *Head & Neck Oncology* **1**, 27 (2009).
<https://doi.org/10.1186/1758-3284-1-27>
- 24 Ohyama, Y. *et al.* Differential expression of fatty acid-binding proteins and pathological implications in the progression of tongue carcinoma. *Molecular and clinical oncology* **2**, 19-25 (2014). <https://doi.org/10.3892/mco.2013.198>
- 25 Seliger, B. *et al.* Identification of fatty acid binding proteins as markers associated with the initiation and/or progression of renal cell carcinoma. *Proteomics* **5**, 2631-2640 (2005). <https://doi.org/10.1002/pmic.200401264>
- 26 Goto, Y. *et al.* Aberrant fatty acid-binding protein-7 gene expression in cutaneous malignant melanoma. *Journal of Investigative Dermatology* **130**, 221-229 (2010).
<https://doi.org/10.1038/jid.2009.195>
- 27 Kawaguchi, K. *et al.* High expression of Fatty Acid-Binding Protein 5 promotes cell growth and metastatic potential of colorectal cancer cells. *FEBS Open Bio* **6**, 190-199 (2016). <https://doi.org/10.1002/2211-5463.12031>
- 28 Fang, L.-Y., Wong, T.-Y., Chiang, W.-F. & Chen, Y.-L. Fatty-acid-binding protein 5 promotes cell proliferation and invasion in oral squamous cell carcinoma. *Journal of Oral Pathology & Medicine* **39**, 342-348 (2009). <https://doi.org/10.1111/j.1600-0714.2009.00836.x>
- 29 Zhang, H. *et al.* The proteins FABP7 and OATP2 are associated with the basal phenotype and patient outcome in human breast cancer. *Breast Cancer Research and Treatment* **121**, 41-51 (2010). <https://doi.org/10.1007/s10549-009-0450-x>

- 30 Slipicevic, A. *et al.* The fatty acid binding protein 7 (FABP7) is involved in proliferation and invasion of melanoma cells. *BMC Cancer* **8**, 1-13 (2008).
<https://doi.org/10.1186/1471-2407-8-276>
- 31 Hotamisligil, G. S. *et al.* Uncoupling of Obesity from Insulin Resistance Through a Targeted Mutation in $\alpha P2$, the Adipocyte Fatty Acid Binding Protein. *Science* **274**, 1377 LP - 1379 (1996).
- 32 Jing, C. *et al.* Human Cutaneous Fatty Acid-binding Protein Induces Metastasis by Up-Regulating the Expression of Vascular Endothelial Growth Factor Gene in Rat Rama 37 Model Cells Human Cutaneous Fatty Acid-binding Protein Induces Metastasis by Up-Regulating the Expressi. *Cancer research*, 4357-4364 (2001).
- 33 Ladanyi, A. *et al.* Adipocyte-induced CD36 expression drives ovarian cancer progression and metastasis. *Oncogene* **37**, 2285-2301 (2018). <https://doi.org/10.1038/s41388-017-0093-z>
- 34 Pascual, G. *et al.* Targeting metastasis-initiating cells through the fatty acid receptor CD36. *Nature* **541**, 41-45 (2017). <https://doi.org/10.1038/nature20791>
- 35 Åbacka, H. *et al.* SMS121, a new inhibitor of CD36, impairs fatty acid uptake and viability of acute myeloid leukemia. *Scientific Reports* **14**, 9104 (2024).
<https://doi.org/10.1038/s41598-024-58689-1>
- 36 Gyamfi, J. *et al.* Interaction between CD36 and FABP4 modulates adipocyte-induced fatty acid import and metabolism in breast cancer. *npj Breast Cancer* **7**, 129 (2021).
<https://doi.org/10.1038/s41523-021-00324-7>
- 37 Created in BioRender. Williams, J.L. (2024). <https://BioRender.com/z80v807>
- 38 Created in BioRender. Williams, J.L. (2024). <https://BioRender.com/j76o085>

**Chapter 4: Defining a new role for surrounding
adipocytes in TNBC tumor growth**

A version of this chapter was published as:
Williams, J.L., Camarda R., et al. (2024). "**Tumor cell-adipocyte gap junctions activate lipolysis and contribute to breast tumorigenesis.**" [bioRxiv: 277939](https://doi.org/10.1101/277939).

Abstract

A pro-tumorigenic role for adipocytes has been identified in breast cancer, and reliance on fatty acid catabolism found in aggressive tumors. The molecular mechanisms by which tumor cells coopt neighboring adipocytes, however, remain elusive. Here, we describe a direct interaction linking tumorigenesis to adjacent adipocytes. We examine breast tumors and their normal adjacent tissue from several patient cohorts, patient-derived xenografts and mouse models, and find that lipolysis and lipolytic signaling are activated in neighboring adipose tissue. We find that functional gap junctions form between breast cancer cells and adipocytes. As a result, cAMP is transferred from breast cancer cells to adipocytes and activates lipolysis in a gap junction-dependent manner. We identify connexin 31 (GJB3), which promotes receptor triple negative breast cancer growth and activation of lipolysis *in vivo*. Thus, direct tumor cell-adipocyte interaction contributes to tumorigenesis and may serve as a new therapeutic target in breast cancer.

Main Text

A variety of cancers, including those of the breast, arise near or within adipose tissue depots [1]. Therefore, during tumor development a heterotypic cell-cell interface exists between adipocytes and cancer cells in these organs. We and others have demonstrated that triple-negative breast cancers (TNBC, estrogen/progesterone/HER2 receptor-negative) utilize and require fatty acid oxidation to fuel bioenergetic metabolism [2,3]. The origin of fatty acids which meet this necessity remains largely unclear. Adipocyte lipolysis has been linked by several studies to

secretion of pro-tumorigenic cytokines by cancer-associated adipocytes, including elevation of pro-inflammatory signals such as tumor necrosis factor- α [4-11]. Multiple models provide evidence that these adipocyte-derived fatty acids can be taken up and oxidized by proximate cancer cells [4-10,12]. These studies, however, have widely modeled the cancer-adipocyte interface *in vitro* using transwell co-culture methods that cannot recapitulate the direct cell-cell contact observed *in vivo* [6-9,11-13]. Furthermore, clinical evidence for elevated lipolysis in breast tumor-adjacent adipocytes has not been well established. Mammary adipocytes undergo enhanced lipolysis when in close proximity to non-tumor epithelial cells, suggesting that local pro-lipolytic mechanisms exist, but have yet to be identified between tumor cells and adipocytes [5,14]. Thus, we set out to study the breast cancer-adipocyte interface and determine the contribution of cell-cell contact to tumorigenesis.

To determine if lipolysis occurs in normal tissue adjacent to breast tumors (NAT) which includes adipocytes, we employed four independent strategies. First, we employed three-component breast (3CB) composition measurement, a radiographic imaging method derived from dual-energy mammography that allows for quantification of a tissue's water, lipid and protein content [15]. We postulated that, if tumors induce lipolysis in adipocytes, we will observe differences in lipid content between NAT nearer the tumor and NAT farther away. Using 3CB imaging, we assessed the lipid content of breast tumors and the first 6 mm of surrounding NAT, segmented into 2 mm "rings," from 46 patients with invasive breast cancer (**Fig 4.1A** and **Table S4.1**). As we have previously demonstrated [16], we found a significant decrease in lipid content in tumor lesions compared to NAT 0-2 mm away (R1) (**Fig 4.1B**). This difference is congruent with breast tumors being epithelial in nature, while adipose tissue is the major constituent of normal

breast [14]. Remarkably, we also found that within NAT there was a significant stepwise decrease in lipid content comparing R3 (4-6 mm) to R2 (2-4 mm), and R2 to R1 (**Fig 4.1B**). In addition, we asked whether changes in lipid content between R3 and R1 NAT correlate with receptor status or tumor grade (**Table S4.1**). We found that NAT surrounding triple-negative (TN) and grade 2/3 tumors trended towards a greater average decrease in lipid content between R3 and R1 than NAT surrounding receptor-positive (RP) and grade 1 tumors, respectively (**Fig S4.1, A and B**). These data suggest that adipocytes near breast tumors have partially depleted lipid stores, and that TN and higher-grade tumors may induce this phenomenon to a greater degree than RP and low-grade tumors. We quantified average adipocyte size in R1 and R3 in the 11 of the 46 patients imaged with 3CB for whom we had access to histological sections of treatment-naïve tumor and NAT at the time of surgical resection (**Fig 4.1A, Fig S4.1C and Table S4.1**). Similar to the change in lipid content observed with 3CB, we found a significant decrease in adipocyte size in R1 compared to R3 in all patients analyzed, suggesting adipocytes are smaller when nearer to breast tumors (**Fig 4.1C**). Finally, we correlated the change in lipid content and adipocyte size on an individual patient basis. We found a marked positive correlation ($R = 0.5818$, $p = 0.0656$) between the change in lipid content and adipocyte area (**Fig 4.1D**). Taken together, these data suggest adipocytes are smaller and have diminished lipid content, two phenotypes that are established indicators of lipolysis [17], when adjacent to breast tumors.

Second, we sought to determine if gene expression changes associated with lipolysis were observed in tumor-adjacent adipocytes. We generated a lipolysis gene expression signature by identifying the 100 genes most upregulated when a differentiated adipocyte cell culture model is stimulated with cAMP, a critical pro-lipolytic signaling molecule [18]. We then used a publicly

available gene expression dataset for primary breast tumors as well as matched NAT 1, 2, 3 and 4 cm away, to determine if enrichment of the lipolysis signature occurred in NAT in comparison to non-tumor breast tissue obtained from healthy individuals using single-set gene set enrichment analysis [19,20]. We found a significant elevation of the cAMP-dependent lipolysis signature in tumor and NAT from all analyzed regions compared to control tissue (**Fig 4.1E**). These data indicate that lipolytic signaling is activated in breast-tumor adjacent adipocytes up to 4 cm away from the primary tumor. While adipose tissue is sparsely innervated, a recent study found that adipocytes can propagate pro-lipolytic sympathetic signals via direct transfer of cAMP through adipocyte-adipocyte gap junctions [21]. We observed elevation of cAMP signaling up to 4 cm away from patient tumors (**Fig 4.1E**), suggesting that tumor-adjacent adipocytes might also disperse a pro-lipolytic stimulus to distant adipocytes via gap junctions.

Third, we sought to determine if there are changes to protein abundance in tumor-adjacent NAT indicative of lipolysis activation. We conducted laser capture microdissection (LCM, 10,000 cells per capture) on primary breast tumors from 75 patients, representing all major PAM50 subtypes. For a subset of patients, we also collected matched stroma and/or NAT. As a control, we conducted LCM on non-tumor breast tissue from 42 healthy subjects (**Table S4.3A**). Global proteomic analysis was performed using liquid chromatography-tandem mass spectrometry (LC-MS/MS) (**Table S4.3B**). Notably, one of the most significantly upregulated proteins in NAT, and indeed one of the most NAT-specific proteins, compared to all other tissues examined was hepatocyte nuclear factor 4- α (HNF4 α) (**Fig 4.1F**). As HNF4 α is an established, essential activator of lipolysis in adipose tissue [22], these data indicate lipolysis is robustly activated in breast-tumor adjacent adipose tissue.

Fourth, we sought to validate the observations made in our clinical datasets using mouse models of breast cancer. Hormone sensitive lipase (HSL) is a critical lipolytic enzyme; its activation by cAMP-dependent protein kinase A (PKA) leads to phosphorylation at serine 563 [17,18], while prolonged activation results in down-regulation of total HSL expression through a negative feedback mechanism [23,24]. We performed immunoblot analysis to probe for HSL, phospho-HSL (S563) and HNF4 α in tumor and NAT, as well as corresponding control mammary tissues, from three well-characterized breast cancer patient-derived xenograft (PDX) models (HCI002, HCI009, HCI010) and a transgenic model of MYC-driven TNBC (MTB-TOM) [25,26]. In all models analyzed, a downregulation of total HSL in NAT compared to control tissue was observed (**Fig 4.1, G and H**). Downregulation of total HSL has been observed in obesity and in an independent analysis of primary breast tumor NAT, and is thought to be the result of a negative feedback loop in adipocytes in response to chronic lipolysis [23,24]. Additionally, in 3 of the 4 models examined we found an increase in HNF4 α protein or in phospho-HSL/total HSL ratio (**Fig 4.1, G and H**), both characteristic of increased lipolysis [17,22]. Taken together, our concurrent findings in 3 independent clinical datasets and several models of patient-derived and transgenic breast cancers in mice indicate that lipolysis is activated, to varying degrees, in breast cancer-adjacent adipose tissue. These findings support the conclusion that “normal” tissue adjacent to tumors is, in fact, not normal [27]; in the context of breast cancer, tumor-adjacent adipocytes have markers of activated lipolysis with corresponding diminished lipid stores.

We next sought to determine the contribution of cell-cell contact to lipolysis activation in breast tumor-adjacent adipocytes. Gap junctions are cell-cell junctions formed by a family of proteins

called connexins, which are known to transport a variety of small molecules (<1 kD), including cAMP [21,28]. Connexins were long thought to play tumor-suppressive roles in cancer, but recent evidence from a variety of tumor types has challenged this notion [28-31]. Given that adipocytes are capable of transferring cAMP and activating lipolysis in a homotypic interaction with other adipocytes[21], we hypothesized that gap junctions may also form between tumor cells and adipocytes in a heterotypic fashion to activate lipolysis via transfer of cAMP. Using a well-established dye transfer assay [30], we first probed for functional gap junction formation between breast cancer cells. We tested whether the TNBC cell line HCC1143 or the more indolent RP cell line T47D could transfer gap-junction dependent dyes to the same tumor cell line. Both lines formed functional gap junctions, but dye transfer between HCC1143 cells was 30-fold increased (**Fig 4.2A**) compared to transfer amongst T47D cells. Thus, we reasoned there may be differences in sensitivity to gap junction inhibition between TN and RP cells. Furthermore, given the upregulation of MYC in the majority of TNBC [32,33], we asked whether MYC expression affects gap junction dependence. We examined if gap junction inhibition alters cellular ATP as a proxy for cell abundance in a panel of TN and RP human breast cell lines with varying MYC levels [2]. Intriguingly, TNBC cell lines with high MYC expression [2], including HCC1143, were significantly more sensitive to 24 hours of treatment with the pan-gap junction inhibitor carbenoxolone (CBX) than the low MYC TNBC or RP cell lines tested (**Fig 4.2B**). In addition, dye uptake in HCC1143 cells was significantly reduced (30.63%, $p < 0.0001$) following treatment with CBX (**Fig 4.2C**). These data suggest that gap junction communication occurs between breast cancer cells, and that a threshold amount of gap junction activity may be required for high MYC TN cell viability.

To delineate the role of connexins in TN compared to RP breast cancer further, we examined the expression of the 21 connexin genes in 771 primary human breast cancers, TN ($n = 123$) and RP ($n = 648$), using publicly available RNA-seq data from The Cancer Genome Atlas (TCGA). Of the 20 connexins for which data was available, 5/20 were significantly downregulated, and 11/20 were significantly upregulated. These 11 upregulated connexins included 5 of the 7 gap junction B (GJB) family members (**Fig 4.2D**). To probe gap junction expression at the cellular level, we also examined scRNA-seq ($n=317$) of primary patient tumors ($n=11$) [34]. Expression of GJBs was observed in a greater fraction (47.2% vs. 29.8%) of TN than RP tumor cells, and GJBs were the most frequently expressed gap junction family for TN, but not for RP tumor cells (**Fig 4.2E** and **Fig S4.2**). As an independent approach to examine *in vivo* expression of connexins in TNBC, we then performed RNA-seq on MTBTOM tumors and non-tumor control tissue (**Table S4.4**). Of the 10 connexins for which data were available, 2/10 were significantly downregulated, 4/10 were significantly upregulated, and 4/10 were not significantly changed in MTBTOM tumors versus control tissue (**Fig 4.2F**). Connexin 31 (*GJB3*, Cx31) was the most significantly elevated connexin in both human TN tumors and the MYC-driven TNBC model. Thus, we focused the remainder of our studies on Cx31. Cx31 has been found to be expressed in keratinocytes, the small intestine, and the colon [35,36]. Although roles for various connexins as oncogenes and/or tumor suppressors have been described [28,29], a pro-tumorigenic function of Cx31 has not been established.

Accordingly, we sought to determine if functional Cx31-containing gap junctions form between breast cancer cells and adipocytes. To validate the presence of cancer-adipocyte gap junctions in TNBC, we began by examining primary patient biopsies for expression of Cx31 and of pan-

cytokeratin to distinguish epithelial tumor cells. We found that both TN tumor cells and adipocytes robustly express Cx31 at the plasma membrane. Further, we found many points of cell-cell contact occurred *in vivo* between tumors and adipocytes (**Fig 4.3A**). To model the cell-cell contact observed *in vivo* between breast cancer cells and adipocytes, we developed three independent co-culture models. First, we performed 3-dimensional *ex vivo* studies by co-culturing breast cancer cells directly within primary patient breast fat (**Fig 4.3B**). We stably transduced HCC1143 (TNBC) and T47D (RP) with an mCherry expression plasmid, then injected either mCherry-HCC1143 or -T47D cells directly into mammary adipose tissue (WD43177) and co-cultured overnight. Tumor cell-adipocyte co-cultures were formalin-fixed, paraffin-embedded and probed for Cx31 and pan-cytokeratin expression, then imaged using immunofluorescent microscopy. We found that both HCC1143 cells and adipocytes robustly expressed Cx31 at the plasma membrane; HCC1143 formed close cell-cell contacts with primary adipocytes (**Fig 4.3B**, top). In contrast, while T47D cells formed cancer cell-cancer cell contacts, we did not observe close cancer cell-adipocyte contacts (**Fig 4.3B**, bottom). These data suggest that Cx31 can be expressed at both the tumor cell and adipocyte plasma membrane, and that breast cancer cells can form close cell-cell contacts with adipocytes.

To determine whether breast cancer cells rely upon Cx31-containing gap junctions to influence adipocyte function, we used CRISPR/Cas9 to generate a series of *GJB3* depleted TN lines (HS578T and HCC1143). In TN MYC-high TN cell line HCC1143, we generated two clones, with $\sim 1/3$ and $\sim 2/3$ *GJB3* expression loss (HCC1143 *GJB3*^{Med} and *GJB3*^{Low}). In TN MYC-low line HS578T, we generated two distinct clones with $\sim 1/3$ *GJB3* expression loss (HS578T *GJB3*^{Med-1} and *GJB3*^{Med-2}). Despite several attempts we were unable to generate TN cell lines

with complete Cx31 loss, strongly suggesting that a basal level of Cx31 expression is required for TN cancer cell growth.

To examine how Cx31 expression impacted cancer cell-adipocyte contact, we performed *ex vivo* co-cultures with primary patient breast fat using the partially depleted Cx31 cell lines. We stably transduced TN HCC1143 *GJB3^{WT}* and *GJB3^{Low}* cell lines, as well as RP line T47D with a GFP expression plasmid, then injected each line directly into primary mammary adipose tissue (WD49393). After overnight incubation, co-cultured tissues were formalin-fixed and probed for expression of Cx31 and lipolysis marker pHSL(S563) [17]. Tissues were then cleared [37] and imaged via whole mount fluorescence microscopy. We found that HCC1143 *GJB3^{WT}* cells formed extended cancer cell-adipocyte contacts, in tight conformation with adjacent adipocytes (**Fig 4.3D**, top). In contrast, Cx31-depleted HCC1143 *GJB3^{Low}* cells formed tangential contacts with adjacent adipocytes (**Fig 4.3D**, middle), which we note closely mimic the tangential cancer cell-adipocyte conformation observed in T47D (RP) co-cultures (**Fig 4.3D**, bottom). In mock co-cultures, our positive control forskolin, which raises intracellular cAMP levels by activating adenylyl cyclase [18], robustly induced pHSL(S563) expression and increased puncta compared to vehicle-treated mammary adipose tissue (**Fig S4.3, A-C**). We observed greater pHSL(S563) expression and elevated puncta in adipose tissue co-cultured with HCC1143 *GJB3^{WT}* cells than tissues with HCC1143 *GJB3^{Low}* or T47D cells (**Fig S4.3, D and E**), indicating more cAMP-dependent PKA activity. These results suggest that Cx31 level in breast cancer can moderate cell contact with surrounding adipocytes and alter lipolytic signaling.

We next sought to determine if Cx31 expression impacted tumor cell-adipocyte communication using a co-culture model in which HCC1143 *GJB3^{WT}*, *GJB3^{Med}* or *GJB3^{Low}* cells were seeded in 2D culture and loaded with gap junction-transferable dye. We added primary mammary adipose tissue from three healthy individuals (WD42295, WD43911, WD50223) directly on top of the monolayers to permit direct contact. Tumor cells and adipocytes were co-cultured for 5 hours and then assayed for gap junction-dependent dye transfer from the cancer cells to adipocytes. We found that robust dye transfer occurred from the HCC1143 *GJB3^{WT}* cells to mammary adipocytes from all three patients (**Fig 4.3E**). However, depletion of Cx31 expression by 1/3 or 2/3 in the *GJB3^{Med}* and *GJB3^{Low}* lines, respectively, resulted in a significant decrease in dye transfer compared to *GJB3^{WT}* control cells (**Fig 4.3E**). These data suggest that functional gap junctions form between TN breast cancer cells and adipocytes in a Cx31-dependent manner.

To determine if breast cancer cell gap junctions are permeable to cAMP, we treated a panel of human TN and RP cell lines with CBX for 24 hours to inhibit pan-gap junction function and ascertain if cAMP was retained in the tumor cells. In 5 of 6 lines tested we found marked increases in the levels of intracellular cAMP concentration in CBX- versus vehicle-treated cells (**Fig 4.3F**). Additionally, significantly higher concentrations of cAMP were observed in high MYC TN cells in comparison to low MYC TN or RP cells (**Fig 4.3F**). The increase in intracellular cAMP upon pan-gap junction inhibition in 5 of 6 lines examined suggests that breast cancer cell gap junctions are indeed permeable to cAMP.

We next tested whether cAMP is directly transferred from breast cancer cells to adipocytes and if the abundance of Cx31 alters transfer. HCC1143 *GJB3^{WT}*, *GJB3^{Med}* or *GJB3^{Low}* cells were seeded

and loaded with a fluorescent cAMP analogue (fluo-cAMP). These monolayer cultures were then co-cultured in direct contact with primary mammary adipose tissue from three healthy individuals (WD47558, WD46812, WD50344), and incubated for 5 hours. Adipocytes were then isolated from the tumor cells and assayed for fluo-cAMP. We found that cAMP transfer occurred from control cells to adipocytes from all three patients (**Fig 4.3G**). However, as we observed with transfer of gap junction-permeable dye (**Fig 4.3E**), depletion of Cx31 resulted in a significant reduction of cAMP transfer (**Fig 4.3G**). Thus, cAMP is transferred from TN breast cancer cells to adipocytes in a Cx31-dependent manner.

We next sought to determine if downstream cAMP signaling is activated in adipocytes in a tumor-adipocyte gap junction-dependent manner. To determine if cAMP signaling is activated in adipocytes upon cell-cell contact with breast cancer cells, we used a primary mouse preadipocyte model that can be differentiated to adipocytes *in vitro* [18,38]. This model is ideal to study downstream signaling during co-culture because changes in adipocyte transcription can be assayed via qRT-PCR using murine-specific primers. Adipocytes were terminally differentiated and then HS578T and HCC1143 *GJB3* partial depletion cell lines were seeded directly on top of adipocyte cultures. After co-culturing the cells for 24 hours we extracted RNA and assayed for changes in murine-specific (thus adipocyte-specific in this system) expression of UCP1, a known cAMP-responsive gene in adipocytes [18], to measure cAMP signaling. We also assayed for mouse aP2 expression as a marker of adipocyte differentiation. Our positive control, forskolin, robustly induced UCP1 expression compared to vehicle-treated cells (**Fig 4.3H**). The HCC1143 *GJB3*^{WT} and *GJB3*^{Med} lines both induced adipocyte UCP1 expression, but UCP1 induction was significantly reduced in the *GJB3*^{Low} co-cultures (**Fig 4.3H**). In contrast, none of the HS578T

lines, including the *GJB3^{WT}* control, were capable of inducing UCP1 expression (**Fig 4.3H**). All conditions, including forskolin treatment, resulted in reduced aP2 expression (**Fig 4.3H**), suggesting effects on adipocyte differentiation are distinct from those observed on cAMP signaling. Given that Cx31 expression is similar in HS578T *GJB3^{WT}* and HCC1143 *GJB3^{Low}* cells (**Fig 4.3C**), and that neither activate cAMP signaling (**Fig 4.3H**), it is possible that a Cx31 expression threshold is required for breast cancer cells to activate cAMP signaling in adjacent adipocytes. Although direct transfer of cAMP among adipocytes in a homotypic interaction has been described [21], this is the first description of gap junction-dependent activation of adipocyte lipolysis in a heterotypic manner, by a tumor cell.

Finally, we sought to determine the contribution of breast cancer Cx31-dependent gap junctions to tumorigenesis. We found that HS578T *GJB3^{Med-1}* and *GJB3^{Med-2}*, and HCC1143 *GJB3^{Med}* cell lines did not display a difference in proliferation compared to their respective *GJB3^{WT}* control lines (**Fig 4.4A**). In contrast, HCC1143 *GJB3^{Low}* cells demonstrate a significant reduction in proliferation, while maintaining 93.7% viability relative to Cas9 controls (**Fig 4.4A**). These data suggest that, even in the absence of breast cancer cell-adipocyte interaction, Cx31 may promote breast cancer cell proliferation. To determine the contribution of Cx31 to breast tumorigenesis *in vivo*, we transplanted each of the HS578T and HCC1143 Cx31 partial depletion lines into mammary fat pads of immunocompromised NOD-SCID/gamma (NSG) female mice and assayed for time of tumor onset and ethical endpoint (when tumor reaches 2cm in any dimension). Remarkably, with the HS578T lines, in which partial *GJB3* knockout had no effect on cell proliferation *in vitro* (**Fig 4.4A**), 0/10 mice that received HS578T *GJB3^{Med-1}* or *GJB3^{Med-2}* xenografts (5 per line) developed tumors within 180 days (**Fig 4.4B**). Among the HCC1143

lines, the *GJB3^{Med}* line displayed a significant delay in both tumor onset and time to ethical endpoint, while only 3 of 5 mice transplanted with the *GJB3^{Low}* line developed tumors, and none reached ethical endpoint within 180 days (**Fig 4.4B**). We performed an independent xenograft model wherein inducible Cx31 hairpins were transduced into the TN-MYC^{High} BT549 human breast cell line and found that Cx31 depletion significantly enhanced tumor-free survival compared to controls (**Fig 4.4C**). Our data indicate that decreasing Cx31 expression is sufficient to impair tumor growth, suggesting that gap junctions promote breast tumorigenesis *in vivo*.

We sought to clarify the effects of Cx31 on lipolysis versus other effects on tumor growth. To determine if control and Cx31 partial expression loss tumors differentially induced lipolysis, we collected tumor and NAT from HCC1143 *GJB3^{WT}*, *GJB3^{Med}* and *GJB3^{Low}* tumor-bearing mice, as well as residual mammary glands from the two *GJB3^{Low}* mice that were transplanted, but never developed tumors. Using immunoblot analysis, we probed for markers of lipolysis. Notably, a marked reduction in total HSL expression was found in 3 of 3 HCC1143 *GJB3^{WT}* NAT samples compared to control tissues (**Fig 4.4D**), consistent with persistent activation of lipolysis leading to HSL downregulation [23,24]. In contrast, we did not observe a consistent change in HSL expression in any of the other NAT samples analyzed from tumors with partial Cx31 expression loss (**Fig 4.4D**). Interestingly, we found a marked increase in phospho-HSL/HSL ratio in both the HCC1143 *GJB3^{WT}* and *GJB3^{Med}* NAT samples, but this difference was significantly reduced in HCC1143 *GJB3^{Low}* NAT (**Fig 4.4D**). The increase in phospho-HSL/HSL in *GJB3^{Med}* NAT may be due to alternative modes of lipolysis activation, such as secreted pro-lipolytic cytokines [4], which is congruent with the observed increase in UCP1 expression during *GJB3^{Med}*-adipocyte co-culture (**Fig 4.3H**). To further interrogate lipolytic

signaling in NAT, we probed for cAMP abundance in HCC1143 *GJB3^{WT}* and *GJB3^{Med}* tumors by mass spectrometry. We found a significant increase in intratumoral cAMP level in HCC1143 *GJB3^{Med}* tumors compared to the *GJB3^{WT}* control tumors (**Fig 4.4E**), consistent with diminished transfer of cAMP to NAT. We examined *GJB3^{WT}* and *GJB3^{Med}* tumors and associated NAT, and assayed for differences in adjacent adipocyte size, as an indicator of lipolysis. We found a significant increase in the average size of adipocytes adjacent to *GJB3^{Med}* tumors compared to *GJB3^{WT}* control tumors (**Fig 4.4F**), again supporting a decreased induction of lipolysis in NAT from Cx31 partial knockout tumors.

Finally, if the delay in HCC1143 *GJB3^{Med}* tumor onset (**Fig 4.4B**) was due to an inability to activate lipolysis in adjacent adipocytes, we reasoned that pharmacological activation of lipolysis should rescue this phenotype. Indeed, we found that daily intra-peritoneal injection of CL316243, a specific β 3-receptor agonist known to activate lipolysis *in vivo* [39], completely rescued the delay in tumor onset observed in HCC1143 *GJB3^{Med}* tumors, but did not further promote the growth of HCC1143 *GJB3^{WT}* tumors (**Fig 4.4G**). Taken together, these data indicate that cAMP signaling, and lipolysis are activated in breast tumor-adjacent adipocytes in a Cx31-dependent manner *in vivo*.

In summary, we find that lipolysis is activated in breast cancer-adjacent adipose tissue and that functional gap junctions form between breast cancer cells, and between breast cancer cells and adipocytes. In addition, cAMP is transferred via breast cancer cell gap junctions, and cAMP signaling is activated in adipocytes adjacent to breast cancer cells in a gap junction-dependent

manner. Finally, we established a previously unappreciated, functional role for Cx31-dependent gap junctions in promoting breast tumor growth and activation of lipolysis in tumor-adjacent adipose tissue *in vivo*, which may represent a new therapeutic target to treat pro-lipolytic breast tumors. Furthermore, the recent discovery of gap junction formation and pro-tumorigenic signal exchange between brain metastatic carcinoma cells and astrocytes [30] suggests that gap junction-dependent heterotypic interaction between tumor and non-tumor cells may be an emerging hallmark of tumorigenesis.

Materials and Methods

3CB patient population

Five hundred women with suspicious mammography findings (BIRADS 4 or greater) were recruited and imaged before their biopsies using a 3-compartment decomposition dual-energy mammography protocol (3CB). This was multicenter study with two recruitment sites:

University of California at San Francisco and Moffitt Cancer Center, Tampa, Florida. All patients received a biopsy of the suspicious area, and breast biopsies were clinically reviewed by the pathologists. A subset of pathology proven triple-negative ($n = 6$) and receptor-positive ($n = 40$) invasive cancers were selected for this study. All women received both cranio-caudal (CC) and mediolateral-oblique (MLO) views. Exclusion criteria for the study were no prior cancer, biopsies, or breast ipsilateral alterations, and no occult findings.

3CB imaging protocol

The 3CB method combines the dual-energy X-ray mammography attenuations and breast thickness map to solve for the three unknowns water, lipid, and protein content [15]. We used Hologic Selenia full-field digital mammography system (Hologic, Inc.) to image women with

3CB. Two dual energy mammograms were acquired on each woman's affected breast using a single compression. The first exposure was made under conditions of regular clinical screening mammogram. The second mammogram was acquired at a fixed voltage (39 kVp) and mAs for all participants. A high energy exposure (39 kVp/Rh filter) was made using an additional 3-mm plate of aluminum in the beam to increase the average energy of the high energy image. We limited the total dose of this procedure to be approximately 110% of the mean-glandular dose of an average screening mammogram. The images were collected under an investigational review board approval to measure breast composition. The breast thickness map was modeled using the SXA phantom [40]. The thickness validation procedure concluded in a weekly scanning of specially designed quality assurance phantom [41]. The calibration standards and 3CB algorithms are described in full elsewhere [15,42]. The region of interests of lesions and three surrounding rings of 2 mm distance outward from lesion boundary were derived for water, lipid, and protein maps. The median lipid measures of regions of interest within lesions, three rings outside of lesions, differences and ratios between lesions and rings were generated for both CC and MLO mammograms. Average values of generated variables of two views were used.

Histological sectioning, hematoxylin and eosin staining, and adipocyte area quantification

Invasive breast carcinomas were obtained from the Pathology Departments of the University of California San Francisco (San Francisco, CA) and Moffitt Cancer Center (Tampa, FL). The study population included 39 hormone receptor positive tumors (32 ER positive (+)/PR+/HER2 negative, 2 ER+/PR-/HER2-, 4 ER+/PR+/HER2+, and 1 ER+/PR-/HER2+), 6 triple negative (ER-/PR-/HER2-) tumors, and 1 ER-/PR-/HER2+ tumor. Thirty-nine tumors were invasive ductal carcinomas and 7 were invasive lobular carcinomas. Tissue was fixed in 10% formalin

and embedded in paraffin, and 4 micron sections were cut for hematoxylin and eosin (H&E) and immunohistochemical ER, PR, and HER2 staining, as well as HER2 fluorescence *in situ* hybridization (FISH) for a subset of tumors. ER, PR, and HER2 were scored according to ASCO/CAP guidelines [43,44]. An H&E-stained slide demonstrating tumor and sufficient (at least 0.5 cm) NAT was chosen from each of 11 tumors with available slides and subjected to whole slide scanning at 400× magnification using an Aperio XT scanner (Leica Biosystems, Buffalo Grove, IL). Images were visualized using ImageScope software (Leica Biosystems). For each tumor, 4 representative images at 50X magnification (at least 50 adipocytes per image) from R1 and R3 were analyzed using Fiji imaging software with the opensource Adiposoft v1.13 plugin [45]. This study was approved by the institutional review board of the respective institutions.

cAMP-dependent lipolysis signature

The cAMP-dependent lipolysis gene signature was generated using RNA-seq data of cAMP-treated adipocytes [18]. Differentially expressed genes were sorted according to their *P* value and the top 100 upregulated genes were chosen for the signature. This signature was then used to calculate enrichment scores using the single-set gene set enrichment analysis (ssGSEA) method [20]. “cAMP 100 signature” enrichment scores were calculated for a dataset containing multiple samples from multiple regions surrounding breast tumors [19]. The dataset includes samples from the tumor itself ($n = 9$), and NAT 1 cm ($n = 7$), 2 cm ($n = 5$), 3 cm ($n = 3$) and 4 cm ($n = 4$) away from the tumor, in addition to healthy normal samples ($n = 10$). The spatial data set of multiple regions surrounding breast tumors was downloaded from EMBL-EBI ArrayExpress (Accession E-TABM-276). Raw CEL files were downloaded and processed using custom

Affymetrix GeneChip Human Genome U133 Plus 2.0 CDF obtained from BrainArray [46]. The processing and normalization were performed using the Robust Multi-array Average (RMA) procedure on Affymetrix microarray data.

Laser Capture Microdissection

Breast tumor tissue was sectioned at 6 μm in a Leica CM 1850 Cryostat (Leica Microsystems GmbH). The sections were mounted on uncharged glass slides without the use of embedding media and placed immediately in 70% ethanol for 30 seconds. Subsequent dehydration was achieved using graded alcohols and xylene treatments as follows: 95 % ethanol for 1 minute, 100% ethanol for 1 minute (times 2), xylene for 2 minutes and second xylene 3 minutes. Slides were then dried in a laminar flow hood for 5 minutes prior to microdissection. Then, sections were laser captured microdissected with PixCell II LCM system (Arcturus Engineering). Approximately 5000 shots using the 30 micron infrared laser beam will be utilized to obtain approximately 10,000 cells per dissection. All samples were microdissected in duplicate on sequential sections.

SDS-PAGE and In-gel Digestion

All membranes containing the microdissected cells from breast tumor tissue were removed and placed directly into a 1.5 mL Eppendorf tube. Membranes containing the microdissected cells were suspended in 20 μL of SDS sample buffer, reduced with DTT and heated in a 70-80°C water bath for approximately 10 min. The supernatant was then electrophoresed approximately 2 cm into a 10% Bis Tris gel, stained with Colloidal Blue with destaining with water, and the region was excised and subjected to in-gel trypsin digestion using a standard protocol. Briefly,

the gel regions were excised and washed with 100 mM ammonium bicarbonate for 15 minutes. The liquid was discarded and replaced with fresh 100 mM ammonium bicarbonate and the proteins reduced with 5 mM DTT for 20 minutes at 55° C. After cooling to room temperature, iodoacetamide was added to 10 mM final concentration and placed in the dark for 20 minutes at room temperature. The solution was discarded and the gel pieces washed with 50% acetonitrile/50 mM ammonium bicarbonate for 20 minutes, followed by dehydration with 100% acetonitrile. The liquid was removed and the gel pieces were completely dried, re-swelled with 0.5 µg of modified trypsin (Promega) in 100 mM NH₄HCO₃, and digested overnight at 37°C. Peptides were extracted by three changes of 60% acetonitrile/0.1% TFA, and all extracts were combined and dried *in vacuo*. Samples were reconstituted in 35 µL 0.1 % formic acid for LC-MS/MS analysis.

LC-MS/MS Analysis, Protein Identification and Quantitation

Peptide digests were analyzed on a Thermo LTQ Orbitrap Velos ion trap mass spectrometer equipped with an Eksigent NanoLC 2D pump and AS-1 autosampler as described previously [47]. Peptide sequence identification from MS/MS spectra employed the RefSeq Human protein sequence database, release version 54, and both database and peptide library search strategies [47]. For initial protein assembly, peptide identification stringency was set at a maximum of 1% reversed peptide matches, *i.e.*, 2% peptide-to-spectrum matches (PSM) FDR and a minimum of 2 unique peptides to identify a given protein within the full data set. To minimize false-positive protein identifications, only proteins with a minimum of 6 matched spectra were considered. The full dataset contained 850,847 filtered spectra corresponding to 31,594 distinct spectrum-peptide sequence matches, which mapped to 24,946 distinct peptide sequences and 2,230

indistinguishable protein identifications. The protein-level FDR for the final assembly was 5.14%. Spectral counts for each protein in the final assembly were calculated as the sum of peptide-spectrum matches that met the criteria described above.

Orthotopic xenograft studies

The human samples used to generate patient-derived xenograft (PDX) tumors, as well as the human non-tumor samples, were previously described [25]. The generation of the MTBTOM tumor model has been previously described [26]. 4-week-old WT FVB/N and immunocompromised NOD/SCID-gamma (NSG) female mice were purchased from Taconic Biosciences. Viably frozen MTB-TOM, HCI002, HCI009 and HCI010 tumor samples were transplanted into the mammary fat pad, following clearance of associated lymph node and epithelium, of respective FVB/N and NSG mice. Tumor growth was monitored daily by caliper measurement in two dimensions. When tumors reached 1 cm (MTBTOM) or 2 cm (PDX) in any dimension mice were euthanized, tumor and NAT were isolated, and flash-frozen in liquid nitrogen. The protocols described in this and other sections regarding animal studies were approved by the UCSF Institutional Animal Care and Use Committee. For the HCC1143 and HS578T control and Cx31 partial expression loss orthotopic xenografts, and for the BT549 shRNA knockdown orthotopic xenografts, 5×10^5 cells were resuspended 1:1 with matrigel (Corning) and injected into the cleared mammary fat pads of 4-week-old WT NSG female mice. Tumor incidence and growth were monitored daily via palpation and caliper measurement, respectively. Mice were euthanized after 180 days or after tumors reached 2cm in any dimension. For HCC1143 *GJB3^{WT}* and *GJB3^{Med}* xenografts, a central slice of tumor and surrounding NAT was fixed in 4% paraformaldehyde and embedded in paraffin for histological sectioning, H&E

staining and adipocyte area quantification, while the remaining tumor and NAT tissues were flash-frozen in liquid nitrogen. For other xenografts, NAT was isolated and flash-frozen in liquid nitrogen. For the CL316243 experiment, mice were randomized into experimental groups immediately post-orthotopic transplant. The following day, drug treatment was initiated and mice received vehicle or 1 mg/kg CL316243, delivered by intraperitoneal injection, daily until tumor incidence was recorded via palpation. For the Cx31 shRNA knockdown experiments, mice were randomized into experimental groups immediately post-orthotopic xenograft, and mice in the shCx31 knockdown group were administered doxycycline dietarily.

Immunoblot analysis

Proteins were extracted using RIPA buffer (Thermo) and proteinase (Roche) plus phosphatase (Roche) inhibitor cocktails. Protein extracts were resolved using 4–12% SDS-PAGE gels (Life Technologies) and transferred to nitrocellulose membranes (Life Technologies). Membranes were probed with primary antibodies overnight on a 4 °C shaker, then incubated with horseradish peroxidase (HRP)-conjugated secondary antibodies, and signals were visualized with ECL (Bio-Rad). The primary antibodies targeting the following proteins were used: β -actin (actin) (sc-47778 HRP, Santa Cruz, 1:10,000), pHSL S563 (4139, Cell Signaling, 1:1000), HSL (4107, Cell Signaling, 1:1000), HNF4 α (ab41898, Abcam, 1:1000), and Cx31 (ab156582, Abcam, 1:1000). Chemiluminescent signals were acquired with the Bio-Rad ChemiDoc XRS+ System equipped with a supersensitive CCD camera. Where indicated, unsaturated band intensities were quantified using Bio-Rad Image Lab software.

Cell culture and virus production

A panel of established TN and RP human breast cancer cell lines, and their culture conditions, have previously been described [48]. No cell line used in this paper is listed in the database of commonly misidentified cell lines that is maintained by the International Cell Line Authentication Committee (ICLAC) (<http://iclac.org/databases/cross-contaminations/>). All lines were found to be negative for mycoplasma contamination. Lentiviruses for Cas9 and sgRNAs were produced in 293T cells using standard polyethylenimine (Polysciences Inc.) transfection protocols.

Dye transfer and FACS analysis

For cancer cell-cancer cell transfer, monolayers of indicated lines (donors) were labelled with 1 μ M CalceinAM dye (Life Technologies) at 37°C for 40 min. Dye-loaded ‘donor’ cells were washed three times with PBS, and then single-cell suspensions of 1.5×10^5 mCherry-labelled cells (recipients) were added for 5 hours. For CBX treatment studies, monolayers of indicated lines (recipients) were pre-treated for 24 hours with 150 μ M CBX or vehicle. Indicated ‘donor’ cells were loaded in suspension with CalceinAM dye (Life Technologies) at 37°C for 40min, washed three times with PBS, and added onto indicated ‘recipient’ cells for 5 hours. Dye transfer was quantified by BD LSRFORTESSA or BD LSR II (BD Biosciences). Gating strategy to identify mCherry-positive, Calcein-positive cell population is described in **Fig. S4.4**. For cancer cell-adipocyte transfer, monolayers of indicated control or Cx31 partial knockout lines (donors) were labelled with 1 μ M CalceinAM dye at 37°C for 40 min. Dye-loaded cells were washed three times with PBS, and then primary mammary adipose tissues (recipient) were added for 5 hours. Primary adipose tissue was isolated from co-culture, washed with PBS, and dye transfer

was quantified by measurement of total adipose fluorescence using a Tecan fluorescent plate reader.

Gene expression analysis

TCGA breast-invasive carcinoma data set was sourced from data generated by TCGA Research Network (<http://cancergenome.nih.gov>), made available on the University of California, Santa Cruz (UCSC) Cancer Browser. Single-cell RNAseq data was sourced from data generated by Chung, et al.[34]. For the MTBTOM data set, 11 endpoint MTBTOM orthotopic xenografts generated as described above, and 3 mammary glands from naïve mice, were flash-frozen in liquid nitrogen. Library preparation and Illumina RNAseq was performed by Q²Solutions (www.q2labsolutions.com). Gene expression analyses were performed using the ‘limma’ R package [49]. For the panel of established TN and RP human breast cancer cell lines [48], library preparation and Illumina RNAseq was performed by Novogene (www.novogene.com). All RNA was isolated using the RNAeasy kit (Qiagen).

ATP quantification

To determine the effects of CBX treatment on ATP levels, tumor cells were seeded in 96-well plates at 5,000–7,000 cells per well and cultured in the presence of 0 or 150 μ M CBX (Sigma) for 24 hours, with triplicate samples for each condition. Relative ATP concentrations were determined using the CellTiter-Glo Luminescent Cell Viability Assay (Promega).

Isolation of primary mammary adipose tissue

Anonymous reduction mammoplasty samples were acquired from the Cooperative Human Tissue Network (CHTN). Samples were washed in DPBS supplemented with 1 % Penicillin/Streptomycin and 0.1 % Gentamicin (all GIBCO). Mammary adipose tissue was separated mechanically from epithelial tissue using a razor blade, and was then cryopreserved in freezing medium (10% DMSO (Sigma) in FBS (X&Y Cell Culture)).

Immunofluorescence staining and microscopy

For adipose tissue cancer cell co-cultures imaged whole mount, 2×10^6 of the indicated GFP-labelled cell line was suspended in 500uL DMEM/F-12(Gibco 11320033) containing 10% FBS and injected into primary mammary adipose tissue from a healthy individual, then cultured at 37°C for 24 hours. For immunofluorescence labeling of co-culture tissues, samples were washed three times in PBS and fixed in 4% paraformaldehyde, permeabilized in 0.5% Triton X-100 for 15min, and blocked in 10% goat serum in PBS with 0.25g/L BSA, 0.2% Triton X-100, and 0.41% Tween-20 overnight. Samples were then incubated overnight with primary antibodies (Cx31, WH0002707M1, Sigma, 1:100, and pHSL(S563), 4139, Cell Sig, 1:100), and then overnight with Alexa Fluor-647 or -546 conjugated antibodies. Finally, using an established protocol for whole mount breast tissue imaging[37], co-culture tissues were cleared through overnight incubation at 4 °C in a 'FUnGI' solution of 50% glycerol (vol/vol), 2.5 M fructose, 2.5 M urea, 10.6 mM Tris Base, and 1 mM EDTA. Confocal images were acquired using a Zeiss LSM900 with Airyscan 2 detector. For pHSL(S563) image quantification, fluorescence was measured using Fiji imaging software, and Difference of Gaussians was used for analysis of puncta number and percent area. For sectioned adipose tissue co-culture, 1×10^6 of the indicated mCherry-labelled cell line was injected into primary mammary adipose tissue and cultured at

37°C for 18 hours. The co-cultures were examined using fluorescent microscopy to identify regions of adipose tissue containing mCherry-positive cancer cells. These regions were isolated and fixed in 4% paraformaldehyde and embedded in paraffin. Primary TNBCs used for immunofluorescence were identified and retrieved from the clinical archives of the University of California San Francisco (UCSF) Department of Pathology. All tumors consisted of estrogen receptor (ER)-, progesterone receptor (PR)-, and HER2-negative invasive ductal carcinomas. Breast tissue was fixed in 10% formalin and embedded in paraffin. Tumor blocks with sufficient tumor and adjacent (at least 0.5 cm) normal tissue were selected, and 4µm sections were cut on plus-charged slides for immunofluorescence. This study was approved by the UCSF institutional review board. For immunofluorescence labeling of sectioned co-cultures and primary TNBC, slides were dewaxed in xylene followed by rehydration in graded ethanol (100, 95, 70%) and deionized H₂O. Antigen retrieval was performed in 10mM Tris, 1mM EDTA, 0.05% Tween 20, pH 9 at 121 °C for 4 min. Subsequently, tissue sections were blocked in 1% bovine serum albumin, 2% fetal bovine serum in PBS for 5 min, and incubated with primary antibodies (Cx31, 12880, Proteintech, 1:50 and pan-cytokeratin, sc-81714, Santa Cruz, 1:50) overnight at 4 °C. Following several PBS washes, sections were incubated with Alexa Fluor-488 or -568 conjugated antibodies, counterstained with DAPI (Sigma), and mounted using Vectashield (Vector). Epifluorescence images were acquired either by spinning disk microscopy on a customized microscope setup as previously described [50-52] except that the system was upgraded with a next generation scientific CCD camera (cMyo, 293 Photometrics) with 4.5 µm pixels allowing optimal spatial sampling using a λ ~60 NA 1.49 objective (CFI 294 APO TIRF; Nikon), or at the UCSF Nikon Imaging Center using a Nikon Ti Microscope equipped with an

Andor Zyla 5.5 megapixel sCMOS camera and Lumencor Spectra-X 6-channel LED illuminator. Images were collected using a Plan Apo λ 20x / 0.75 lens.

Generation of Cx31 partial expression loss lines

LentiCas9-Blast (Addgene plasmid #52962) and lentiGuide-Puro (Addgene plasmid #52963)

were gifts from Feng Zhang. sgRNAs against Cx31 were constructed using the Feng Zhang Lab

CRISPR Design Tool (crispr.mit.edu). sgRNAs used were as follows:

Cx31 exon 1 sg1: CCAGATGCGCCCGAACGCTGTGG (HS578T *GJB3*^{Med-1} and HCC1143 *GJB3*^{Med})

Cx31 exon 1 sg2: CCGGGTGCTGGTATACGTGGTGG (HS578T *GJB3*^{Med-2} and HCC1143 *GJB3*^{Low})

ShRNAs against Cx31 and GFP control were constructed using Tet-pLKO-Puro (Addgene plasmid #21915). shRNAs used were as follows:

shCx31:

Cx31.shRNA3_forward:

ccggAAGCTCATCATTGAGTTCCTCctcgagGAGGAACTCAATGAT GAGCTTttttg

Cx31.shRNA3_reverse: aattcaaaaaAAGCTCATCATTGAGTTCCTCctcgagGAGGAACTCAAT GATGAGCTT

shGFP [53]:

shGFP_forward: CCGGTACAACAGCCACAACGTCTATCTCGACATAGACTTGTGGCTG TTGTATTTTTG

shGFP_reverse: CAAAATACAACAGCCACAACGTCTATGTGCGAGATAGACGTTGTGG CTGTTGTACCGG

Lentiviral transduction was performed in DMEM supplemented with 10% FBS and polybrene 10 μ g/mL. For sgRNA transduction, Cas9-expressing cells were enriched by Blasticidin (10-15 μ g/mL Gemini BioProducts) selection for seven days. Cas9⁺ cells were subsequently transduced with lentiGuide-Puro (with sgRNAs targeting Cx31) followed by puromycin (1 μ g/mL; Gibco) for seven days. Thereafter, clonal selection was performed and clones screened for loss of target

gene protein expression by immunoblot analysis. For shRNAs, cells were transduced with Tet-pLKO-Puro (with shRNAs targeting Cx31 or GFP control[53]) followed by puromycin (2 ug/mL; Gibco) for seven days, after which knockdown of target protein was confirmed by immunoblot analysis.

cAMP quantification

For *in vitro* studies, tumor cells were seeded in 96-well plates at 5,000–7,000 cells per well and cultured in the presence of 0 or 150 μ M CBX (Sigma) for 24 hours, with triplicate samples for each condition. Changes in cAMP concentration were determined using the cAMP-Glo Assay (Promega). For *in vivo* studies, frozen tissue was homogenized using a TissueLyser in 300 μ l of 40:40:20 acetonitrile:methanol:water with the addition of 1 nM (final concentration) of D3-[15N]serine as an internal extraction standard (Cambridge Isotopes Laboratories Inc, DNLM-6863). 10 μ l of cleared supernatant (via centrifugation at 15,000 r.p.m., 10 min, at 4 °C) was used for SRM–LC-MS/MS using a normal-phase Luna NH2 column (Phenomenex). Mobile phases were buffer A (composed of 100% acetonitrile) and buffer B (composed of 95:5 water:acetonitrile). Solvent modifiers were 0.2% ammonium hydroxide with 50 mM ammonium acetate for negative ionization mode. cAMP levels were analyzed using the MassHunter software package (Agilent Technologies) by quantifying the transition from parent precursor mass to product ions.

cAMP transfer

For cancer cell-adipocyte transfer, monolayers of indicated control or Cx31 partial knockout lines (donors) were labelled with 2 μ M fluo-cAMP (Biolog Life Science Institute) at 37°C for 30 min.

cAMP-loaded cells were washed three times with PBS, and then primary mammary adipose tissues (recipient) were added for 5 hours. Primary adipose tissue was isolated from co-culture, washed with PBS, and cAMP transfer was quantified by measurement of total adipose fluorescence using a Tecan fluorescent plate reader.

Preadipocyte differentiation and qRT-PCR

Primary mouse preadipocytes were differentiated as previously described [54]. Monolayers of differentiated adipocytes were washed with PBS, and then treated with vehicle or 10 μ M forskolin (Sigma), or seeded with 1 X 10⁵ of the indicated cancer lines. Total RNA was isolated from co-cultures after 20 hours using the RNeasy kit (Qiagen). One μ g of total RNA was reverse transcribed using iScript cDNA synthesis kit (Bio-Rad). The relative expression of UCP1, aP2, and GAPDH was analyzed using a SYBR Green Real-Time PCR kit (Thermo) with an Applied Biosystems QuantStudio 6 Flex Real-Time PCR System thermocycler (Thermo). Variation was determined using the $\Delta\Delta$ CT method [55](48) with GAPDH mRNA levels as an internal control.

Mouse-specific primers used were as follows:

GAPDH forward: CCAGCTACTCGCGGCTTTA
GAPDH reverse: GTTCACACCGACCTTCACCA
UCP1 forward: CACCTTCCCGCTGGACACT
UCP1 reverse: CCCTAGGACACCTTTATACCTAATGG
aP2 forward: ACACCGAGATTTTCCTTCAAAGTG
aP2 reverse: CCATCTAGGGTTATGATGCTCTTCA

Proliferation assays

To determine the effects of Cx31 partial knockout on cell proliferation and viability, the indicated cell lines were seeded in 6-well plates at 1.5 X 10⁵ cells/well. Cells were harvested at 24, 48 and 72 h. Cell counts and cell viability by trypan blue exclusion were determined using

the Countess Automated Cell Counter (Life Technologies) according to the manufacturer's instructions.

Statistical analysis

Prism software was used to generate and analyze Spearman correlation (**Fig 4.1D**) and the survival plots (**Figs. 4.4B, 4.4C and 4.4G**). Correlation *P* values were generated using ordinary one-way ANOVA (**Figs. 4.1H, 4.3F, 4.3H, 4.4D and 4.4F**), ordinary one-way ANOVA with multiple comparisons (**Fig 4.2B**), repeated measures one-way ANOVA (**Figs. 4.1B, 4.1F, 4.3E, and 4.3G**), repeated measures mixed effects model (Figs. 4.1C, 4.1E and 4.1G), and unpaired two-tailed t test (**Figs. 4.4A, 4.4E, S4.1A, and S4.1B**). Survival plot *P* values was generated using a log-rank test. All differential expression analyses (**Figs. 4.2D and 4.2F**) were done using the 'limma' R package [49].

Code availability

Publicly available data sets were acquired as noted. Our annotations of the TCGA data set are available (<https://bitbucket.org/jeevb/brca>). All data and code related to these studies are available in the main text, supplementary materials and indicated repositories. The raw RNAseq data will be deposited on GEO.

Figures

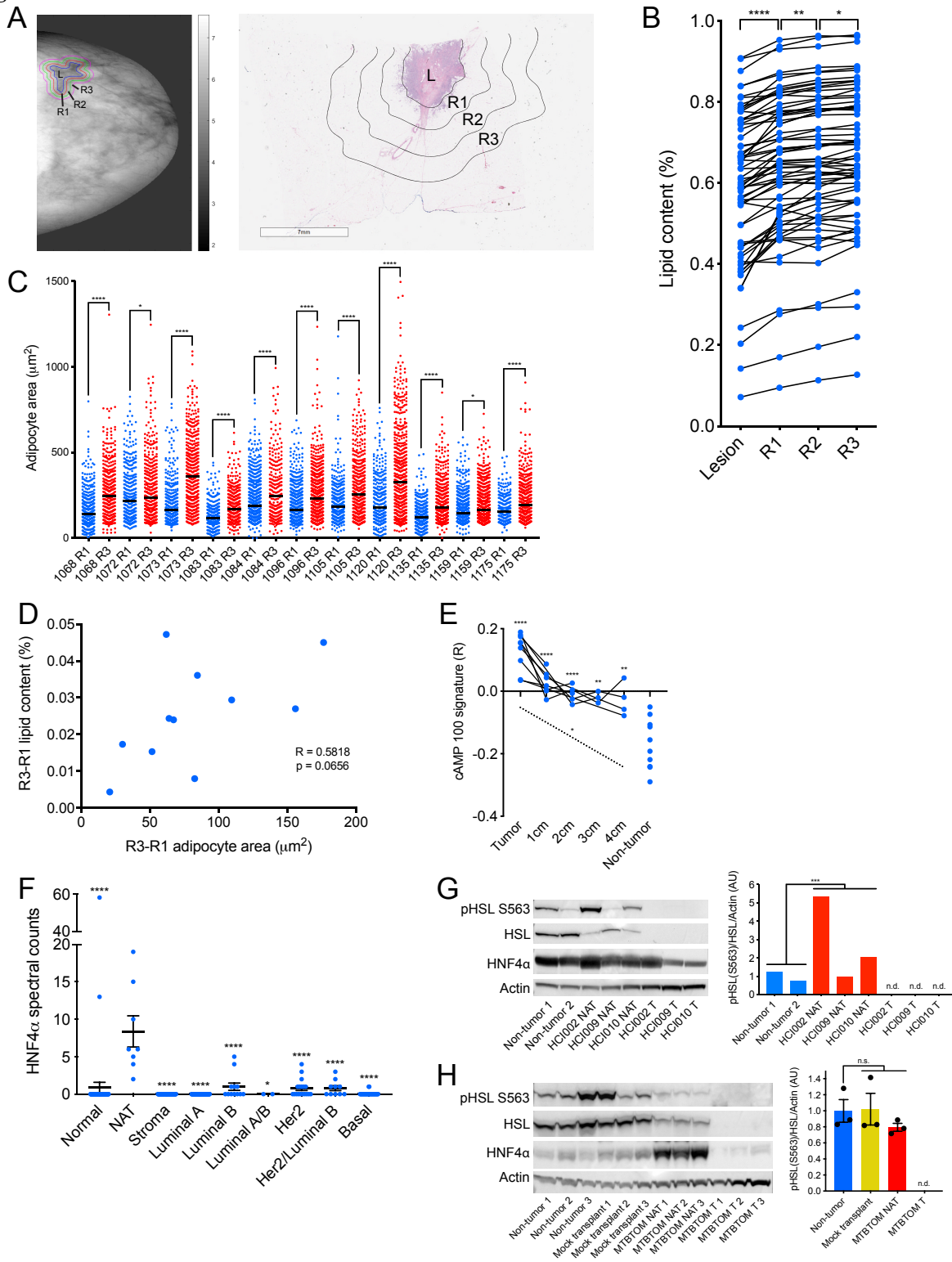


Figure 4.1. Lipolysis and lipolytic signaling are activated in breast tumor-adjacent adipocytes from breast cancer patients and mouse models of breast cancer. Figure caption continued on the next page.

Figure caption continued from the previous page. (A) Representative lipid content image (left) and hematoxylin and eosin stained excision specimen (right) from patients with invasive breast cancer. The lesion (L), and NAT 0-2 mm (R1), 2-4 mm (R2), and 4-6 mm (R3) away are indicated. (B) Percent lipid content (lipid content / lipid + water + protein content) of L, R1, R2 and R3 from patients (n = 46) with invasive breast cancer. (C) Adipocyte area in R1 and R3 from a subset of patients (n = 11) in B. The black line indicates mean adipocyte area, and each patient identifier is indicated. Each point represents individual adipocyte. (D) Correlation of change in lipid content in B and change in average adipocyte area in C from R3 to R1 for matched patients in C. Spearman correlation and two-tailed t test were used to generate the correlation coefficient and associated P value. (E) ssGSEA enrichment scores for cAMP- dependent lipolysis signature in primary breast tumors (n = 9), NAT 1 cm (n = 7), 2 cm (n = 5), 3 cm (n = 3), and 4 cm (n = 4), and healthy non-tumor breast tissue (n = 10). Dotted line indicates fixed effects analysis across matched samples. (F) HNF4a peptide counts from LC-MS/MS of primary tissue from healthy control breast tissue (n = 42), NAT (n = 4), stroma (n = 36), and luminal A (n = 38), luminal B (n = 6), luminal A/B (n = 1), HER2-amplified (n = 9), HER2-amplified/luminal B (n = 5), and basal (n = 16) tumors. Each point represents individual sample LCM on which LC-MS/MS was performed. LCM and LC-MS/MS was performed in technical duplicate on sequential histological slides from each patient. (G) Immunoblot analysis (left) showing expression levels of lipolysis activators HSL and HNF4a, and phosphorylated HSL (pHSL S563) in healthy non-tumor mammary gland and NAT and tumor tissues from a panel of PDXs. Quantification (right) of pHSL/HSL ratio, normalized to b-actin levels. (H) Immunoblot analysis (left) showing expression levels of lipolysis activators HSL and HNF4a, and phosphorylated HSL (pHSL S563) in healthy non-tumor mammary gland, mock-transplanted mammary gland, and NAT and tumor tissues from MTBTOM allografts. Quantification (right) of pHSL/HSL ratio, normalized to b-actin levels. For (B) and (E) black lines indicate matched samples from individual patients. For (F) and (H) mean \pm s.e.m. is shown. *P < 0.05, **P < 0.01, ***P < 0.001, ****P < 0.0001; repeated measures one-way ANOVA (B) and (F), repeated measures mixed effects model (C), (E), and (G), ordinary one-way ANOVA (H).

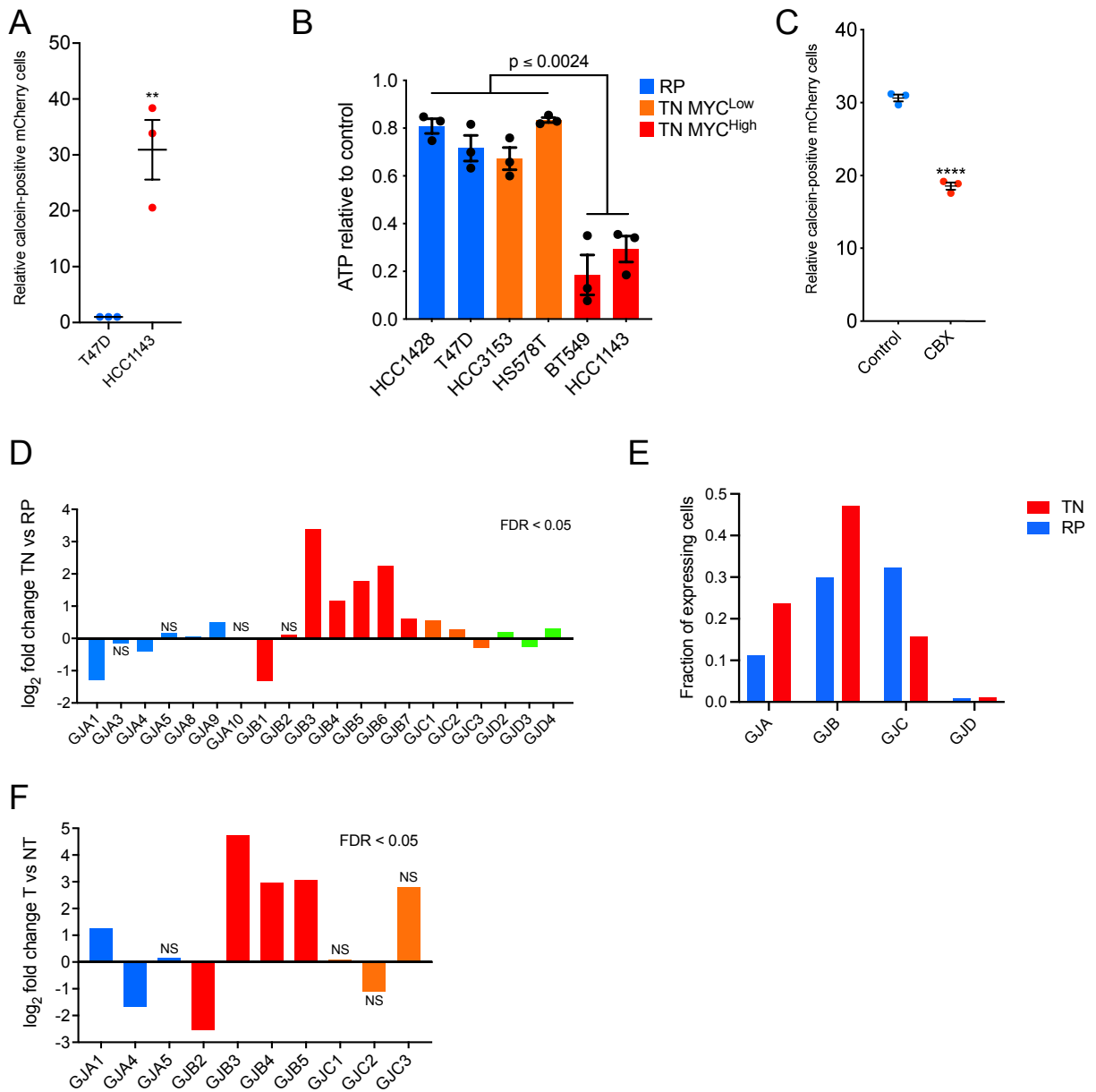


Figure 4.2. Breast cancer cells form functional gap junctions and express Cx31.

(A) Relative frequency of dye transfer from Calcein AM- loaded cells (donor) to mCherry-labelled cells (recipient) as determined by FACS (fluorescence- activated cell sorting) analysis. (B) ATP levels in TN high MYC, TN low MYC, and RP cell lines after treatment with 150 μ M CBX for 24 hours relative to untreated (control) cells. (C) Relative frequency of dye transfer from Calcein AM- loaded cells (donor) to mCherry-labeled cells (recipient) treated with 150uM CBX or vehicle control for 24 hours, as determined by FACS analysis. (D) Fold change (log₂) in expression of indicated connexin genes in TN (n = 123) versus RP (n = 648) tumors based on RNA-seq data acquired from TCGA of 771 breast cancer patients. Figure caption continued on the next page.

Figure caption continued from the previous page. (E) Fraction of cells in (n=11) patient tumors of RP and TNBC subtypes expressing indicated gap junction (GJ) family members, based on sc-RNA-seq of 317 tumor cells. (F) Fold change (log₂) in expression of indicated connexin genes in T (n = 11) versus NT (n = 3) tissues based on RNA-seq data from MTBTOM allograft-bearing mice or healthy controls, respectively. For (A) and (C) mean ± s.e.m. of three independent biological replicates is shown. **P < 0.01, ****P < 0.0001; unpaired two-tailed t test (A) and (C), ordinary one-way ANOVA (B). For (D) and (F), all differential expression analysis was done using the ‘limma’ R package.

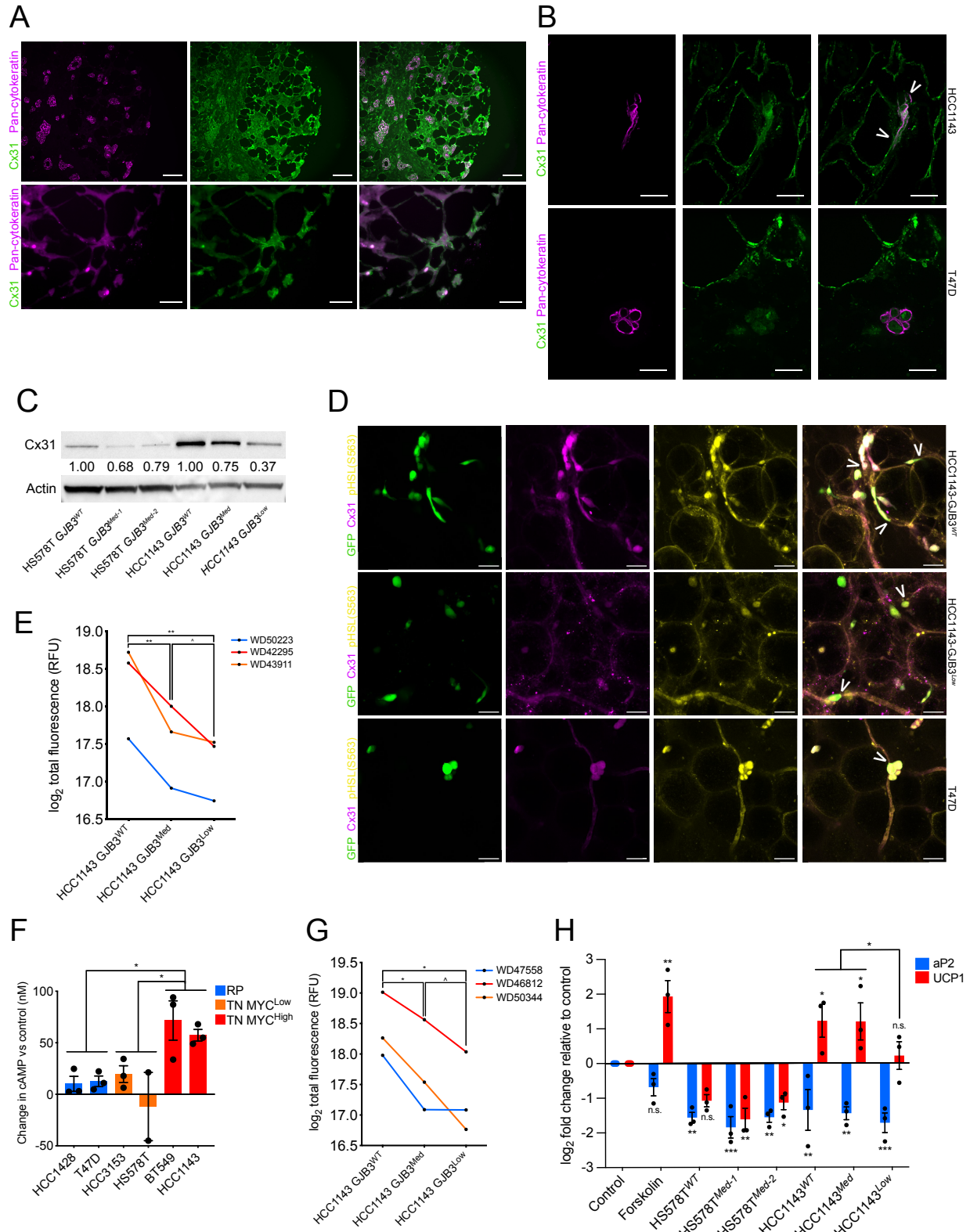


Figure 4.3. Breast cancer cell-adipocyte gap junctions form, transfer cAMP, and activate lipolytic signaling in a Cx31-dependent manner. Figure caption continued on the next page.

Figure caption continued from the previous page. (A) Staining with Cx31 (green) and pan-cytokeratin (magenta) of primary TNBC patient biopsies. Scale bar, top 100 μm , bottom 25 μm . (B) Staining with Cx31 (green) and pan-cytokeratin (magenta) of primary mammary tissue from a healthy individual (WD43177) injected with TN mCherry-HCC1143 cells and co-cultured overnight. White arrowheads indicate co-staining of Cx31 with contact point between HCC1143 and adipocyte plasma membranes. Scale bar, 25 μm . (C) Immunoblot analysis showing protein expression levels of Cx31 in vitro in a panel of clonally derived control GJB3 WT and partial depletion TN lines with one-third and two-thirds loss of GJB3 expression. For the Cx31-depleted lines each clone is referred to by level of GJB3 expression (e.g. GJB3Med expresses two-thirds WT level, and GJB3Low expresses one third GJB3WT level). Quantification of Cx31 level normalized to b-actin level is indicated. (D) Staining with Cx31 (magenta) and pHSL(S563) (yellow) of primary mammary tissue from a healthy individual (WD49393) injected with GFP-expressing HCC1143-GJB3WT (top), HCC1143-GJB3Low (middle), or T47D cells (bottom) and co-cultured overnight. White arrowheads indicate co-staining of Cx31 and pHSL(S563) at contact point between GFP cancer cells and adipocytes. Scale bar, 50 μm . (E) Dye transfer from indicated HCC1143 control and Cx31-depleted lines to primary mammary adipose tissue of indicated (n = 3) healthy individuals. (F) cAMP levels in TN high MYC, TN low MYC, and RP cell lines after treatment with 150 μM CBX for 24 hours, relative to untreated (control) cells. (G) cAMP transfer from indicated HCC1143 control and Cx31 partial expression loss lines to primary mammary adipose tissue of indicated (n = 3) healthy individuals. (H) Fold change in UCP1 and aP2 expression in differentiated adipocytes after treatment with vehicle (control) or 10 μM forskolin, or co-cultured with indicated Cx31 partial expression loss lines for 24 hours. For (F) and (H) mean \pm s.e.m. of three independent biological replicates is shown. $^{\wedge}\text{P} < 0.10$, $^*\text{P} < 0.05$, $^{**}\text{P} < 0.01$, $^{***}\text{P} < 0.001$; repeated measures one-way ANOVA for (E) and (G), ordinary one-way ANOVA for (F) and (H).

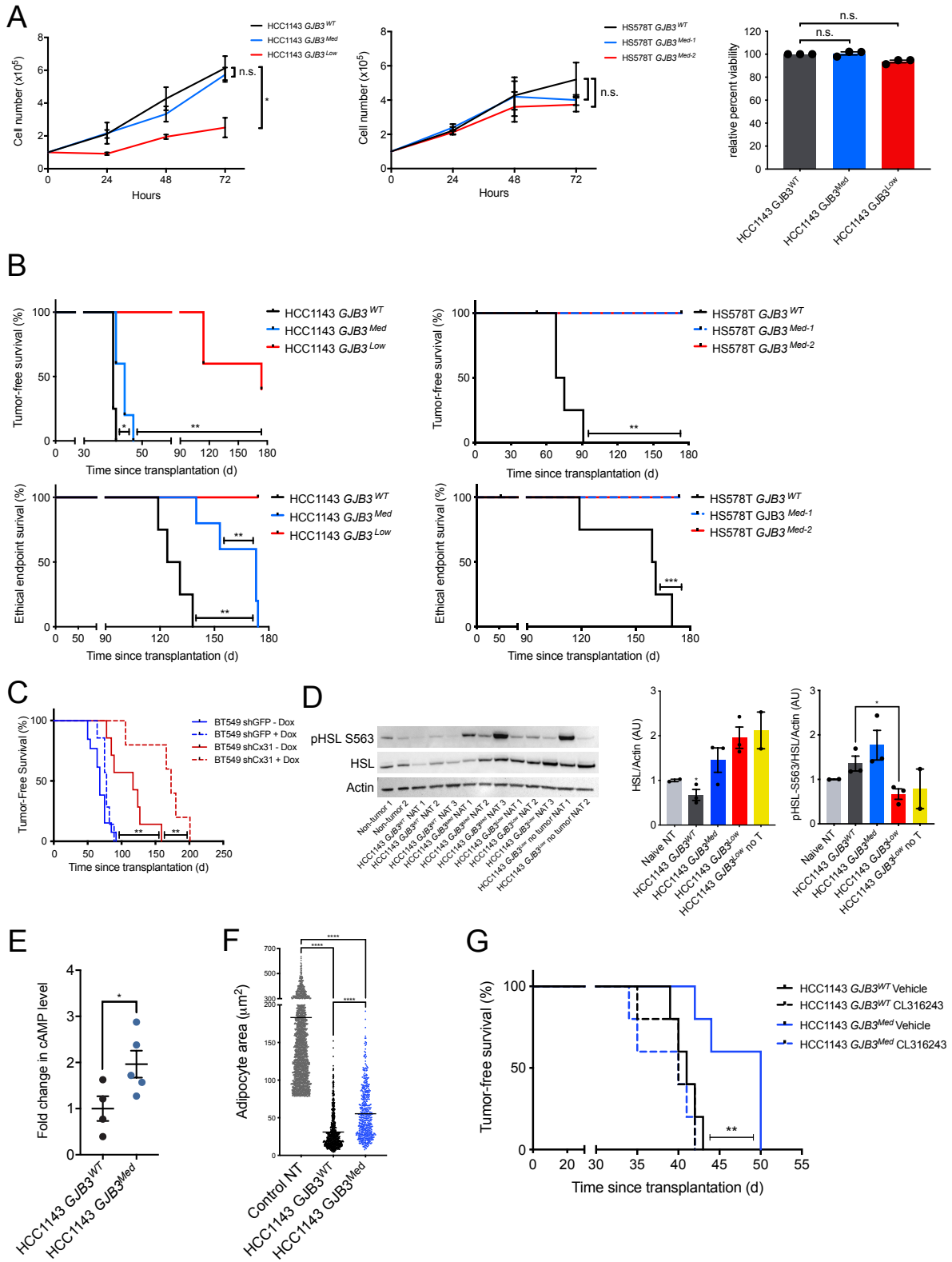


Figure 4.4. Cx31 loss impairs breast cancer cell growth in vitro, tumorigenesis, and activation of lipolysis in adjacent adipocytes in vivo. Figure caption continued on the next page.

Figure caption continued from the previous page. (A) Cell growth of indicated Cx31 partial expression loss lines in HCC1143 (left) and HS578T (middle) over 72 hours, and cell viability at 72 hours of indicated partial GJB3 depletion lines normalized to WT control (right). (B) Kaplan-Meier analysis of tumor onset (top) and ethical endpoint survival (bottom) of mice bearing indicated Cx31 partial expression loss orthotopic xenografts (n = 5 per group). Ethical endpoint survival indicates the percentage of mice bearing xenografts < 2cm in any dimension. (C) Kaplan-Meier analysis of tumor onset in mice bearing indicated xenografts with inducible Cx31 (shCx31) or GFP (shGFP) hairpin, with doxycycline (shGFP n = 7, shCx31 n = 5) and without doxycycline (shGFP n = 13, shCx31 n = 5). (D) Immunoblot analysis (left) showing expression levels of HSL and phosphorylated HSL (pHSL S563) in healthy non-tumor mammary gland and NAT from mice bearing indicated Cx31 partial expression loss xenografts or mice that were transplanted, but subsequently did not develop a tumor. Quantification of total HSL (middle) and of pHSL/HSL ratio (right), normalized to b-actin levels. (E) Fold change in cAMP levels in HCC1143 GJB3Med xenografts versus HCC1143 GJB3WT xenografts. (F) Adipocyte area adjacent to HCC1143 GJB3Med xenografts (n = 5) and HCC1143 GJB3WT xenografts (n = 4) and area in control non-tumor (NT) mice (n=3). The black line indicates mean adipocyte area. Each point represents an individual adipocyte. (G) Kaplan-Meier analysis of tumor onset of mice bearing indicated Cx31 partial expression loss orthotopic xenografts (n = 5 per group) and treated with vehicle or with 1mg/kg CL316243. For (D) and (E) mean \pm s.e.m. is shown. *P < 0.05, **P < 0.01, ***P < 0.001, ****P < 0.0001; unpaired two-tailed t test (A) and (E), log-rank test (B), (C) and (G), ordinary one-way ANOVA (D) and (F).

Supplementary Figures

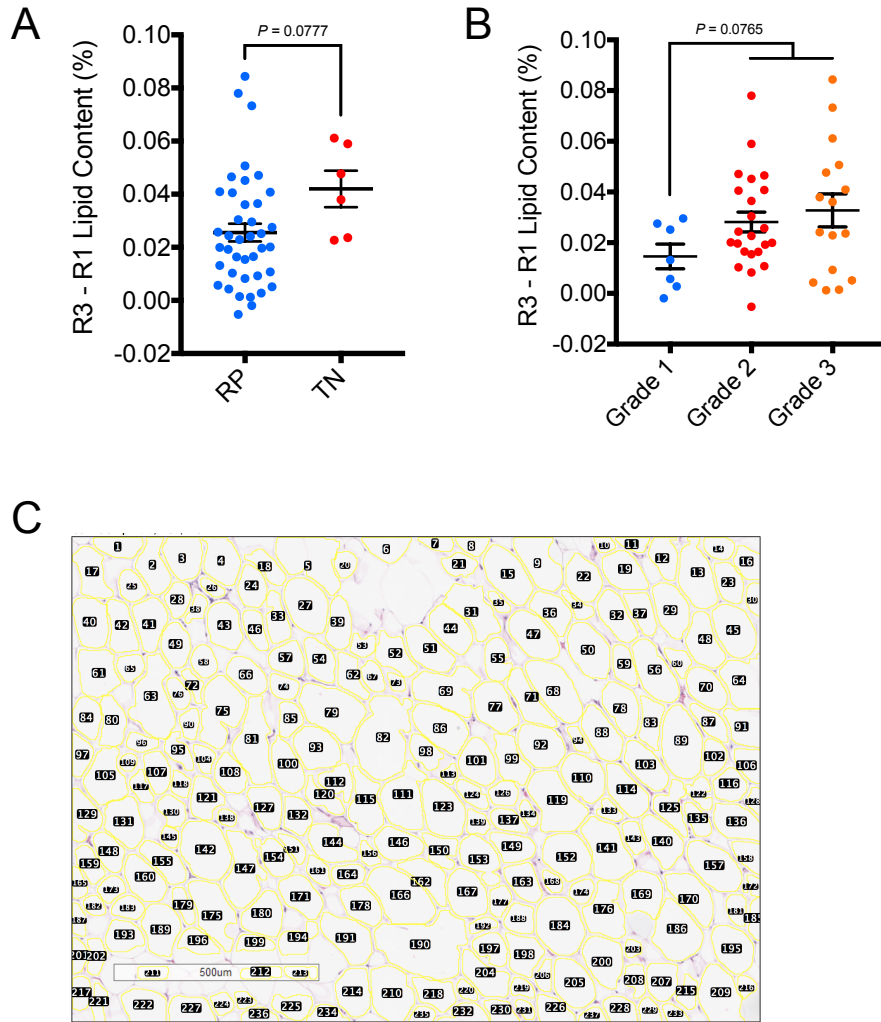


Figure S4.1. NAT lipid content by receptor status and tumor grade, and adipocyte area quantification.

- (A) Change in lipid content in R3 of NAT versus R1 of NAT from TN and RP patients.
- (B) Change in lipid content in R3 of NAT versus R1 of NAT from grade 1, 2 and 3 patients.
- (C) Example of Adiposoft software output on manual mode before curation to identify whole, individual adipocytes. *P* values indicated; unpaired two-tailed *t* test (A) and (B).

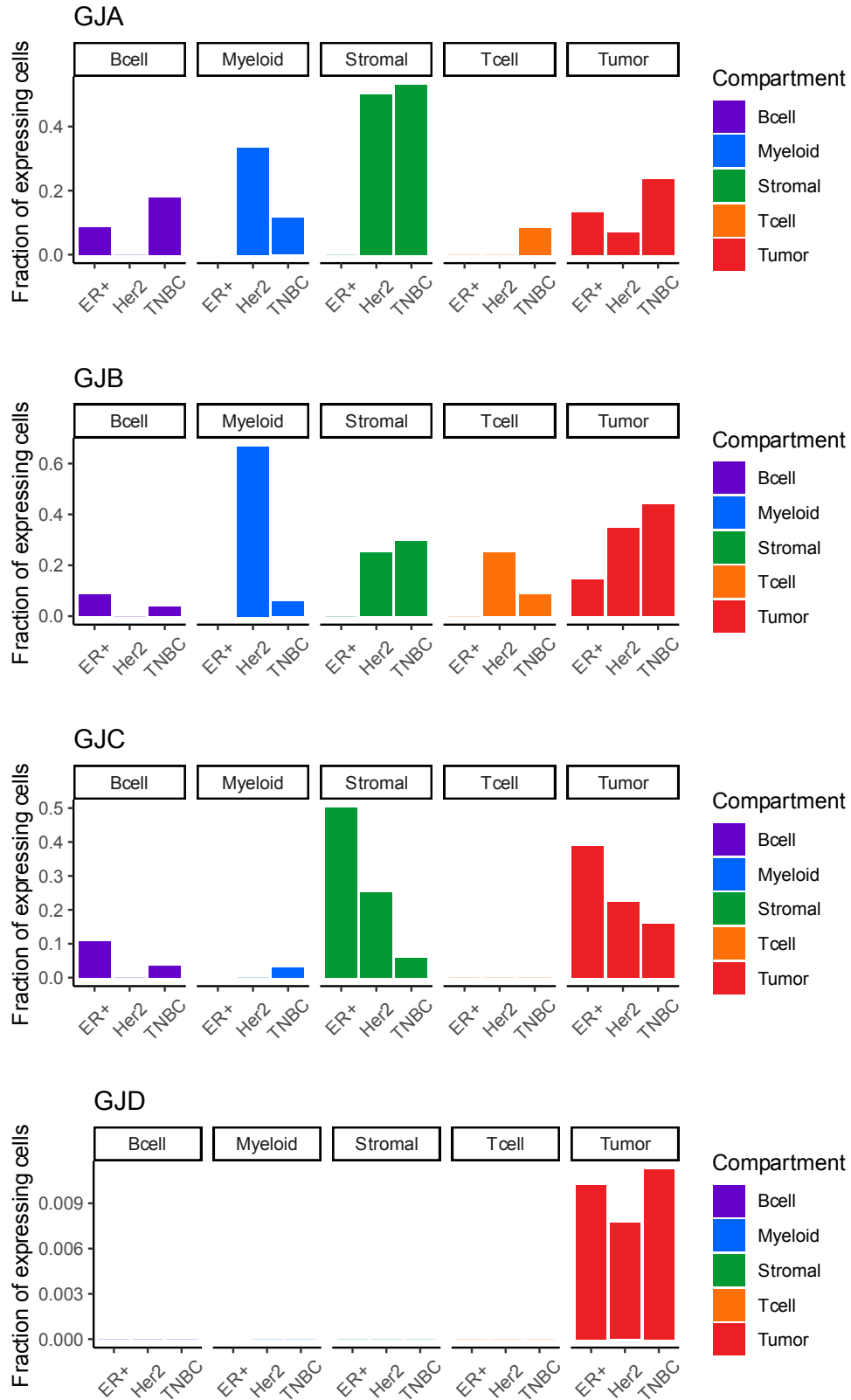


Figure S4.2. Fraction of cells expressing gap junction family by tumor compartment cell type. Figure caption continued on the next page.

Figure caption continued from the previous page. Single cell (n = 515) RNA-seq of B cell (n = 83), myeloid cell (n = 38), stromal cell (n = 23), T cell (n = 54) and tumor (n = 317) cell compartments from the patient (n = 11) tumor microenvironment

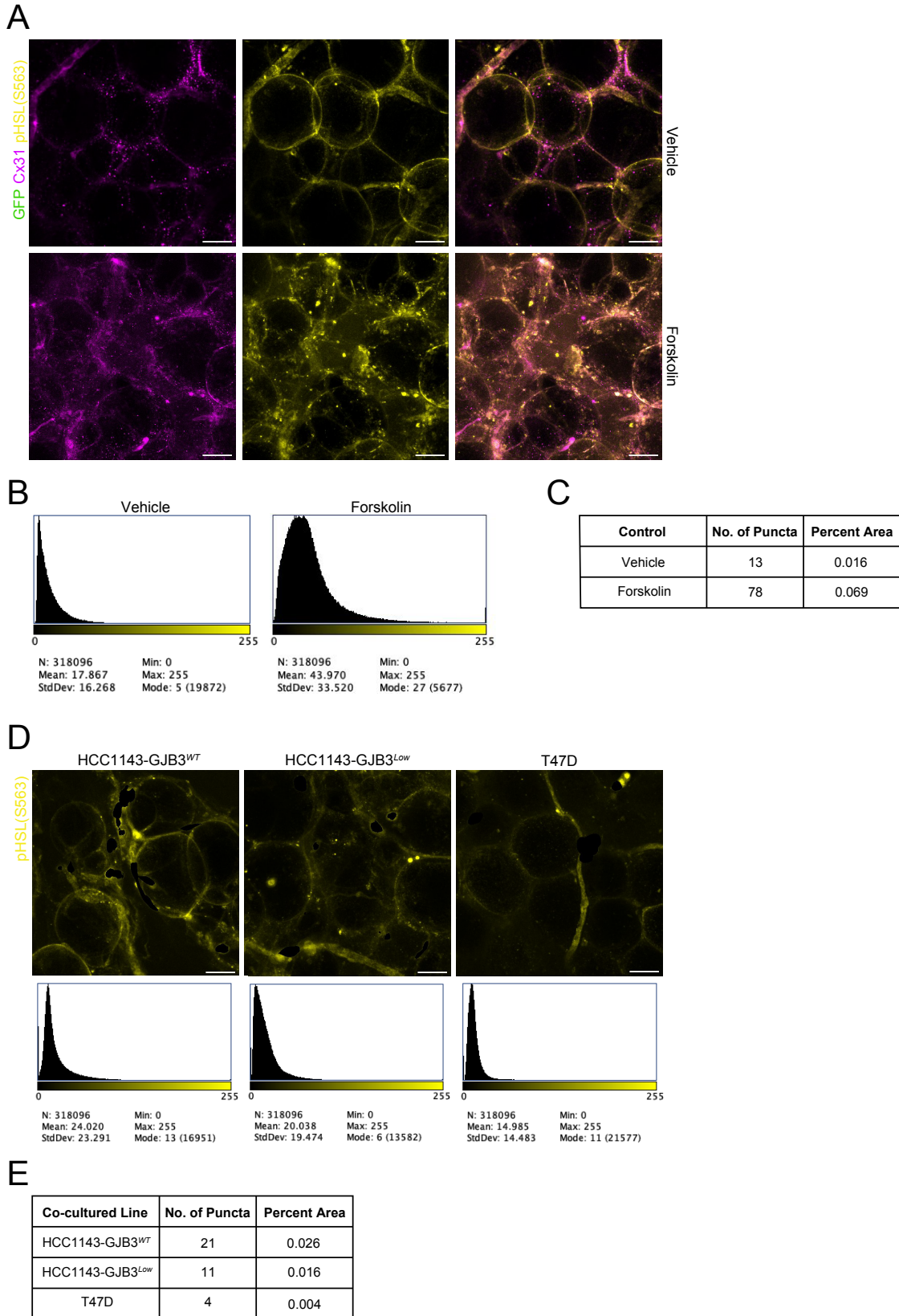


Figure S4.3. Quantification of lipolysis signaling in primary mammary adipose tissue from indicated cancer cell co-cultures and controls. Figure caption continued on the next page.

Figure caption continued from the previous page. (A) Staining with Cx31 (magenta) and pHSL(S563) (yellow) of control mammary adipose tissue injected with either vehicle (top) or 10 μ M forskolin (bottom) and cultured for 24 hours. Scale bar, 50 μ m. (B) Histogram of pHSL(S563) expression in indicated co-culture control tissues. (C) Quantification of pHSL(S563) puncta number and percent total area in indicated co-culture control tissues. (D) Staining (top) and histogram (bottom) of pHSL(S563) in mammary adipose tissue co-cultured with indicated GFP-tagged cancer cell lines. Cancer cell pHSL(S563) signal was masked out using GFP tag. Scale bar, 50 μ m. (E) Quantification of pHSL(S563) puncta number and percent total area in mammary adipose tissue co-cultured with indicated cell line.

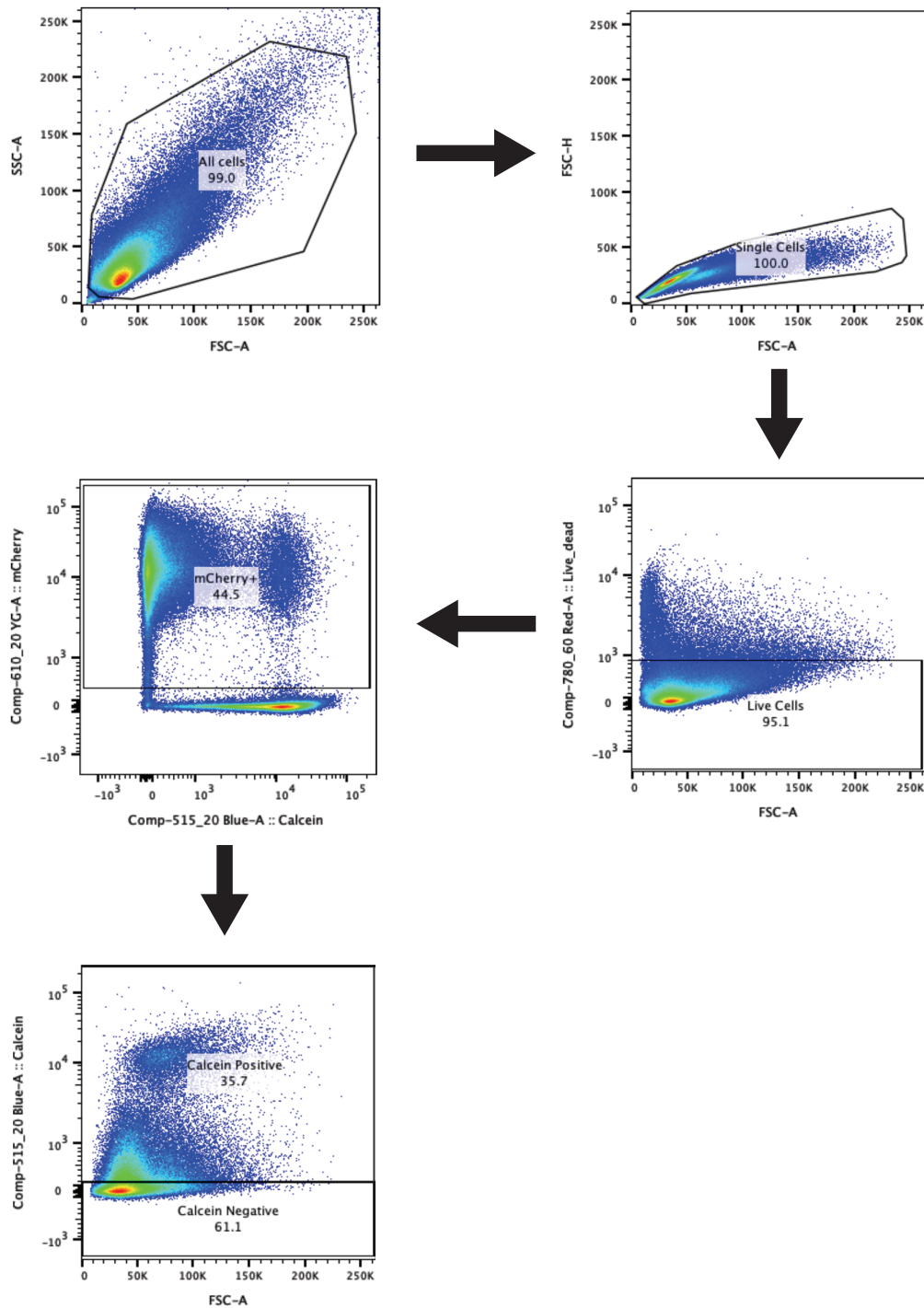


Figure S4.4. Flow cytometry gating strategy to identify mCherry-positive, Calcein AM-positive cells.

Representative experimental control sample, HCC1143 cells. Side scatter and forward scatter were used to distinguish all cells from debris. Forward scatter was used to distinguish singlets (single cells) from all cells. Live cells were identified as negative for live/dead staining. Live single cells positive for mCherry were identified. Of mCherry-positive cells, CalceinAM-positive and -negative populations were distinguished.

Table S4.2. Sample specifications and study sources for applied clinical samples and datasets.

Figure/Table	Study Name/Title	Author Name	Sample Type	Data Collected	Sample Number										Reference no./ Citation
Fig. 3.1B	<i>Mammographic quantitative image analysis and biologic image composition for breast lesion characterization and classification</i>	Drukker et al. 2014	Breast mammography imagery of primary lesion	Three-Compartment Breast (3CB) imaging	3CB			Pathology			RCB				Reference no. 16
Fig. S3.1					Triple-Negative		Receptor-Positive		11/46			Unknown			
Tab. S3.1					6		40								
Fig. 3.1D															
Fig. 3.1E	<i>Epithelial progeny of estrogen-exposed breast progenitor cells display a cancer-like methylome</i>	Cheng et al. 2008	Microdissection of tissues from patient mastectomy	IHC on primary breast lesion and surrounding tissue by radius, contralateral and normal tissue	Primary Tumor	NAT 1cm	NAT 2cm	NAT 3cm	NAT 4cm	Healthy NT			Reference no. 19		
					9	7	5	3	4	10					
Tab. S3.2A	Data first reported here	Williams/C amarda et al.	Laser capture microdissection of primary patient tumors and adjacent tissue, and healthy patient control tissue.	LC-MS/MS	Healthy Control	NAT	Stroma	Lum.A	Lum.B	Lum.A/B	Her2-Amp	Her2-Amp/Lum.B	Basal	First reported here	
Tab. S3.2B															
Fig. 3.1F					42	4	36	38	16	1	9	5	16		
Fig. 3.2C	<i>The Cancer Genome Atlas Program</i>	TCGA	Primary breast cancer lesion tissue	RNA-Seq	Triple-Negative				Receptor-Positive				TCGA Research Network, https://www.cancer.gov/tcga		
					123				648						
Fig. 3.3	Data first reported here	Williams/C amarda et al.	Primary breast adipose tissue from a healthy individual, Werb Lab, UCSF	IHC	8 samples prefixed 'WD'										First reported here
Fig. 3.2E	<i>Single-cell RNA-seq enables comprehensive tumour and immune cell profiling in primary breast cancer</i>	Chung et al. 2017	Primary breast cancer lesion tissue	scRNA-Seq	317 cells total from 11 tumors were sequenced										Reference no. 34
Fig. S3.2															

Additional Supplementary Table Legends:

Table S4.1. Patient ID, receptor status, histological section availability, percent lipid content (lipid content / lipid + water + protein content) of L, R1, R2 and R3, and Scarff- Bloom- Richardson (SBR) grade from patients ($n = 46$) with invasive breast cancer.

Table S4.3. LC-MS/MS of LCM samples from 75 patients with invasive breast cancer and 42 healthy subjects. (A) Sample number, ID number, tissue type, and tumor subtype (when applicable) of 75 patients and 42 healthy subjects. (B) Spectral counts of proteins detected via LC-MS/MS from samples in (A).

Table S4.4. RNA expression changes in MTB-TOM tumors ($n = 11$) compared to non- tumor mammary glands ($n = 3$). Differential expression analysis was performed using the 'limma' R package [49].

References

- 1 Goodwin, P. J. & Chlebowski, R. T. Obesity and Cancer: Insights for Clinicians. *J Clin Oncol* **34**, 4197-4202 (2016). <https://doi.org/10.1200/jco.2016.70.5327>
- 2 Camarda, R. *et al.* Inhibition of fatty acid oxidation as a therapy for MYC-overexpressing triple-negative breast cancer. *Nat Med* **22**, 427-432 (2016).
<https://doi.org/https://10.1038/nm.4055>
- 3 Park, J. H. *et al.* Fatty Acid Oxidation-Driven Src Links Mitochondrial Energy Reprogramming and Oncogenic Properties in Triple-Negative Breast Cancer. *Cell Reports* **14**, 2154-2165 (2016). <https://doi.org/10.1016/j.celrep.2016.02.004>
- 4 Ye, H. *et al.* Leukemic Stem Cells Evade Chemotherapy by Metabolic Adaptation to an Adipose Tissue Niche. *Cell Stem Cell* **19**, 23-37 (2016).
<https://doi.org/10.1016/j.stem.2016.06.001>
- 5 Hoy, A. J., Balaban, S. & Saunders, D. N. Adipocyte–Tumor Cell Metabolic Crosstalk in Breast Cancer. *Trends in Molecular Medicine* **23**, 381-392 (2017).
<https://doi.org/10.1016/j.molmed.2017.02.009>
- 6 Nieman, K. M. *et al.* Adipocytes promote ovarian cancer metastasis and provide energy for rapid tumor growth. *Nat Med* **17**, 1498-1503 (2011).
- 7 Balaban, S., Lee, L. S., Schreuder, M. & Hoy, A. J. Obesity and cancer progression: Is there a role of fatty acid metabolism? *BioMed Research International* **2015** (2015).
<https://doi.org/10.1155/2015/274585>
- 8 Wang, Y. Y. *et al.* Mammary adipocytes stimulate breast cancer invasion through metabolic remodeling of tumor cells Mammary adipocytes stimulate breast cancer

- invasion through metabolic remodeling of tumor cells. **2** (2017).
<https://doi.org/10.1172/jci.insight.87489>
- 9 Wen, Y. A. *et al.* Adipocytes activate mitochondrial fatty acid oxidation and autophagy to promote tumor growth in colon cancer. *Cell Death Dis* **8**, e2593 (2017).
<https://doi.org/10.1038/cddis.2017.21>
- 10 Wang, C., Gao, C., Meng, K., Qiao, H. & Wang, Y. Human adipocytes stimulate invasion of breast cancer MCF-7 cells by secreting IGFBP-2. *PLoS ONE* **10** (2015).
<https://doi.org/10.1371/journal.pone.0119348>
- 11 Muller, C. Tumour-surrounding adipocytes are active players in breast cancer progression. *Annales d'Endocrinologie* **74**, 108-110 (2013).
<https://doi.org/10.1016/j.ando.2013.02.007>
- 12 Dirat, B. *et al.* Cancer-associated adipocytes exhibit an activated phenotype and contribute to breast cancer invasion. *Cancer Research* **71**, 2455-2465 (2011).
<https://doi.org/10.1158/0008-5472.CAN-10-3323>
- 13 Dirat, B. A., Bochet, L., Escourrou, G., Valet, P. & Muller, C. Unraveling the obesity and breast cancer links: a role for cancer-associated adipocytes? *Endocr Dev* **19**, 45-52 (2010). <https://doi.org/10.1159/000316896>
- 14 Hovey, R. C. & Aimo, L. Diverse and active roles for adipocytes during mammary gland growth and function. *J Mammary Gland Biol Neoplasia* **15**, 279-290 (2010).
<https://doi.org/10.1007/s10911-010-9187-8>
- 15 Laidevant, A. D., Malkov, S., Flowers, C. I., Kerlikowske, K. & Shepherd, J. A. Compositional breast imaging using a dual-energy mammography protocol. *Med Phys* **37**, 164-174 (2010). <https://doi.org/10.1118/1.3259715>

- 16 Drukker, K. *et al.* Mammographic quantitative image analysis and biologic image composition for breast lesion characterization and classification. *Med Phys* **41**, 031915 (2014). <https://doi.org/10.1118/1.4866221>
- 17 Duncan, R. E., Ahmadian, M., Jaworski, K., Sarkadi-Nagy, E. & Sul, H. S. Regulation of lipolysis in adipocytes. *Annu Rev Nutr* **27**, 79-101 (2007). <https://doi.org/10.1146/annurev.nutr.27.061406.093734>
- 18 Shinoda, K. *et al.* Genetic and functional characterization of clonally derived adult human brown adipocytes. *Nat Med* **21**, 389-394 (2015). <https://doi.org/10.1038/nm.3819>
- 19 Cheng, A. S. L. *et al.* Epithelial progeny of estrogen-exposed breast progenitor cells display a cancer-like methylome. *Cancer Research* **68**, 1786-1796 (2008). <https://doi.org/10.1158/0008-5472.CAN-07-5547>
- 20 Verhaak, R. G. *et al.* Prognostically relevant gene signatures of high-grade serous ovarian carcinoma. *J Clin Invest* **123**, 517-525 (2013). <https://doi.org/10.1172/jci65833>
- 21 Zhu, Y. *et al.* Connexin 43 Mediates White Adipose Tissue Beiging by Facilitating the Propagation of Sympathetic Neuronal Signals. *Cell Metab* **24**, 420-433 (2016). <https://doi.org/10.1016/j.cmet.2016.08.005>
- 22 Palanker, L., Tennessen, J. M., Lam, G. & Thummel, C. S. Drosophila HNF4 regulates lipid mobilization and beta-oxidation. *Cell Metab* **9**, 228-239 (2009). <https://doi.org/10.1016/j.cmet.2009.01.009>
- 23 Large, V. *et al.* Decreased expression and function of adipocyte hormone-sensitive lipase in subcutaneous fat cells of obese subjects. *J Lipid Res* **40**, 2059-2066 (1999).
- 24 Wang, F. *et al.* Mammary fat of breast cancer: Gene expression profiling and functional characterization. *PLoS ONE* **9** (2014). <https://doi.org/10.1371/journal.pone.0109742>

- 25 DeRose, Y. S. *et al.* Tumor grafts derived from women with breast cancer authentically reflect tumor pathology, growth, metastasis and disease outcomes. *Nat Med* **17**, 1514-1520 (2011). <https://doi.org/10.1038/nm.2454>
- 26 D'Cruz, C. M. *et al.* c-MYC induces mammary tumorigenesis by means of a preferred pathway involving spontaneous Kras2 mutations. *Nat Med* **7**, 235-239 (2001). <https://doi.org/10.1038/84691>
- 27 Aran, D. *et al.* Comprehensive analysis of normal adjacent to tumor transcriptomes. *Nat Commun* **8**, 1077 (2017). <https://doi.org/10.1038/s41467-017-01027-z>
- 28 Aasen, T., Mesnil, M., Naus, C. C., Lampe, P. D. & Laird, D. W. Gap junctions and cancer: communicating for 50 years. *Nat Rev Cancer* **16**, 775-788 (2016). <https://doi.org/10.1038/nrc.2016.105>
- 29 Gleisner, M. A., Navarrete, M., Hofmann, F., Salazar-Onfray, F. & Tittarelli, A. Mind the Gaps in Tumor Immunity: Impact of Connexin-Mediated Intercellular Connections. *Front Immunol* **8**, 1067 (2017). <https://doi.org/10.3389/fimmu.2017.01067>
- 30 Chen, Q. *et al.* Carcinoma–astrocyte gap junctions promote brain metastasis by cGAMP transfer. *Nature* **533**, 493-498 (2016).
- 31 Osswald, M. *et al.* Brain tumour cells interconnect to a functional and resistant network. *Nature* **528**, 93-98 (2015). <https://doi.org/10.1038/nature16071>
- 32 Horiuchi, D. *et al.* MYC pathway activation in triple-negative breast cancer is synthetic lethal with CDK inhibition. *The Journal of Experimental Medicine* **209**, 679-696 (2012). <https://doi.org/10.1084/jem.20111512>
- 33 Koboldt, D. C. *et al.* Comprehensive molecular portraits of human breast tumours. *Nature* **490**, 61-70 (2012). <https://doi.org/10.1038/nature11412>

- 34 Chung, W. *et al.* Single-cell RNA-seq enables comprehensive tumour and immune cell profiling in primary breast cancer. *Nat Commun* **8**, 15081 (2017).
<https://doi.org/10.1038/ncomms15081>
- 35 Wenzel, K., Manthey, D., Willecke, K., Grzeschik, K. H. & Traub, O. Human gap junction protein connexin31: molecular cloning and expression analysis. *Biochem Biophys Res Commun* **248**, 910-915 (1998). <https://doi.org/10.1006/bbrc.1998.9070>
- 36 Willebrords, J., Maes, M., Crespo Yanguas, S. & Vinken, M. Inhibitors of connexin and pannexin channels as potential therapeutics. *Pharmacol Ther* **180**, 144-160 (2017).
<https://doi.org/10.1016/j.pharmthera.2017.07.001>
- 37 Rios, A. C. *et al.* Intraclonal Plasticity in Mammary Tumors Revealed through Large-Scale Single-Cell Resolution 3D Imaging. *Cancer Cell* **35**, 618-632.e616 (2019).
<https://doi.org/10.1016/j.ccell.2019.02.010>
- 38 Aune, U. L., Ruiz, L. & Kajimura, S. Isolation and Differentiation of Stromal Vascular Cells to Beige/Brite Cells. *JoVE*, e50191 (2013). <https://doi.org/doi:10.3791/50191>
- 39 Wang, Q. A., Tao, C., Gupta, R. K. & Scherer, P. E. Tracking adipogenesis during white adipose tissue development, expansion and regeneration. *Nat Med* **19**, 1338-1344 (2013).
<https://doi.org/10.1038/nm.3324>
- 40 Malkov, S., Wang, J., Kerlikowske, K., Cummings, S. R. & Shepherd, J. A. Single x-ray absorptiometry method for the quantitative mammographic measure of fibroglandular tissue volume. *Med Phys* **36**, 5525-5536 (2009). <https://doi.org/10.1118/1.3253972>
- 41 Malkov, S., Wang, J., Duewer, F. & Shepherd, J. A. 769-774 (Springer Berlin Heidelberg, 2012).

- 42 Malkov, S. *et al.* International Workshop on Digital Mammography. **9699**, 211–218 (2016).
- 43 Hammond, M. E. *et al.* American Society of Clinical Oncology/College of American Pathologists guideline recommendations for immunohistochemical testing of estrogen and progesterone receptors in breast cancer (unabridged version). *Arch Pathol Lab Med* **134**, e48-72 (2010). <https://doi.org/10.5858/134.7.e48>
- 44 Wolff, A. C. *et al.* Recommendations for human epidermal growth factor receptor 2 testing in breast cancer: American Society of Clinical Oncology/College of American Pathologists clinical practice guideline update. *J Clin Oncol* **31**, 3997-4013 (2013). <https://doi.org/10.1200/jco.2013.50.9984>
- 45 Galarraga, M. *et al.* Adiposoft: Automated software for the analysis of white adipose tissue cellularity in histological sections. *Journal of Lipid Research* **53**, 2791-2796 (2012). <https://doi.org/10.1194/jlr.D023788>
- 46 Dai, M. *et al.* Evolving gene/transcript definitions significantly alter the interpretation of GeneChip data. *Nucleic Acids Res* **33**, e175 (2005). <https://doi.org/10.1093/nar/gni179>
- 47 Zhang, B. *et al.* Proteogenomic characterization of human colon and rectal cancer. *Nature* **513**, 382-387 (2014). <https://doi.org/10.1038/nature13438>
- 48 Neve, R. M. *et al.* A collection of breast cancer cell lines for the study of functionally distinct cancer subtypes. *Cancer Cell* **10**, 515-527 (2006). <https://doi.org/10.1016/j.ccr.2006.10.008>
- 49 Smyth, G. K. in *Bioinformatics and Computational Biology Solutions Using R and Bioconductor* (eds Robert Gentleman *et al.*) 397-420 (Springer New York, 2005).

- 50 Ettinger, A. & Wittmann, T. in *Methods in Cell Biology* Vol. 123 (eds Jennifer C. Waters & Torsten Wittman) 77-94 (Academic Press, 2014).
- 51 Stehbens, S., Pemble, H., Murrow, L. & Wittmann, T. in *Methods in Enzymology* Vol. 504 (ed P. Michael conn) 293-313 (Academic Press, 2012).
- 52 Stehbens, S. J. *et al.* CLASPs link focal-adhesion-associated microtubule capture to localized exocytosis and adhesion site turnover. *Nat Cell Biol* **16**, 561-573 (2014).
<https://doi.org/10.1038/ncb2975>
- 53 Rohrberg, J. *et al.* MYC Dysregulates Mitosis, Revealing Cancer Vulnerabilities. *Cell Rep* **30**, 3368-3382.e3367 (2020). <https://doi.org/10.1016/j.celrep.2020.02.041>
- 54 Kajimura, S. *et al.* Initiation of myoblast to brown fat switch by a PRDM16-C/EBP- β transcriptional complex. *Nature* **460**, 1154-1158 (2009).
<https://doi.org/10.1038/nature08262>
- 55 Livak, K. J. & Schmittgen, T. D. Analysis of relative gene expression data using real-time quantitative PCR and the 2(-Delta Delta C(T)) Method. *Methods* **25**, 402-408 (2001). <https://doi.org/10.1006/meth.2001.1262>

Chapter 5: Additional publications from thesis work

In Vivo Optical Metabolic Imaging of Long-Chain Fatty Acid Uptake in Orthotopic Models of Triple-Negative Breast Cancer

Targeting a tumor's metabolic dependencies is a clinically actionable therapeutic approach; however, identifying subtypes of tumors likely to respond remains difficult. The use of lipids as a nutrient source is of particular importance, especially in breast cancer. Imaging techniques offer the opportunity to quantify nutrient use in preclinical tumor models to guide development of new drugs that restrict uptake or utilization of these nutrients. We describe a fast and dynamic approach to image fatty acid uptake in vivo and demonstrate its relevance to study both tumor metabolic reprogramming directly, as well as the effectiveness of drugs targeting lipid metabolism. Specifically, we developed a quantitative optical approach to spatially and longitudinally map the kinetics of long-chain fatty acid uptake in in vivo murine models of breast cancer using a fluorescently labeled palmitate molecule, Bodipy FL c16. We chose intra-vital microscopy of mammary tumor windows to validate our approach in two orthotopic breast cancer models: a MYC-overexpressing, transgenic, triple-negative breast cancer (TNBC) model and a murine model of the 4T1 family. Following injection, Bodipy FL c16 fluorescence increased and reached its maximum after approximately 30 min, with the signal remaining stable during the 30–80 min post-injection period. We used the fluorescence at 60 min (Bodipy60), the mid-point in the plateau region, as a summary parameter to quantify Bodipy FL c16 fluorescence in subsequent experiments. Using our imaging platform, we observed a two- to four-fold decrease in fatty acid uptake in response to the downregulation of the MYC oncogene, consistent with findings from in vitro metabolic assays. In contrast, our imaging studies report an increase in fatty acid uptake with tumor aggressiveness (6NR, 4T07, and 4T1), and uptake was significantly decreased after treatment with a fatty acid transport inhibitor, perphenazine, in both normal mammary pads and in

the most aggressive 4T1 tumor model. Our approach fills an important gap between in vitro assays providing rich metabolic information at static time points and imaging approaches visualizing metabolism in whole organs at a reduced resolution.

Article

In Vivo Optical Metabolic Imaging of Long-Chain Fatty Acid Uptake in Orthotopic Models of Triple-Negative Breast Cancer

Megan C. Madonna ^{1,*} , Joy E. Duer ² , Joyce V. Lee ³, Jeremy Williams ³, Baris Avsaroglu ³, Caigang Zhu ⁴, Riley Deutsch ¹, Roujia Wang ¹, Brian T. Crouch ¹, Matthew D. Hirschey ⁵, Andrei Goga ^{3,6,7} and Nirmala Ramanujam ^{1,8}

¹ Department of Biomedical Engineering, Duke University, Durham, NC 27708, USA; riley.deutsch@duke.edu (R.D.); roujia.wang@duke.edu (R.W.); brian.crouch@duke.edu (B.T.C.); nimmi.ramanujam@duke.edu (N.R.)

² Department of Biology, Duke University, Durham, NC 27708, USA; jduer@wakehealth.edu

³ Department of Cell and Tissue Biology, University of California, San Francisco (UCSF), San Francisco, CA 94143, USA; joyce.lee3@ucsf.edu (J.V.L.); jeremy.williams@ucsf.edu (J.W.); baris.avsaroglu@ucsf.edu (B.A.); andrei.goga@ucsf.edu (A.G.)

⁴ Department of Biomedical Engineering, University of Kentucky, Lexington, KY 40506, USA; caigang.zhu@uky.edu

⁵ Duke Molecular Physiology Institute, Durham, NC 27701, USA; matthew.hirschey@duke.edu

⁶ Department of Medicine, University of California, San Francisco, CA 94143, USA

⁷ Helen Diller Family Comprehensive Cancer Center, University of California, San Francisco, CA 94143, USA

⁸ Department of Pharmacology & Cancer Biology, School of Medicine, Duke University, Durham, NC 27708, USA

* Correspondence: megan.madonna@duke.edu



Citation: Madonna, M.C.; Duer, J.E.; Lee, J.V.; Williams, J.; Avsaroglu, B.; Zhu, C.; Deutsch, R.; Wang, R.; Crouch, B.T.; Hirschey, M.D.; et al. In Vivo Optical Metabolic Imaging of Long-Chain Fatty Acid Uptake in Orthotopic Models of Triple-Negative Breast Cancer. *Cancers* **2021**, *13*, 148. <https://doi.org/10.3390/cancers13010148>

Received: 2 November 2020

Accepted: 31 December 2020

Published: 5 January 2021

Publisher's Note: MDPI stays neutral with regard to jurisdictional claims in published maps and institutional affiliations.



Copyright: © 2021 by the authors. Licensee MDPI, Basel, Switzerland. This article is an open access article distributed under the terms and conditions of the Creative Commons Attribution (CC BY) license (<https://creativecommons.org/licenses/by/4.0/>).

Simple Summary: A dysregulated metabolism is a hallmark of cancer. Once understood, tumor metabolic reprogramming can lead to targetable vulnerabilities, spurring the development of novel treatment strategies. Beyond the common observation that tumors rely heavily on glucose, building evidence indicates that a subset of tumors use lipids to maintain their proliferative or metastatic phenotype. This study developed an intra-vital microscopy method to quantify lipid uptake in breast cancer murine models using a fluorescently labeled palmitate molecule, Bodipy FL c16. This work highlights optical imaging's ability to both measure metabolic endpoints non-destructively and repeatedly, as well as inform small animal metabolic phenotyping beyond in vivo optical imaging of breast cancer alone.

Abstract: Targeting a tumor's metabolic dependencies is a clinically actionable therapeutic approach; however, identifying subtypes of tumors likely to respond remains difficult. The use of lipids as a nutrient source is of particular importance, especially in breast cancer. Imaging techniques offer the opportunity to quantify nutrient use in preclinical tumor models to guide development of new drugs that restrict uptake or utilization of these nutrients. We describe a fast and dynamic approach to image fatty acid uptake in vivo and demonstrate its relevance to study both tumor metabolic reprogramming directly, as well as the effectiveness of drugs targeting lipid metabolism. Specifically, we developed a quantitative optical approach to spatially and longitudinally map the kinetics of long-chain fatty acid uptake in in vivo murine models of breast cancer using a fluorescently labeled palmitate molecule, Bodipy FL c16. We chose intra-vital microscopy of mammary tumor windows to validate our approach in two orthotopic breast cancer models: a MYC-overexpressing, transgenic, triple-negative breast cancer (TNBC) model and a murine model of the 4T1 family. Following injection, Bodipy FL c16 fluorescence increased and reached its maximum after approximately 30 min, with the signal remaining stable during the 30–80 min post-injection period. We used the fluorescence at 60 min (Bodipy₆₀), the mid-point in the plateau region, as a summary parameter to quantify Bodipy FL c16 fluorescence in subsequent experiments. Using our imaging platform, we observed a two- to four-fold decrease in fatty acid uptake in response to the downregulation of the MYC oncogene, consistent with findings from in vitro metabolic assays. In contrast, our imaging studies report an increase in fatty acid uptake with tumor aggressiveness (6NR, 4T07, and 4T1), and uptake

MYC Dysregulates Mitosis, Revealing Cancer Vulnerabilities

Tumors that overexpress the *MYC* oncogene are frequently aneuploid, a state associated with highly aggressive cancers and tumor evolution. However, how *MYC* causes aneuploidy is not well understood. Here, we show that *MYC* overexpression induces mitotic spindle assembly defects and chromosomal instability (CIN) through effects on microtubule nucleation and organization. Attenuating *MYC* expression reverses mitotic defects, even in established tumor cell lines, indicating an ongoing role for *MYC* in CIN. *MYC* reprograms mitotic gene expression, and we identify *TPX2* to be permissive for spindle assembly in *MYC*-high cells. *TPX2* depletion blocks mitotic progression, induces cell death, and prevents tumor growth. Further elevating *TPX2* expression reduces mitotic defects in *MYC*-high cells. *MYC* and *TPX2* expression may be useful bio-markers to stratify patients for anti-mitotic therapies. Our studies implicate *MYC* as a regulator of mitosis and suggest that blocking *MYC* activity can attenuate the emergence of CIN and tumor evolution.

MYC Dysregulates Mitosis, Revealing Cancer Vulnerabilities

Julia Rohrberg,^{1,*} Daniel Van de Mark,^{1,6} Meelad Amouzgar,^{1,6} Joyce V. Lee,¹ Moufida Taïleb,¹ Alexandra Corella,^{1,7} Seda Kilinc,¹ Jeremy Williams,^{1,2} Marie-Lena Jokisch,¹ Roman Camarda,^{1,2} Sanjeev Balakrishnan,^{1,9} Rama Shankar,⁴ Alicia Zhou,^{1,8} Aaron N. Chang,^{5,10} Bin Chen,⁴ Hope S. Rugo,³ Sophie Dumont,¹ and Andrei Goga^{1,3,11,*}

¹Department of Cell & Tissue Biology, University of California, San Francisco, San Francisco, CA, USA

²Biomedical Sciences Graduate Program, University of California, San Francisco, San Francisco, CA, USA

³Department of Medicine, University of California, San Francisco, San Francisco, CA, USA

⁴Department of Pediatrics and Human Development and Department of Pharmacology and Toxicology, College of Human Medicine, Michigan State University, Grand Rapids, MI, USA

⁵Baylor College of Medicine, Houston, TX, USA

⁶These authors contributed equally

⁷Present address: Divisions of Human Biology and Clinical Research, Fred Hutchinson Cancer Research Center, Mailstop D4-100, 1100 Fairview Avenue N, Seattle, WA 98109-1024, USA

⁸Present address: Color Genomics, 863A Mitten Rd., Burlingame, CA 94010, USA

⁹Present address: Dovetail Genomics, Santa Cruz, CA, USA

¹⁰Present address: Fulcrum Therapeutics, One Kendall Square, Bldg. 700, Suite B7102, Cambridge, MA 02139, USA

¹¹Lead Contact

*Correspondence: julia.rohrberg@ucsf.edu (J.R.), andrei.goga@ucsf.edu (A.G.)

<https://doi.org/10.1016/j.celrep.2020.02.041>

SUMMARY

Tumors that overexpress the *MYC* oncogene are frequently aneuploid, a state associated with highly aggressive cancers and tumor evolution. However, how *MYC* causes aneuploidy is not well understood. Here, we show that *MYC* overexpression induces mitotic spindle assembly defects and chromosomal instability (CIN) through effects on microtubule nucleation and organization. Attenuating *MYC* expression reverses mitotic defects, even in established tumor cell lines, indicating an ongoing role for *MYC* in CIN. *MYC* reprograms mitotic gene expression, and we identify *TPX2* to be permissive for spindle assembly in *MYC*-high cells. *TPX2* depletion blocks mitotic progression, induces cell death, and prevents tumor growth. Further elevating *TPX2* expression reduces mitotic defects in *MYC*-high cells. *MYC* and *TPX2* expression may be useful biomarkers to stratify patients for anti-mitotic therapies. Our studies implicate *MYC* as a regulator of mitosis and suggest that blocking *MYC* activity can attenuate the emergence of CIN and tumor evolution.

INTRODUCTION

Aneuploidy, a state of abnormal chromosome number, is a hallmark of cancer, with >70% of common solid tumors found to be aneuploid (Boveri, 2008; Cimini, 2008). Aneuploidy is frequently caused by chromosomal instability (CIN), chromosome missegregation that leads to chromosome loss or gain (Lengauer et al., 1997; Thompson and Compton, 2008). CIN is a major driver of tumor evolution and promotes drug resistance and

metastasis (Bakhoun et al., 2018; Greaves, 2015; Turajlic and Swanton, 2017); however, the major mechanisms that induce CIN remain poorly understood.

The *MYC* oncogene is frequently overexpressed in a wide variety of aggressive and metastatic tumors and has been associated with aneuploidy (Felsner and Bishop, 1999a; Karlsson et al., 2003; McCormack et al., 1998; Soucek and Evan, 2010). One of the key biological functions of *MYC* is its ability to facilitate entry and progression through G1 and S phases of the cell cycle by regulating gene transcription (Bretonnes et al., 2015). However, whether *MYC* also affects mitotic progression and induces CIN is unclear. We and others have found that cells with elevated *MYC* activity are sensitive to mitotic interruption such as treatment with microtubule-targeting agents, mitotic kinase inhibitors, or small interfering RNA (siRNA)-mediated depletion of spindle-related genes (Dauch et al., 2016; Goga et al., 2007; Horiuchi et al., 2012; Kessler et al., 2012; Littler et al., 2019; Martins et al., 2015; Menssen et al., 2007; Pereira et al., 2017; Topham et al., 2015). However, a molecular mechanism for the synthetic-lethal interactions of *MYC* with mitotic regulators is missing. Clarifying such a mechanism could reveal novel treatment strategies for aggressive *MYC*-overexpressing cancers.

Chromosome segregation is mediated by the mitotic spindle, while spindle error detection occurs through the spindle assembly checkpoint (SAC). The SAC delays chromosome segregation until appropriate attachments of chromosomes to spindle microtubules are established (Joglekar, 2016). In cancer cells, where CIN is common, chromosomes frequently missegregate as a result of microtubule-chromosome attachment errors that are not detected by the SAC (Bakhoun et al., 2009). Various defects in spindle formation can cause attachment errors and CIN (Cimini, 2008). One key mediator of spindle formation is the microtubule-binding protein *TPX2*, which is overexpressed in many aggressive human tumors, and its overexpression is highly correlated with CIN (Carter et al., 2006; Hu et al., 2012). However,



Chapter 6: Concluding remarks

Summary

Defining the cellular adaptations that permit altered fatty acid metabolism (FAM) and aggressive growth in TNBC has both clinical value and a broader bearing in elucidating tumor-microenvironment interactions. In *Chapter 2*, we reviewed the role of driver oncogenes in tissue-specific alteration to tumor metabolism, the importance of modeling tumor metabolism *in vivo*, and how potent oncogene MYC can drive disparate metabolic changes through carcinogenesis based on tumor tissue of origin. We described strategies for *in vivo* modeling of MYC-driven tumor metabolism, and technological advancements including the shift from snapshot metabolomics towards kinetic flux analysis. MYC drives tumor metabolic reprogramming in a tissue-specific fashion, and glucose and glutamine metabolism can each increase or decrease based on tissue of origin; understanding specific dependencies in each context could bear clinical significance. MYC also drives changes to downstream utilization of glutamine, with various cancers showing relative increases and decreases to glutathione levels and regulation that lend different therapeutic vulnerabilities. Finally, we outline various MYC-driven changes to lipid metabolism, with dysregulation observed in MYC-driven hepatoblastoma and hepatocellular carcinoma but mechanistic links not well-established. In TNBC with elevated MYC (a majority), prior studies identified elevated FAO, and targeting FAO machinery was shown to block *in vivo* tumor progression.

To look for targetable features in TNBC lipid metabolism, I next explored the intracellular adaptations that permit increased FAO. In *Chapter 3* I examined the role of fatty acid binding proteins in TNBC, and their link to MYC level. Upregulation of Fatty acid binding protein 5 (FABP5) has been identified in patient TN tumors and a mouse model for MYC-driven breast cancer, and its role in lipid metabolism is interrogated. I observed elevated FABP5 in

patient-derived triple-negative (TN) cell lines, but increased expression across TN MYC-high and -low lines suggested, in contrast to prior evidence, that levels may not be solely regulated by MYC. Consistent with prior findings, I found that inhibition of FABP5/7 with an available compound impaired TNBC cell proliferation and disrupted lipid homeostasis, indicating therapeutic potential for targeting FABP5. A prior study showed transient FABP5 silencing impaired cell proliferation and lipid metabolism, in line with results of pharmacological inhibition, however I found that complete genetic knockout did not recapitulate deficits to growth and FAM. It is possible that other FABPs compensate following FABP5 loss, suggesting it may be difficult to model specific contributions to FAM using persistent genetic knockout. Preclinical studies indicate that targeting FA import machinery including CD36 could be sufficient to disrupt lipid metabolism in breast cancer. Proposed cell-extrinsic contributions of CD36 to breast tumorigenesis through adipocyte reprogramming emphasize a need to consider TNBC interactions with the tumor microenvironment to decode its dysregulated FAM.

In *Chapter 4*, I described a mechanism by which MYC-driven TNBC drive reprogramming of FAM in adipocytes through cancer cell-adipocyte contact. Studying breast tumors and normal adjacent tissue from several patient cohorts and patient-derived xenograft models, we showed that lipolysis and lipolytic signaling are activated in tumor-adjacent adipocytes. We investigated the tumor-adipocyte interface and found that functional gap junctions form between cancer cells and, and that cAMP, a critical lipolytic signaling molecule, is transferred in a gap junction-dependent manner. We observed specific elevation of connexin 31 (GJB3) in patient TN tumors and a mouse model for MYC-driven breast cancer, and engineered GJB3-depleted TN MYC-high and -low cell lines to define its contributions to tumor progression. I performed direct cancer cell-adipocyte co-cultures using normal patient breast fat

and determined that GJB3 depletion lowered transfer of gap junction-dependent dye and of cAMP to breast adipocytes. Using immunofluorescence and tissue clearing, I imaged direct co-cultures and saw marked contact between GJB3-WT TN cells and breast adipocytes, with contrasting, tangential contact by RP cells or GJB3-depleted TN cells. We performed *in vivo* studies with GJB3-depleted and -knockdown PDX lines, and found GJB3 depletion was sufficient to block tumor growth. GJB3-depleted tumors displayed increased intracellular cAMP, and proximate adipocytes displayed increased size and decreased lipolysis compared to WT. From this study we concluded that pro-lipolytic tumor cell-adipocyte interactions contribute to tumorigenesis, may have potential as new therapeutic target in breast cancer.

These studies, in summary, portray how TNBC both permit altered intracellular FAM and transduce pro-tumorigenic signals that alter FAM in the tumor niche. Altered metabolism is a hallmark of cancer, and is often reflective of the tumor microenvironment; here we observed altered FAM both in and near tumor cells. The invasive tumor front abuts adipocytes in a range of cancer contexts, and defining mechanistic roles for cancer cell-adipocyte contact in tumor growth has relevance in unraveling links between obesity and cancer, and in targeting tumor metastasis to fat depots, both current topics of interest. While prior studies examining roles of adipocytes in tumorigenesis have broadly identified *indirect*, autocrine, paracrine and endocrine signaling from adipocytes to tumors, this work highlights the importance of modeling *direct* cancer cell-adipocyte contact, and of accounting for the tumor microenvironment when examining altered metabolism in cancer.

Future Directions

The foundational observation that most TNBCs feature and depend upon elevated fatty acid oxidation (FAO), insights into altered intracellular fatty acid (FA) trafficking (*Chapter 3*), and the discovery of cancer cell signaling to alter FAM in surrounding tissue (*Chapter 4*), beget new and important questions about bioenergetic reliance on FAO in this aggressive subset of breast cancers. I emerged with greater appreciation for contact-dependent cancer cell signaling with the tumor microenvironment, for the unforeseen contributions of gap junctions in TNBC tumor growth, and for the role of tumor-adjacent lipolysis in TNBC progression. Still, a direct connection between adipocyte lipolysis in the TNBC tumor microenvironment and the import and catabolism of released FA by tumor cells has yet to be established. Given evidence that they induce lipolysis in surrounding adipocytes, *do TNBC tumors rely on FA liberated from adipocyte lipolysis for tumor growth?* Metabolic tracing co-culture studies would be required to delineate whether FA derived from adipocyte lipolysis undergo import and FAO in proximate breast cancer cells. *Do TNBC feature altered FA import machinery?* Given the metabolic shift to FAO in these aggressive breast cancers and evidence that Cx31 tumor cell-adipocyte gap junctions are pro-tumorigenic (*Chapter 4*), understanding whether pro-lipolytic cAMP signaling from these tumors specifically satisfies a need for available FA in TNBC cells would lend new insight to how tumor cells can coopt surrounding tissue to fulfill their metabolic requirements. In any case, with *in vivo* data indicating genetic depletion of Cx31 is sufficient to impair tumor growth, *would selective GJB3 (Cx31) inhibition block TNBC growth in a clinical setting?* There are some selective Cx43 hemichannel inhibitors available for GJA1 (Cx43), the most well-characterized gap junction in cancer.

This work also gives rise to broader questions about the contributions of cancer cell-adipocyte gap junctions to tumorigenesis in other cancer contexts. Our ability to quantify lipid content and adipocyte size in normal adjacent tissue (NAT) of breast cancer patients in *Chapter 4* is owed to a pioneering study (from our collaborator John Shepherd, PhD) wherein advanced mammographic imaging termed ‘three compartment breast lesion detection’ (3CB) was used to quantify compositional thicknesses of water, protein, and lipid for breast cancer screening patients. These data and associated tumor and NAT pathology allowed us to assess clinical evidence of lipolysis across a significant number of breast cancer patients and at standardized margins from respective breast lesions. The co-culture and *in vivo* work that followed reveals mechanistic evidence for an established clinical trend. Though tumor cells border adipocytes in a range of primary and metastatic cancers, exploration of tumor-adjacent lipolysis in other fat depots such as the omentum would not be bolstered by this sort of powerful clinical dataset. Mouse models do, however, exist for ovarian cancers with omental tropism. *Does gap-junction dependent lipolysis contribute to tumorigenesis in other cancers with adipose microenvironments, such as omental metastases? Is there a role for gap junction-dependent lipolysis in driving obesity-linked cancers? Are gap junctions or lipolysis in the tumor microenvironment viable therapeutic targets in other cancer contexts?*

Publishing Agreement

It is the policy of the University to encourage open access and broad distribution of all theses, dissertations, and manuscripts. The Graduate Division will facilitate the distribution of UCSF theses, dissertations, and manuscripts to the UCSF Library for open access and distribution. UCSF will make such theses, dissertations, and manuscripts accessible to the public and will take reasonable steps to preserve these works in perpetuity.

I hereby grant the non-exclusive, perpetual right to The Regents of the University of California to reproduce, publicly display, distribute, preserve, and publish copies of my thesis, dissertation, or manuscript in any form or media, now existing or later derived, including access online for teaching, research, and public service purposes.

Signed by:



A8A58055114D45F...

Author Signature

12/12/2024

Date